nature chemistry

SUPPLEMENTARY INFORMATION

https://doi.org/10.1038/s41557-019-0292-z

In the format provided by the authors and unedited.

Building in vitro transcriptional regulatory networks by successively integrating multiple functional circuit modules

Samuel W. Schaffter[1] **and Rebecca Schulman**[1,2]

[1]Department of Chemical and Biomolecular Engineering, Johns Hopkins University, Baltimore, MD, USA. [2]Department of Computer Science, Johns Hopkins University, Baltimore, MD, USA. e-mail: sschaff6@jhu.edu; rschulm3@jhu.edu

Supplementary Information

Building *in vitro* transcriptional regulatory networks by successively integrating multiple functional circuit modules

Samuel W. Schaffter[1] and Rebecca Schulman[1, 2,*]

[1]Department of Chemical and Biomolecular Engineering – Johns Hopkins University, [2]Department of Computer Science – Johns Hopkins University

email: Samuel W. Schaffter - sschaff6@jhu.edu
[*]email: Rebecca Schulman - rschulm3@jhu.edu

Table of contents

1. Specifications for genelet networks, component structures, and component sequences

1.1. Networks

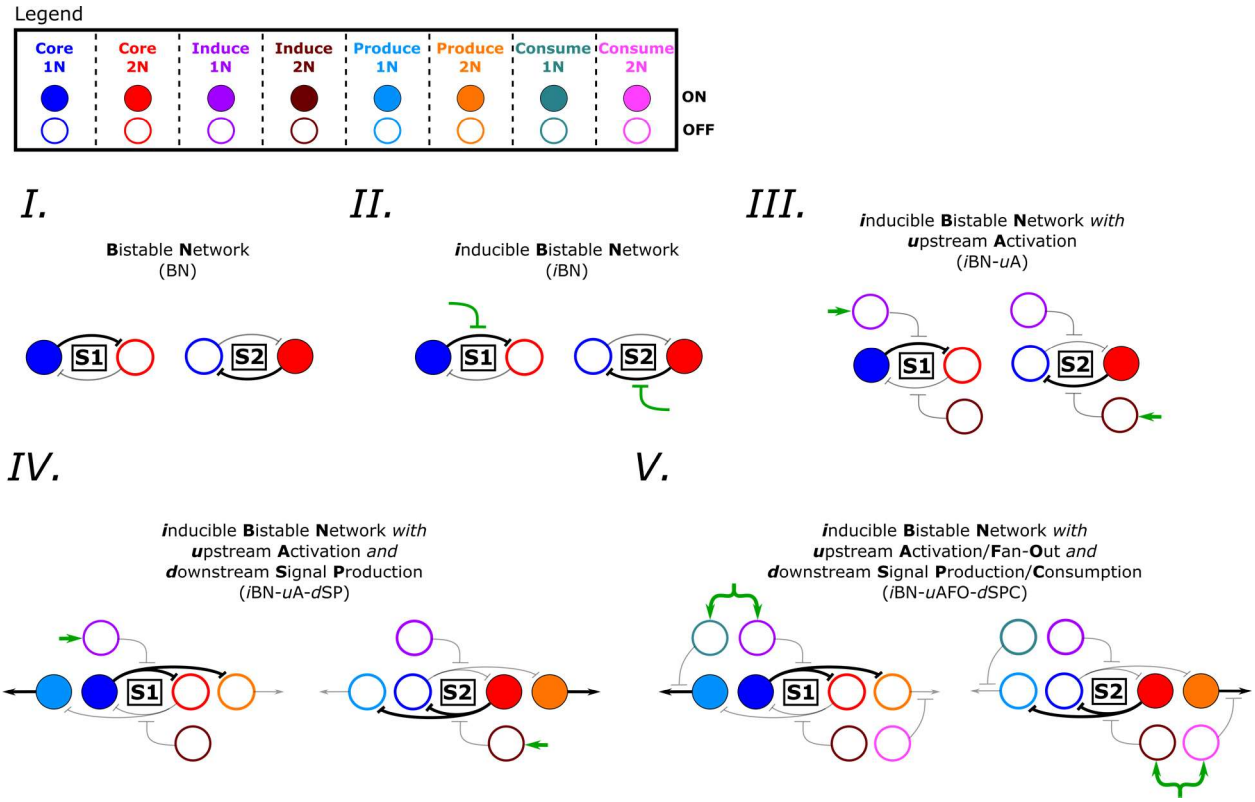

Values of Roman numerals correspond to the main text figure numbers where each of the networks are introduced and characterized. Network interactions shown in green indicate exogenous additions of components.

1.2. Concentrations of reagents during genelet network characterization

***i*BN experiments:**

Component	Concentration
Core 1	100 nM
Core 2	75 nM
dA_1	1000 nM
dA_2	1000 nM
T7 RNAP	4.82 U/µL
RNase H	4.46 x 10^{-3} U/µL
YIPP	1.35 x 10^{-3} U/µL

***i*BN-*u*AFO-*d*SPC experiments:**

Component	Concentration
Core 1	100 nM
Core 2	100 nM
dA_1	1000 nM
blocked dA_2	1000 nM
Induce 1	750 nM
Induce 2	750 nM
Produce 1	35 nM
Produce 2	35 nM
Consume 1	105 nM
Consume 2	105 nM
rO_1 *HP reporter*	100 nM
DFHBI dye	15000 nM
T7 RNAP	9.64 U/µL
RNase H	4.46 x 10^{-3} U/µL
YIPP	1.35 x 10^{-3} U/µL

***i*BN-*u*A experiments:**

Component	Concentration
Core 1	100 nM
Core 2	75 nM
dA_1	1000 nM
dA_2	1000 nM
Induce 1	750 nM
Induce 2	750 nM
T7 RNAP	4.82 U/µL
RNase H	8.92 x 10^{-3} U/µL
YIPP	1.35 x 10^{-3} U/µL

***i*BN-*u*A-*d*SP experiments:**

Component	Concentration
Core 1	100 nM
Core 2	100 nM
dA_1	1000 nM
blocked dA_2	1000 nM
Induce 1	750 nM
Induce 2	750 nM
Produce 1	35 nM
Produce 2	35 nM
rO_1 *reporter*	1000 nM
DFHBI dye	15000 nM
T7 RNAP	9.64 U/µL
RNase H	4.46 x 10^{-3} U/µL
YIPP	1.35 x 10^{-3} U/µL

1.3. Genelet and activator schematics

Some of the longer non-template (nt) strands were ordered with truncated 3' sequences due to synthesis length limitations. Transcription still proceeds through the single-stranded regions at the end of the transcript domains since the template (t) strand is being read[1].

Genelet and activators of the *i*BN (main text Fig. 2):

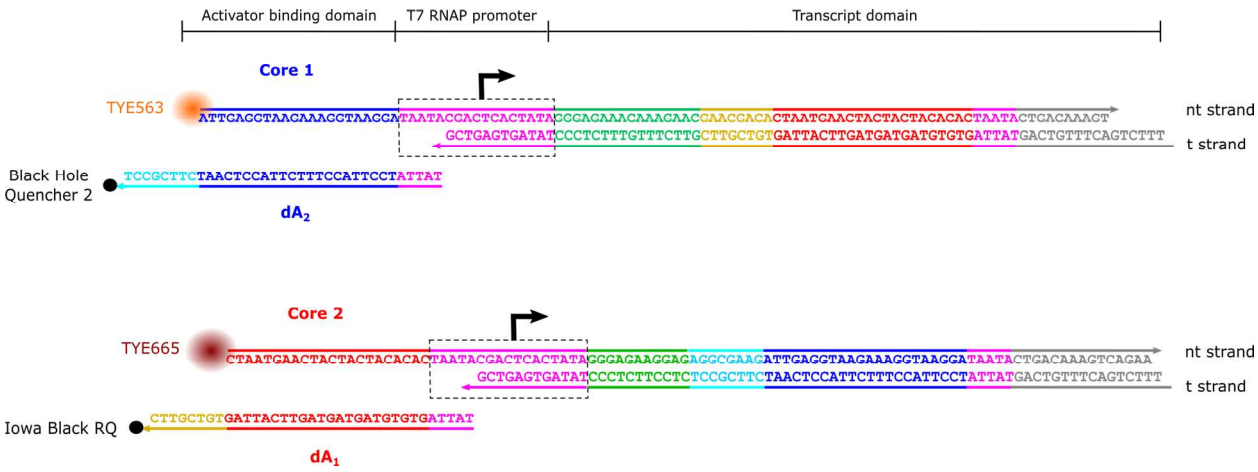

Induce genelets and activators added to the *i*BN to build the *i*BN-*u*A (main text Fig. 3):

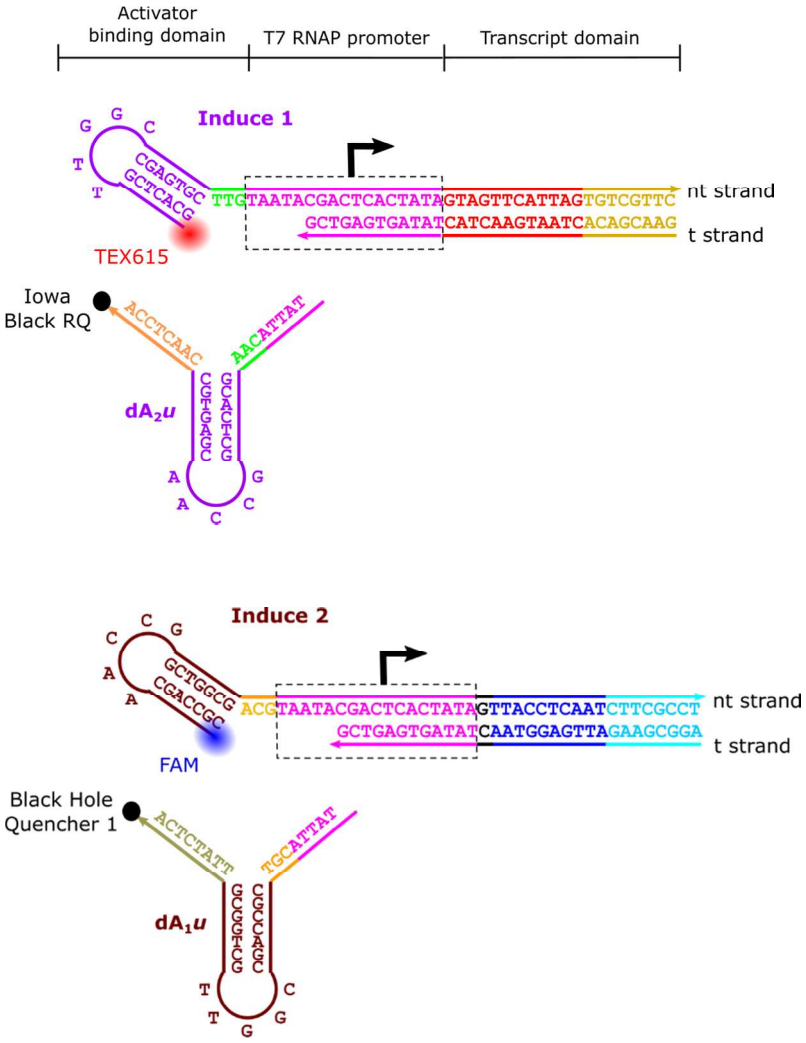

Core 1 with blocked dA_2 and Produce genelets and activators added to the *i*BN-*u*A to build the *i*BN-*u*A-*d*SP (main text Fig. 4):

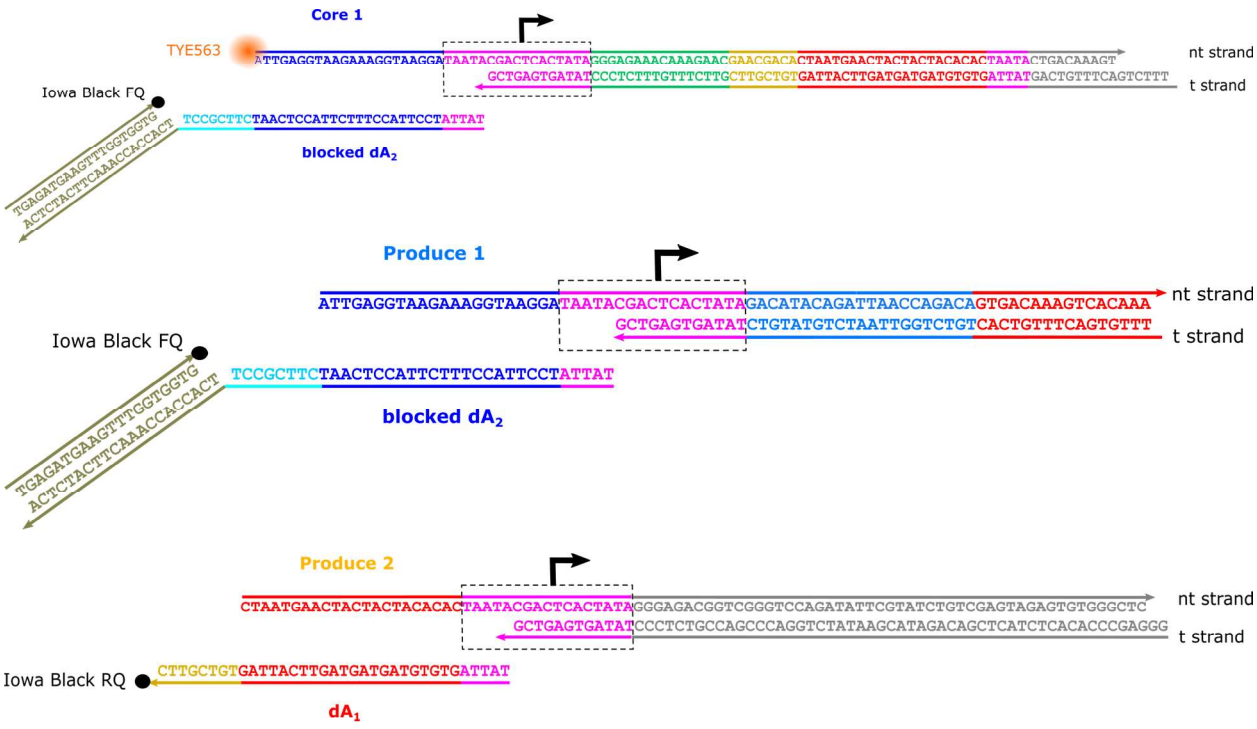

Consume genelets and activators added to the *i*BN-*u*A-*d*SP to build the *i*BN-*u*AFO-*d*SPC (main text Fig. 5):

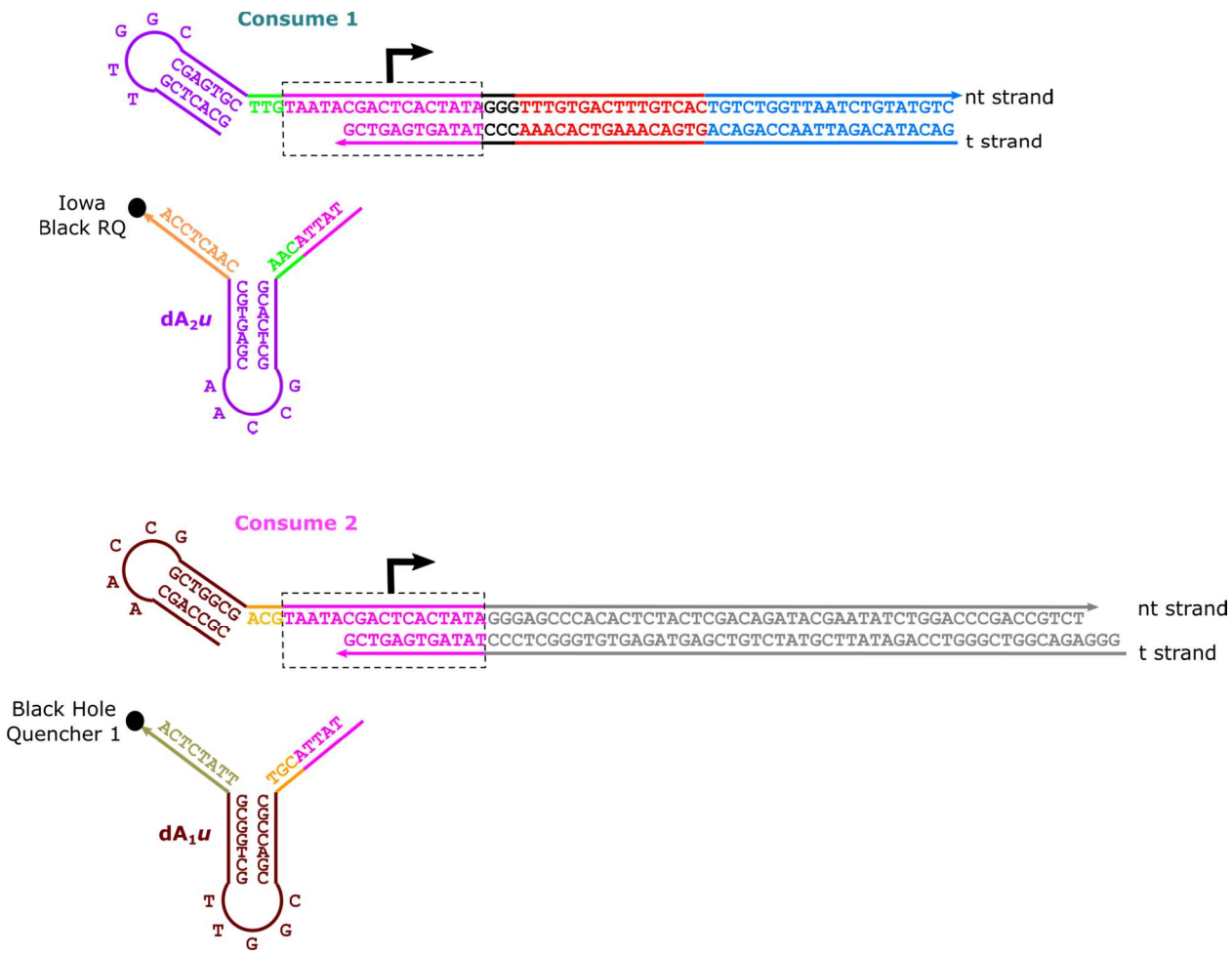

1.4. Repressor and inducer RNA schematics

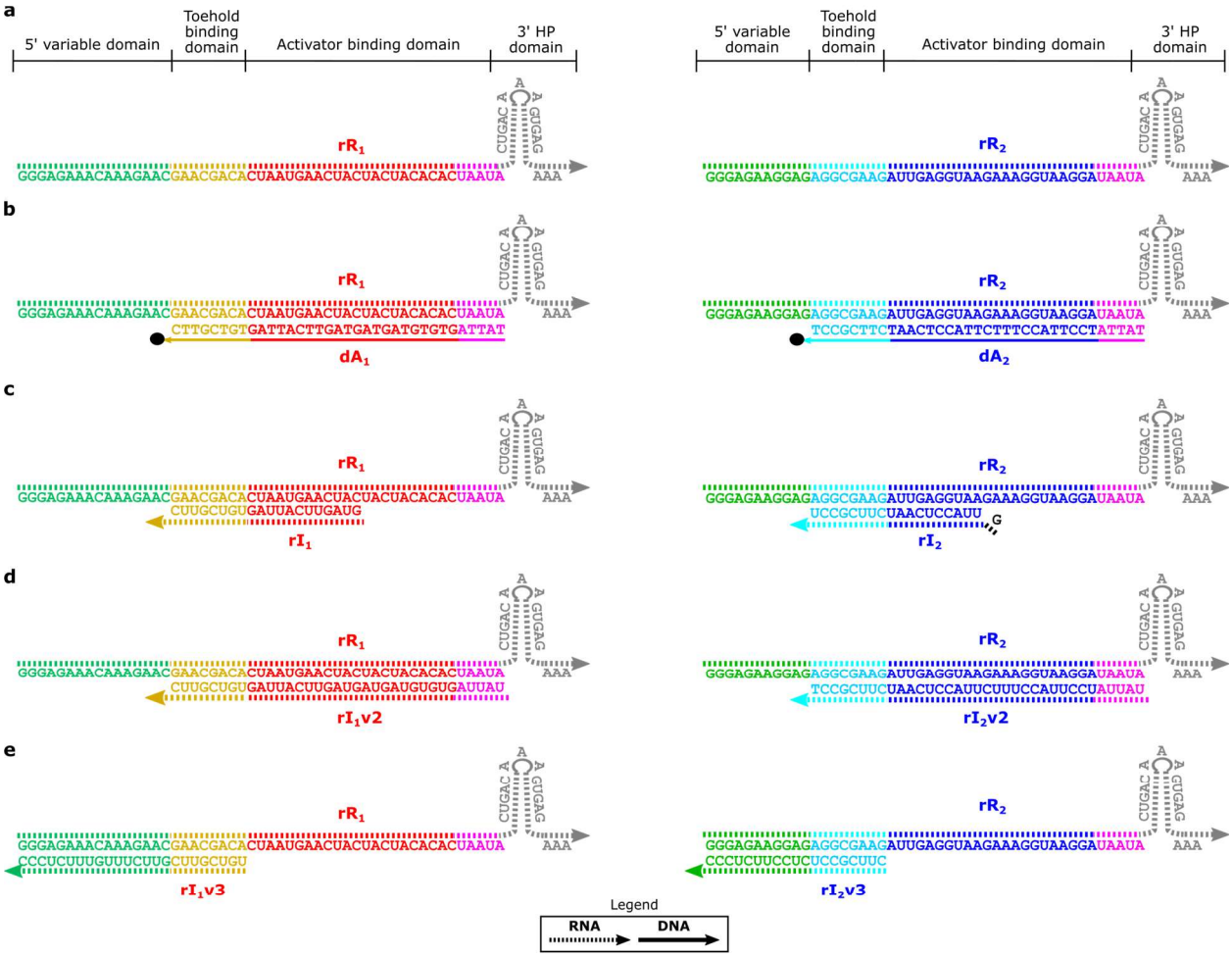

a, The RNA repressors that Core 1 (left) and Core 2 (right) are designed to transcribe.
b, The RNA repressors in (**a**) shown hybridized to their respective DNA activators.
c, The inducer RNAs that switch the state of the bistable network in Fig. 2 of the main text and Supplementary Fig. 4 hybridized to their respective RNA repressors (with partial complementarity to the activator binding domain). The additional 5' guanine on rI_2 was included because a guanine is required at the +1 position of the T7 RNA polymerase promoter sequence for efficient transcription[2], meaning that when this sequence is transcribed it must have a 5' guanine. We included the guanine in the synthesized RNA sequence rI_2 to best characterize its performance as an inducer. The designed terminal 5' base of rI_1 happened to be guanine so an additional 5' guanine base was not needed for transcription of this inducer RNA.
d, Variant 2 inducer RNAs used to switch states in Supplementary Fig. 5 shown hybridized to their respective RNA repressors (with full complementarity to the activator binding domain).
e, Variant 3 inducer RNAs used to switch states in Supplementary Fig. 6 shown hybridized to their respective RNA repressors (with no complementarity to the activator binding domain).

1.5. Synthesized DNA and RNA sequences

Supplementary Table 1 | DNA and RNA oligonucleotides synthesized for this study. Non-template and template strands of genelets are labeled with -nt and -t, respectively. All strands were ordered from Integrated DNA Technologies, Inc (IDT) and the modifications marked with / / are labeled as defined by IDT.

GENELETS	
Core 1-nt	/5TYE563/ATTGAGGTAAGAAAGGTAAGGATAATACGACTCACTATAGGGAGAAACAAAGA ACGAACGACACTAATGAACTACTACTACACACTAATACTGACAAAGT
Core 1-t	5’TTTCTGACTTTGTCAGTATTAGTGTGTAGTAGTAGTTCATTAGTGTCGTTCGTTCTTTGT TTCTCCCTATAGTGAGTCG
Core 2-nt	/5TYE665/CTAATGAACTACTACTACACACTAATACGACTCACTATAGGGAGAAGGAGAGG CGAAGATTGAGGTAAGAAAGGTAAGGATAATACTGACAAAGTCAGAA
Core 2-t	5’TTTCTGACTTTGTCAGTATTATCCTTACCTTTCTTACCTCAATCTTCGCCTCTCCTTCTC CCTATAGTGAGTCG
Induce 1-nt	/5TEX615/GCACTCGTTGGCCGAGTGCTTGTAATACGACTCACTATAGTAGTTCATTAGTG TCGTTC
Induce 1-t	5’GAACGACACTAATGAACTACTATAGTGAGTCG
Induce 2-nt	/56FAM/CGCCAGCAACCGGCTGGCGACGTAATACGACTCACTATAGTTACCTCAATCTTCG CCT
Induce 2-t	5’AGGCGAAGATTGAGGTAACTATAGTGAGTCG
Produce 1-nt	5’ATTGAGGTAAGAAAGGTAAGGATAATACGACTCACTATAGACATACAGATTAACCAGACA GTGACAAAGTCACAAA
Produce 1-t	5’TTTGTGACTTTGTCACTGTCTGGTTAATCTGTATGTCTATAGTGAGTCG
Produce 2-nt	5’CTAATGAACTACTACTACACACTAATACGACTCACTATAGGGAGACGGTCGGGTCCAGAT ATTCGTATCTGTCGAGTAGAGTGTGGGCTC
Produce 2-t	5’GGGAGCCCACACTCTACTCGACAGATACGAATATCTGGACCCGACCGTCTCCCTATAGTG AGTCG
Consume 1-nt	GCACTCGTTGGCCGAGTGCTTGTAATACGACTCACTATAGGGTTTGTGACTTTGTCACTGTC TGGTTAATCTGTATGTC
Consume 1-t	GACATACAGATTAACCAGACAGTGACAAAGTCACAAACCCTATAGTGAGTCG
Consume 2-nt	CGCCAGCAACCGGCTGGCGACGTAATACGACTCACTATAGGGAGCCCACACTCTACTCGACA GATACGAATATCTGGACCCGACCGTCT
Consume 2-t	GGGAGACGGTCGGGTCCAGATATTCGTATCTGTCGAGTAGAGTGTGGGCTCCCTATAGTGAG TCG
additional KWW 1-nt	/56FAM/AACGACTGAGACTGAAAGAACATAATACGACTCACTATAGGTTTCTGACTTTGTC AGTATTAGTGTGTAGTAGTAGTTCATTAGTGTCGTTCGTTCTTTG
additional KWW 1- t	5’GGGAGAAACAAAGAACGAACGACACTAATGAACTACTACTACACACTAA TACTGACAAAGTCAGAAACCTATAGTGAGTCG
additional KWW 2-nt	/5TexRdXN/AAATCCACCAACTCACTCACCATAATACGACTCACTATAGGTTTCTGACTTT GTCAGTATTATCCTTACCTTTCTTACCTCAATCTTCGCCTCTCCTTCT
additional KWW 2-t	5’GGGAGAAGGAGAGGCGAAGATTGAGGTAAGAAAGGTAAGGATAATACTG ACAAAGTCAGAAACCTATAGTGAGTCG

prototype HPC 1-nt	/5TEX615/GCACTCGTTGGCCGAGTGCTTGTAATACGACTCACTATAGGTGTCGTTCGTTC TTTGTTTCTCCC
prototype HPC 1-t	5’GGGAGAAACAAAGAACGAACGACACCTATAGTGAGTCG
prototype HPC 2-nt	/56FAM/CGCCAGCAACCGGCTGGCGACGTAATACGACTCACTATAGGCTTCGCCTCTCCTT CTCCC
prototype HPC 2-t	5’GGGAGAAGGAGAGGCGAAGCCTATAGTGAGTCG
ACTIVATORS	
dA_1	5’TATTAGTGTGTAGTAGTAGTTCATTAGTGTCGTTC/3IAbRQSp/
dA_2	5’TATTATCCTTACCTTTCTTACCTCAATCTTCGCCT/3BHQ_2/
dA_1-nTH	5’TATTAGTGTGTAGTAGTAGTTCATTAG
dA_2-nTH	5’TATTATCCTTACCTTTCTTACCTCAAT
dA_1u	5’TATTACGTCGCCAGCCGGTTGCTGGCGTTATCTCA/3BHQ_1/
dA_2u	5’TATTACAAGCACTCGGCCAACGAGTGCCAACTCCA/3IAbRQSp/
dA_1u2	5’TATTACGTCGCCAGCCGGTTGCTGGCGCAACTCCA/3BHQ_1/
dA_1u3	5’TATTACGTCGCCAGCCGGTTGCTGGCGTCCAGCTC/3BHQ_1/
extended dA_2	TATTATCCTTACCTTTCTTACCTCAATCTTCGCCTTCACCACCAAACTTCATCTCA
quenched blocker	TGAGATGAAGTTTGGTGGTG/3IABkFQ/
KWW dA_1u	5’TATTATGGTGAGTGAGTTGGTGGATTTGTGGAGTG/3IAbRQSp/
KWW dA_2u	5’TATTATGTTCTTTCAGTCTCAGTCGTTATTGTGCT/3BHQ_1/
DNA REPRESSORS	
dR_1s	5’GAACGACACTAATGAACTACTACTACACACTAATA
dR_2s	5’AGGCGAAGATTGAGGTAAGAAAGGTAAGGATAATA
dR_1u	5’TGAGATAACGCCAGCAACCGGCTGGCGACGTAATA
dR_2u	5’TGGAGTTGGCACTCGTTGGCCGAGTGCTTGTAATA
dR_1u2	5’TGGAGTTGCGCCAGCAACCGGCTGGCGACGTAATA
dR_1u3	5’GAGCTGGACGCCAGCAACCGGCTGGCGACGTAATA
RNAS	
rR_1s	5’GAACGACACUAAUGAACUACUACUACACACUAAUA
rR_2s	5’AGGCGAAGAUUGAGGUAAGAAAGGUAAGGAUAAUA
rI_1	5’GUAGUUCAUUAGUGUCGUUC
rI_2	5’GUUACCUCAAUCUUCGCCU
rI_1v2	5’UAUUAGUGUGUAGUAGUAGUUCAUUAGUGUCGUUC
rI_2v2	5’UAUUAUCCUUACCUUUCUUACCUCAAUCUUCGCCU
rI_1v3	5’GGUGUCGUUCGUUCUUUGUUUCUCCC
rI_2v3	5’CUUCGCCUCUCCUUCUCCC

REPORTER COMPLEXES	
rO$_1$_reporter_F	5'GTCACTGTCTGGTTAATCTGTATGTC/3TEX615/
rO$_1$_reporter_Q	/5IAbRQ/GACATACAGATTAACCAGACA
rO$_1$_HP_reporter	/5TEX615/TGTCTGGTTAATCTGTTTAACC/3IAbRQSp/
dO$_1$	5'GACATACAGATTAACCAGACAGTGAC

2. Bistability of the mutually repressive genelet network

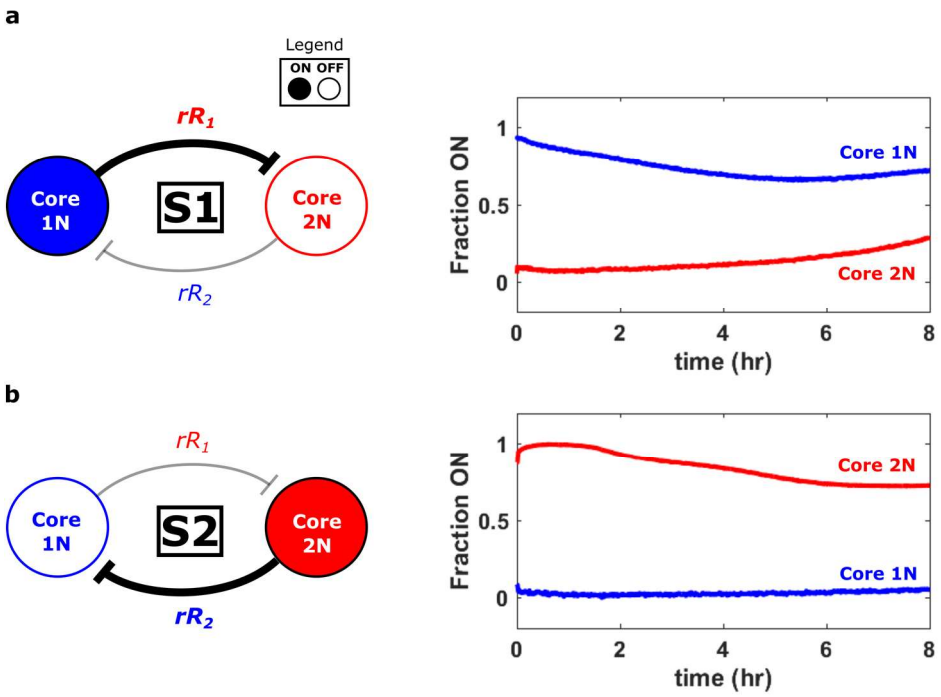

Supplementary Figure 1 | The mutually repressive genelet network is bistable[3]. **a**,**b**, Normalized activation levels of network nodes after initialization in S1 (**a**) or S2 (**b**). In each case the network remained in the state it was initialized in for at least 8 hours. Experiments were conducted as described in the Methods of the main text for the *i*BN.

3. Mechanisms of switching between the states of a bistable mutually repressive genelet network with RNA signals

A double negative feedback network in which two genetic elements mutually repress one another is a fundamental genetic network motif[4]. Given the correct parameters (gene activator and repressor expression/degradation rates), mutually repressive gene networks can exhibit bistability[5]. In a bistable mutually repressive network, gene expression levels will be attracted to one of two stable steady states where only one of the genes has a high expression level. Which stable steady state the circuit arrives at is dependent on the initial gene expression levels. If the expression levels of the genes in the network are perturbed slightly, the network will be drawn back to the state it was in prior to the perturbation but if the expression levels are changed enough, the network can be pushed to switch to the other stable state[5]. The network can be induced to switch states by either changing the expression levels of the genes in the network directly (adding activators or repressors of expression) or indirectly (adding molecules that change the *activity* of the activators or repressors of expression).

We sought to develop a mechanism to switch the state of the bistable genelet network (Fig. 1, main text) using an RNA molecule as a trigger. Supplementary Fig. 2a shows two ways that an RNA molecule could induce the bistable network to switch from S1 to S2. Mechanism 1 switches the state of the network by repressing the transcription of the node that is currently on. When the bistable network is in S1, a switch *via* mechanism 1 could be achieved by the addition of rR_2. rR_2 would turn off Core 1N which would allow Core 2N to turn on, switching the network to S2. Mechanism 2 switches the state of the network using an inducer RNA (shown as rI_1 in Supplementary Fig. 2a) that binds to the currently expressed repressor, preventing that repressor from acting downstream. When the network is in S1, such an inhibition of repressor rR_1 would allow Core 2N to turn on which would lead to the repression of Core 1N.

To investigate the relative speeds and efficiencies of the first two mechanisms for switching the state of the network, we simulated the responses of the bistable network to the addition of the RNA switching signals described above (rR_2 or rI_1). Our simulations were based on simple mass action kinetic models previously developed for genelet based circuits[6–8] (equations (1)-(6)).

The results of the simulations showed that both the addition of rR_2 or rI_1 could drive the network to switch to S2 but the switch completed much faster when rI_1 was added than when rR_2 was added (Supplementary Fig. 2b). The simulation results showed a long delay between the time rR_2 was added and the time Core 2N began to turn on for the simulation of switching *via* mechanism 1. This delay is a result of the slow degradation of rR_1 that accumulated while the network was in S1 and must be removed before Core 2N can begin to turn on. The simulations show that switching the states of the network by adding rI_1 (mechanism 2) does not result in such a delay since rI_1 immediately inactivates any excess rR_1 in the network by binding to it.

To understand the effects of the repressor and inducer concentrations on switching dynamics, we also simulated the response of the bistable network to different concentrations of either rR_2 or rI_1. For mechanism 1, the simulations showed that the switching threshold for rR_2 is between 2 μM and 3 μM and that the time required to change states is not dependent on the concentration of rR_2 added (Supplementary Fig. 2c). Instead, because rR_1 must be degraded before the state can change, the switching time is determined by the degradation rate of rR_1 and there is a long delay between the

addition of rR_2 and the completion of the state change regardless of the concentration of rR_2 used. For mechanism 2, the simulations showed that the switching threshold for rI_1 is between 3 µM and 4 µM and that the time required to change states is also not highly dependent on the concentration of rI_1 added (Supplementary Fig. 2d).

To validate the predictions made in these simulations, we experimentally tested whether switching the network from S1 to S2 *via* mechanism 1 would result in the predicted delay in Core 2N turning on. This experiment showed a significant delay in Core 2N turning on, in line with our simulation predictions (Supplementary Fig. 3). Based on these results, we selected mechanism 2 as the mechanism for switching the state of the network.

$$(1)\ \frac{d[rR_i]}{dt} = -k_{GAI}[\text{Core j:}dA_i][rR_i] - k_{AI}[dA_i][rR_i] - k_{IIC}[rI_i][rR_i] + k_P[\text{Core i:}dA_j]$$

$$(2)\ \frac{d[dA_i]}{dt} = k_D[dA_i{:}rR_i] - k_{GA}[\text{Core j}][dA_i] - k_{AI}[dA_i][rR_i]$$

$$(3)\ \frac{d[\text{Core i:}dA_j]}{dt} = k_{GA}[\text{Core i}][dA_j] - k_{GAI}[\text{Core i:}dA_j][rR_j]$$

$$(4)\ \frac{d[rI_i]}{dt} = -k_{IIC}[rI_i][rR_i]$$

Mass balances are used to infer the concentrations of some of species in equations (1)-(4) over time:

$$(5)[dA_i{:}rR_i] = [dA_i]_{TOTAL} - [dA_i] - [\text{Core j:}dA_i]$$

$$(6)[\text{Core i}] = [\text{Core i}]_{TOTAL} - [\text{Core i:}dA_j]$$

In equations (1)-(6) if $i=1$ then $j=2$ and if $i=2$ then $j=1$

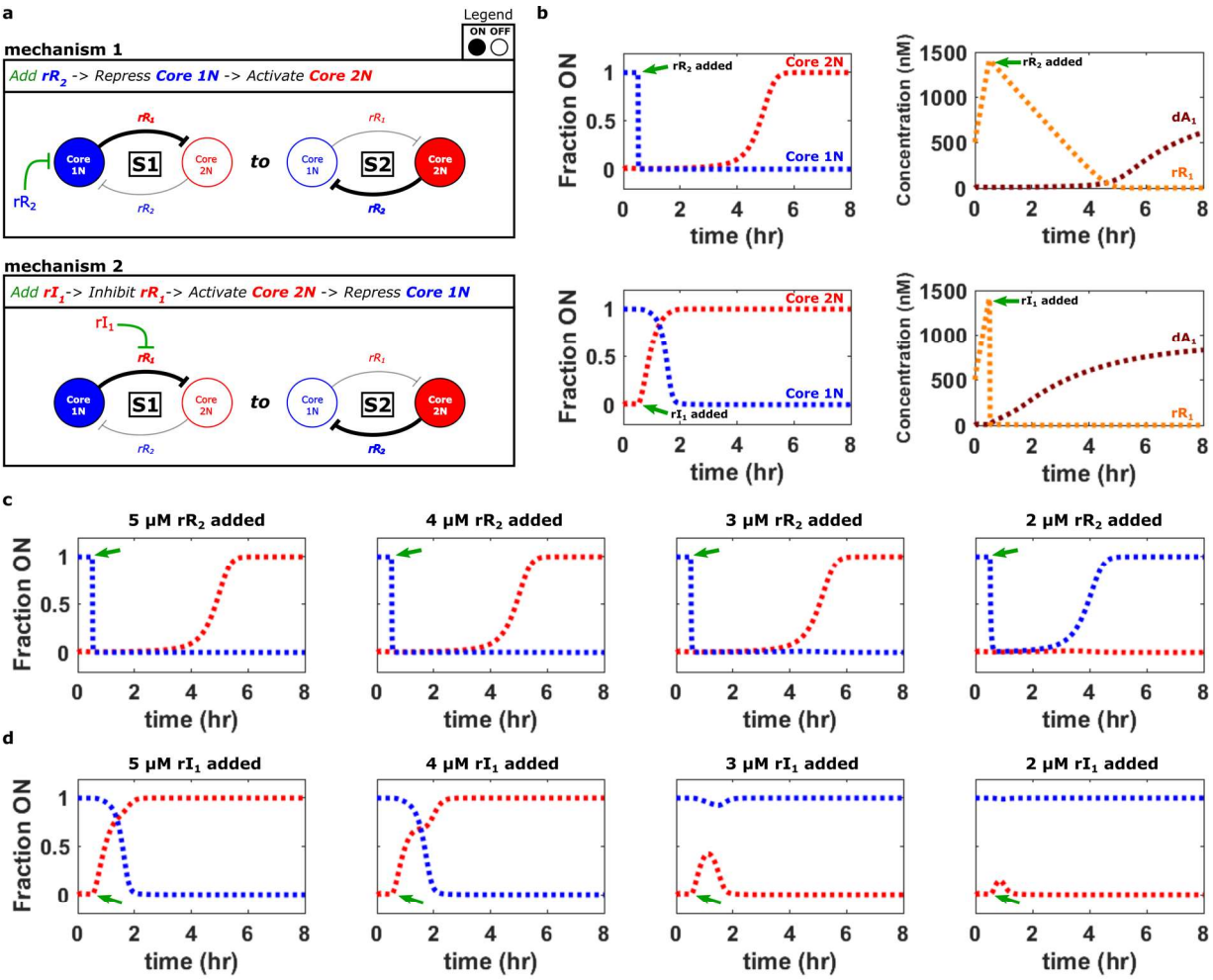

Supplementary Figure 2 | Comparison of the dynamics of two mechanisms for switching the state of the bistable network with RNA species as predicted by a simple kinetic model. a, Schematics of the mechanisms by which an RNA species could switch the state of the bistable network from S1 to S2. **b**, Predictions of the kinetic model presented in equations (1)-(6) of the dynamics of switching for mechanism 1 (top) and mechanism 2 (bottom). 10 μM of rR_2 or rI_1 was introduced in the simulations after 30 minutes (green arrows in plots). **c**,**d**, Predictions of the kinetic model presented in equations (1)-(6) for switching with different concentrations of rR_2 (mechanism 1) (**c**) or different concentrations of rI_1 (mechanism 2) (**d**). The RNA species were introduced in the simulations after 30 minutes (green arrows in plots) to the final concentrations shown above the plots. For simulations, [genelets]: 100 nM each, [activators]: 1000 nM each, [rR_1]: 1500 nM initially, $k_P = 6 \times 10^{-3}\ s^{-1}$, $k_D = 1 \times 10^{-4}\ s^{-1}$, k_{GA}, k_{GAI}, k_{AI} $k_{IIC} = 1 \times 10^{4}\ M^{-1}\ s^{-1}$.

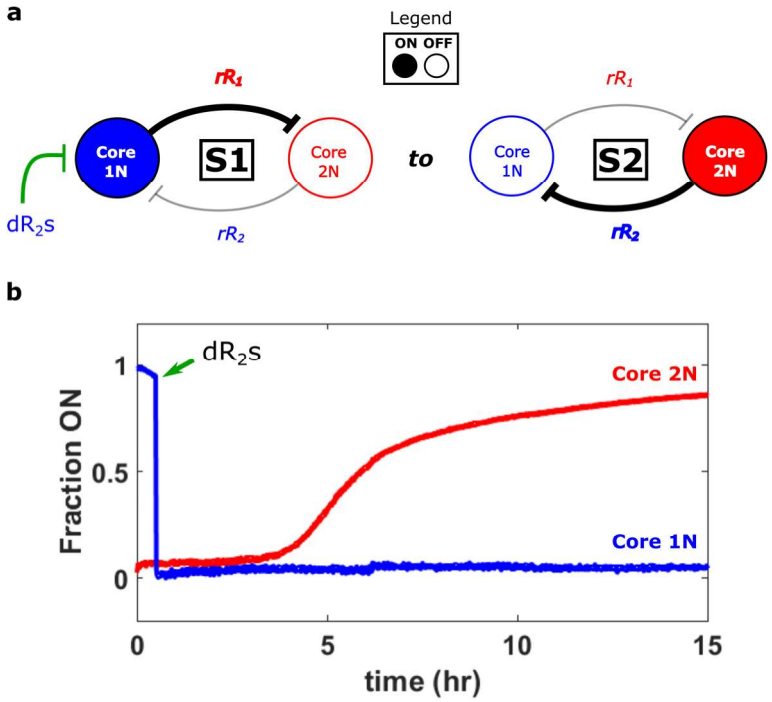

Supplementary Figure 3 | Switching the bistable network from S1 to S2 by turning Core 1N off with the DNA repressor dR_2s (similar to mechanism 1, Supplementary Fig. 2; sequence in Supplementary Table 1). **a**, The mechanism by which dR_2s switches the state of the network. dR_2s should permanently repress Core 1N because it is not degraded by RNase H. This strand was used to emulate the effect of adding a high concentration of rR_2, the RNA repressor of Core 1N. **b**, Normalized activation levels of network nodes during a switch from S1 to S2 *via* addition of dR_2s. The network was initialized in S1 and dR_2s was added to a final concentration of 1.5 μM after 30 minutes in S1. Reactions were otherwise conducted as described in the Methods of the main text for the *i*BN. A long delay was observed after Core 1N was turned off before Core 2N begins to turn on as predicted by our simulations (Supplementary Fig. 2b).

4. Switching states with different inducer RNA designs

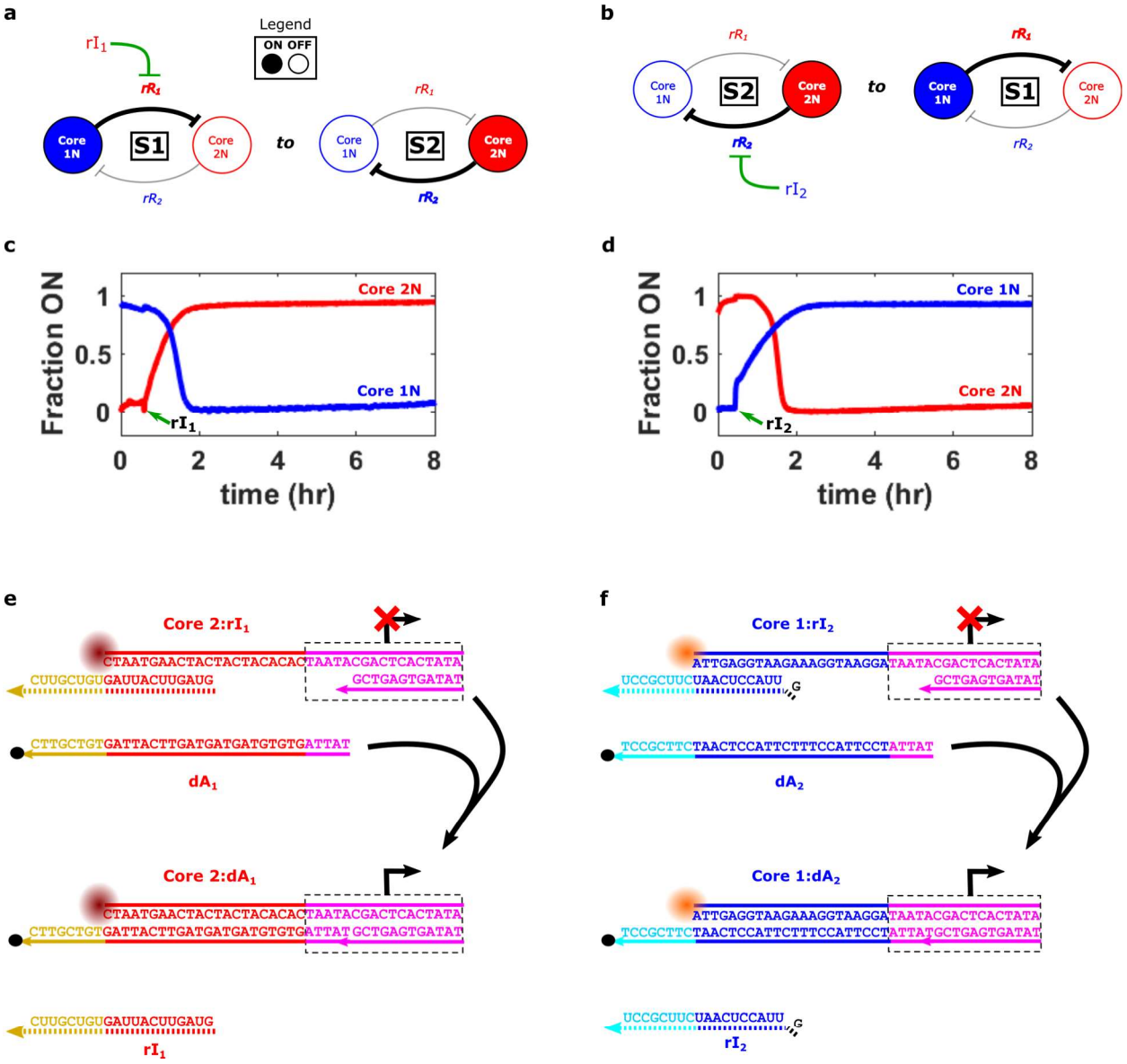

Supplementary Figure 4 | Switching the state of the bistable network with inducer RNAs rI_1 and rI_2 (Supplementary Section 1.4). **a**,**b**, The mechanism for switching the state of the network from S1 to S2 with rI_1 (**a**) and from S2 to S1 with rI_2 (**b**). **c**,**d**, Normalized activation levels of network nodes during a switch from S1 to S2 *via* addition of rI_1 (**c**) or from S2 to S1 *via* addition of rI_2 (**d**). rI_1 or rI_2 was added after 30 minutes to a final concentration of 5 μM (green arrows in plots). Switching states with these inducer RNA variants yield switching kinetics similar to those predicted by our simulations (Supplementary Fig. 2b). Reactions were conducted as described in the Methods of the main text for the *i*BN. **e**, A potential complex that could form through an undesired hybridization reaction between rI_1 and Core 2 (top). However, this undesired Core 2:rI_1 species still has 15 bases unbound on the activator binding domain of Core 2, which could allow dA_1 to bind and displace rI_1 in the depicted reaction. **f**, A potential complex that could form through an undesired hybridization reaction between rI_2 and Core 1 (top). The Core 1:rI_2 species still has 17 bases unbound on the activator binding domain of Core 1 which could allow dA_2 to bind and displace rI_2.

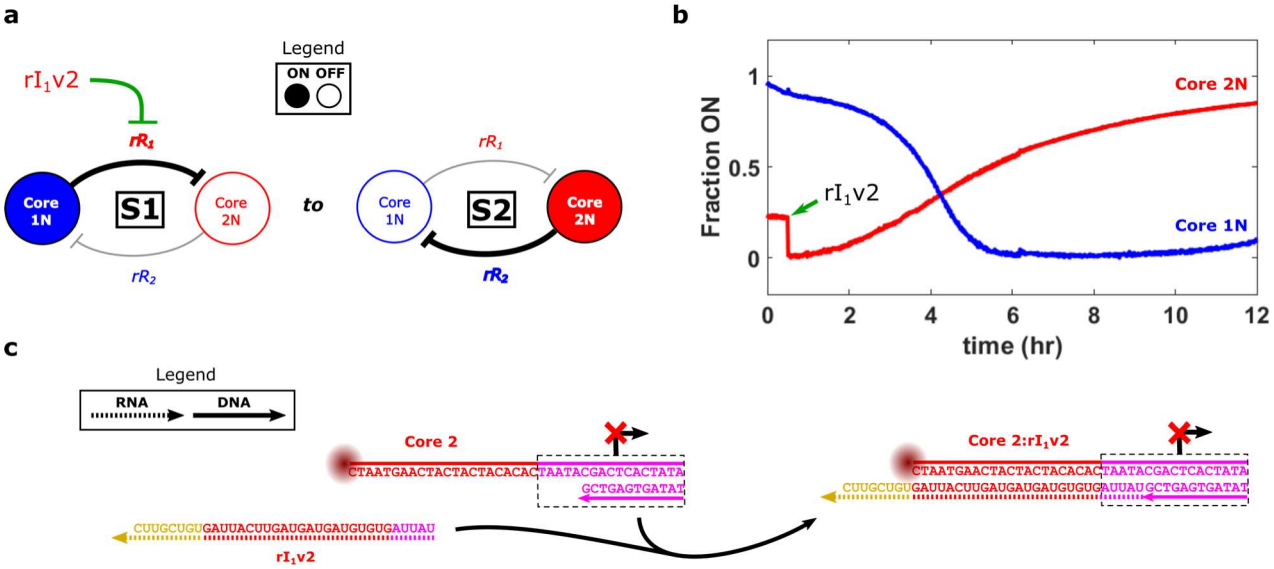

Supplementary Figure 5 | Switching from S1 to S2 *via* addition of rI$_1$v2 (Supplementary Section 1.4). **a**, The mechanism by which rI$_1$v2 switches the network from S1 to S2. **b**, Normalized activation levels of network nodes during a switch from S1 to S2 *via* addition of rI$_1$v2. rI$_1$v2 was added after 30 minutes to a final concentration of 5 μM. Both Core 2N turning on and Core 1N turning off were slow in response to rI$_1$v2. **c**, A potential undesired hybridization reaction between rI$_1$v2 and Core 2 that could be a factor in the slow state change. rI$_1$v2 has the same sequence as dA$_1$ so rI$_1$v2 could bind the activator binding domain of Core 2. The structure of the resulting complex would prevent dA$_1$ from binding Core 2 while rI$_1$v2 is bound to it. And since rI$_1$v2 is RNA, transcription from Core 2 will not occur when rI$_1$v2 is bound. rI$_1$v2 thus undesirably acts as a repressor of Core 2N. Reactions were conducted as described in the Methods of the main text for the *i*BN.

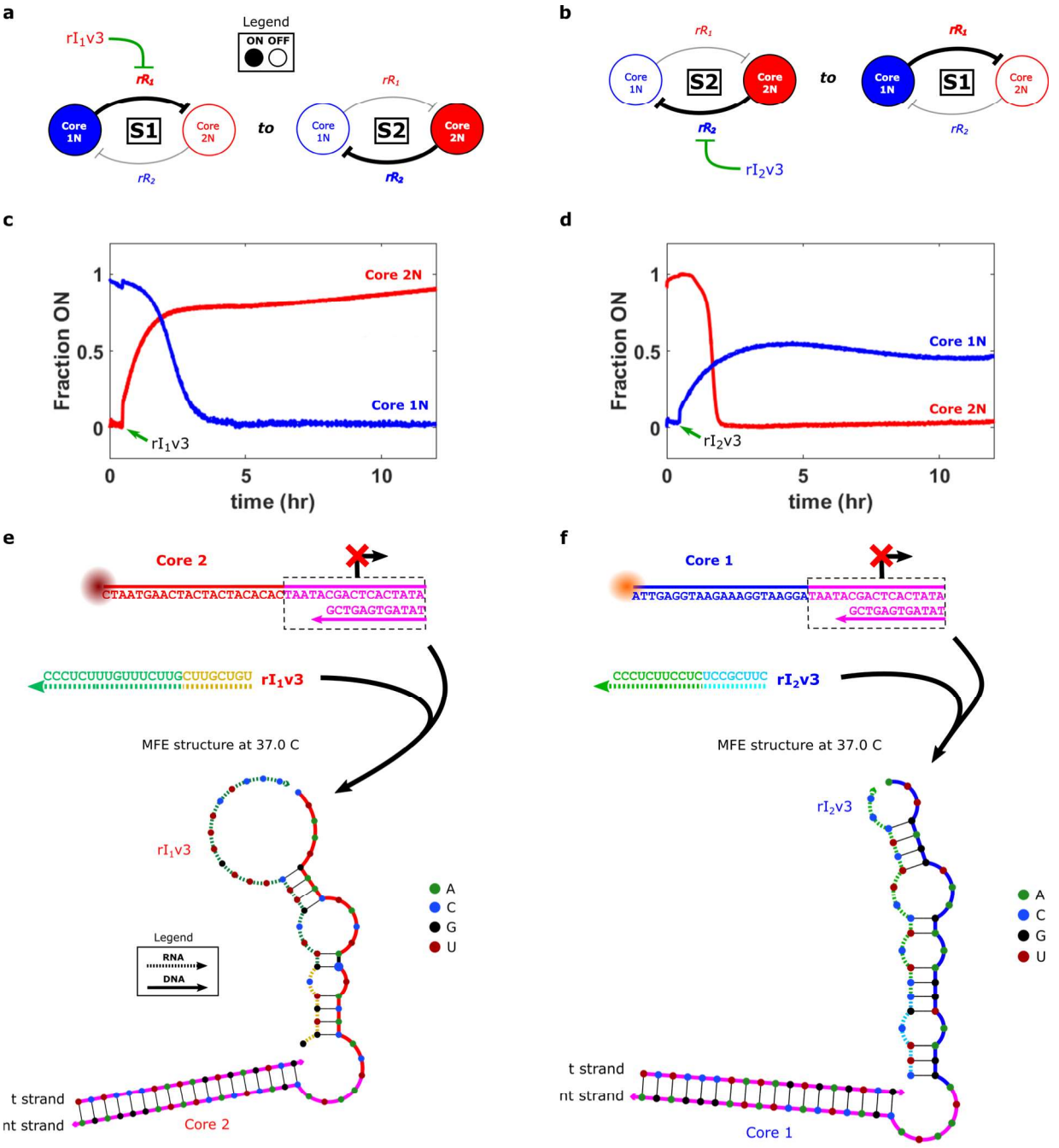

Supplementary Figure 6 | Switching the state of the bistable network in response to rI_1v3 and rI_2v3 (Supplementary Section 1.4). **a**,**b**, The mechanism for switching the state of the network from S1 to S2 with rI_1v3 (**a**) and from S2 to S1 with rI_2v3 (**b**). **c**,**d**, Normalized activation levels of network nodes during a switch from S1 to S2 *via* addition of rI_1v3 (**c**) or from S2 to S1 *via* addition of rI_2v3 (**d**). rI_1v3 or rI_2v3 was added after 30 minutes to a final concentration of 10 µM (green arrows in plots). Reactions were conducted as described in the Methods of the main text for the *i*BN. **e**, The lowest free energy secondary structure of rI_1v3 bound to the activator binding domain of Core 2, as predicted by NUPACK[9] (Supplementary Section 8.2). **f**, The lowest free energy structure of rI_2v3 bound to the activator binding domain of Core 1, as predicted by NUPACK. These undesired interactions between these inducer RNA variants and the genelets could prevent the activators from binding to the genelets, resulting in the incomplete switching behavior or the slower switching kinetics than observed in our simulations (Supplementary Fig. 2b).

5. Additional experiments with the *i*BN

5.1. Characterization of switching states

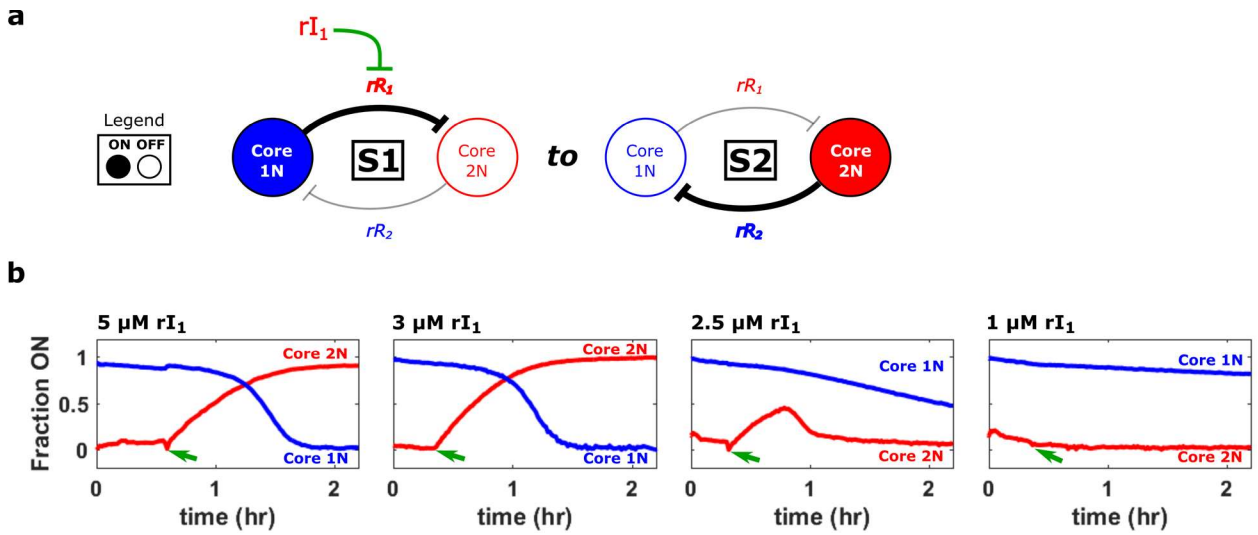

Supplementary Figure 7 | The dynamics of the *i*BN initialized in S1 in response to different concentrations of rI_1 added after 30 minutes. a, The mechanism for switching the state of the *i*BN from S1 to S2 with rI_1. **b**, Normalized activation levels of network nodes during switches from S1 to S2 *via* addition of different amounts of rI_1. rI_1 was added after about 30 minutes to the final concentrations shown above the plots. Green arrows indicate when rI_1 was added in each case. Reactions were otherwise conducted as described in the Methods of the main text for the *i*BN. Adding less than 3 μM rI_1 does not switch the network to S2 and adding 3 μM or more rI_1 results in similar switching kinetics.

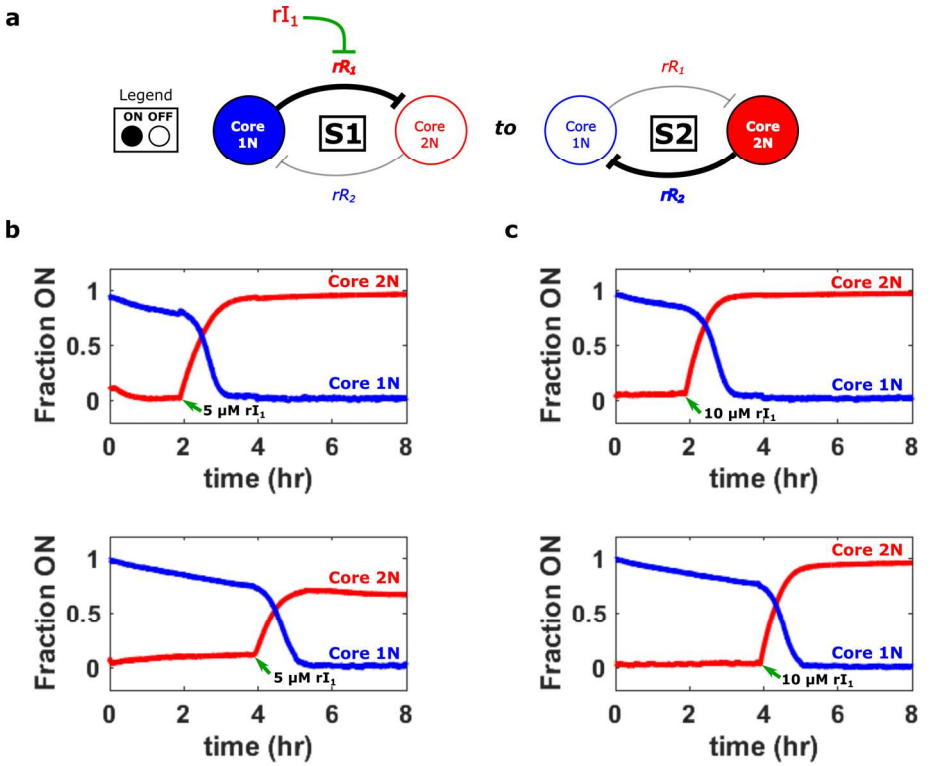

Supplementary Figure 8 | The dynamics of the *i*BN initialized in S1 in response to different amounts of rI_1 at different times. **a**, The mechanism for switching from S1 to S2 with rI_1. **b**,**c**, Normalized activation levels of network nodes during switches from S1 to S2 *via* addition of rI_1 to a final concentration of 5 μM (**b**) or 10 μM (**c**) after the network spent 2 hours (top plots) or 4 hours (bottom plot) in S1. In (**b**), 5 μM rI_1 was enough inducer to switch the network from 100% Core 1N ON to 100% Core 2N ON after 2 hours in S1. After 4 hours in S1, 5 μM rI_1 only resulted in ~70% of Core 2N ON. In (**c**), 10 μM rI_1 was enough to completely switch states after 2 or 4 hours in S1. This observation suggest that longer times in S1 result in higher concentrations of rR_1 which increases the amount of rI_1 required to switch states. Reactions were conducted as described in the Methods of the main text for the *i*BN.

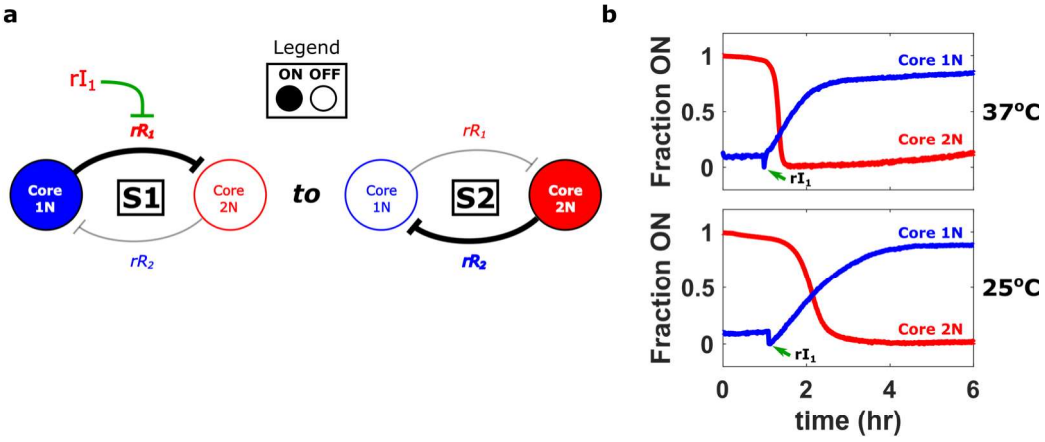

Supplementary Figure 9 | Switching the *i*BN from S1 to S2 at room temperature. **a**, The mechanism for changing the *i*BN from S1 to S2. **b**, Normalized activation levels of network nodes during a switch from S1 to S2 at 37°C (top) or at 25°C (bottom). 10 μM of rI_1 was added after 1 hour in S1 for both reactions (green arrows in plots). Reactions conducted as described in the Methods of the main for the *i*BN with *[T7 RNAP]* = 3.57 U/μL and *[RNase H]* = 0.018 U/μL.

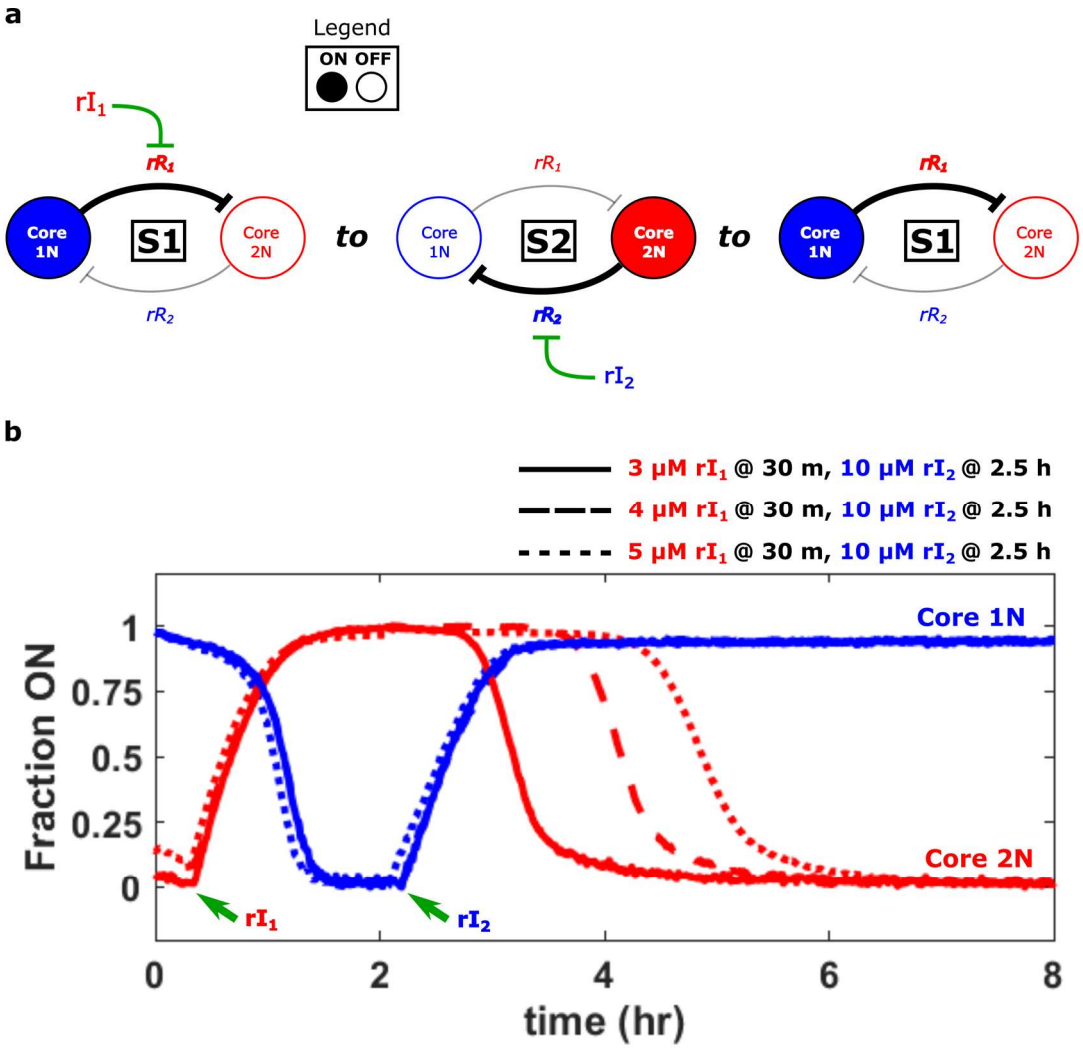

Supplementary Figure 10 | The timing of a second induced state change of the *i*BN depends on the concentration of the inducer RNA that directs the first switch. **a**, The mechanism for switching the *i*BN from S1 to S2 to S1. **b**, Normalized activation levels of network nodes during switches from S1 to S2 to S1. rI_1 was added to a final concentration of 3 µM (solid lines), 4 µM (dashed lines), or 5 µM (dotted lines) after 30 minutes and rI_2 was added at 2.5 hours to a final concentration of 10 µM in all three experiments. The data for the experiment where 3 µM rI_1 was added to switch from S1 to S2 is also presented in Fig. 2d of the main text. Reactions were conducted as described in the Methods of the main text for the *i*BN. The higher the concentration of rI_1 used to induce the first state change, the longer the delay before the network switches states after the addition of rI_2. This delay is due to excess rI_1 still present in the network after the first state change that must all be removed before the second state change can begin.

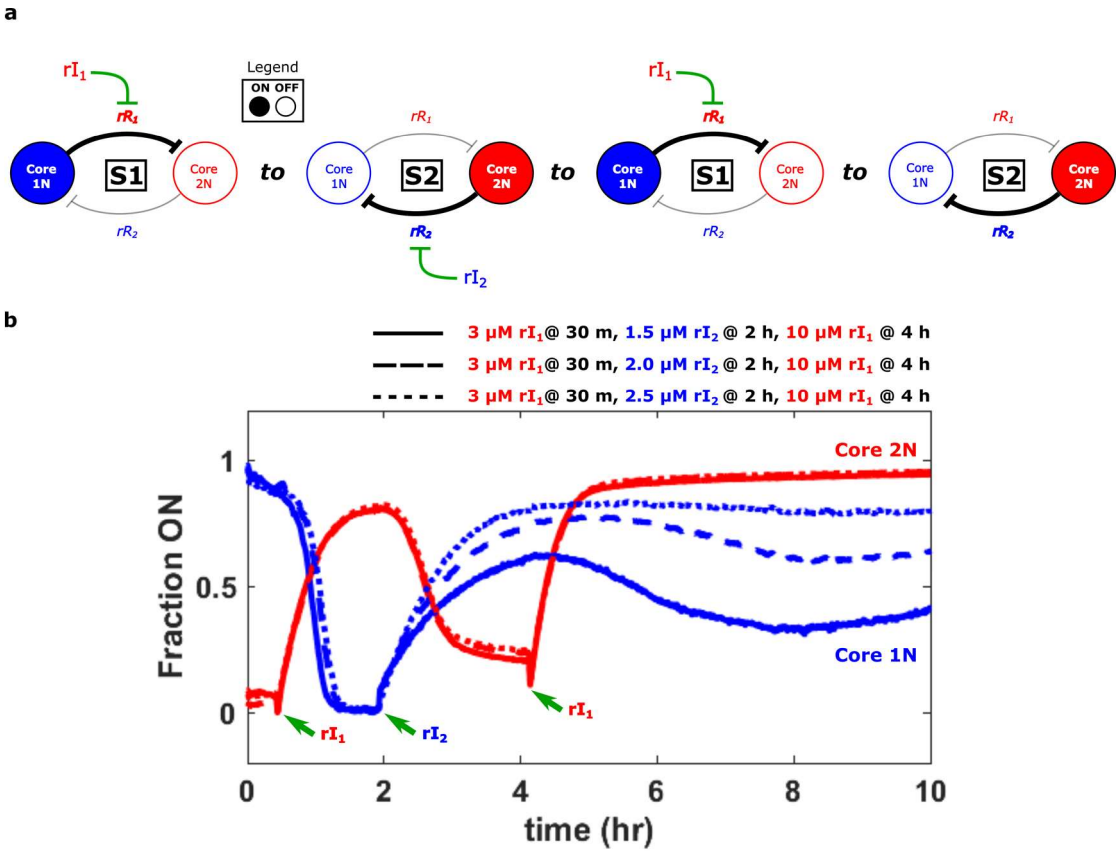

Supplementary Figure 11 | An attempt to change the state of the *i*BN three times. a, The mechanism for switching the *i*BN from S1 to S2 to S1 to S2 *via* addition of inducer RNA signals. **b**, Normalized activation levels of network nodes during switches from S1 to S2 to S1 to S2 when inducer RNAs are added at different concentrations and times. rI_1 was added to a final concentration of 3 μM after 30 minutes and rI_2 was added to a final concentration of 1.5 μM (solid lines), 2 μM (dashed lines), or 2.5 μM (dotted lines) after 2 hours, rI_1 was added again at 4 hours to a final concentration of 10 μM in all three experiments. Reactions were conducted as described in the Methods of the main text for the *i*BN with *[T7 RNAP]* = 5 U/μL, *[RNase H]* = 0.0089 U/μL. The first two state changes work well but during the final state change Core 2N is not able to completely turn Core 1N back off.

5.2. Limitations in batch operation times

The results in Supplementary Fig. 11 show that an attempted third sequential state change does not fully complete. In the third state change, we observed that Core 2N is able to turn on but cannot then completely shut Core 1N off to finish the state change. Such a phenomenon illustrates how genelet circuits in general and the bistable switch circuits studied in this work in particular have a finite lifetime over which they function well in a closed system. Understanding how this lifetime is determined and how it might be increased is central to exploiting the dynamic behaviors of these networks.

The switching of genelets between off and on states relies in part on the digestion of RNA repressor signals. Previous genelet studies have suggested that incompletely digested RNA waste products may build up over time, and that these RNA fragments might affect circuit function[7,10,11]. These interfering RNA products can arise, as an example, because RNase H can only cleave RNA at sites in an RNA-DNA duplex that are greater than 5-7 bases from the 3' end of the DNA strand in the duplex[12]. As a result, short RNA strands that are complementary to the 3' repression toeholds of the activators could accumulate over the course of an experiment[10]. Such fragments could reversibly bind to the repression toeholds of the genelet activators, competing with repressors for binding on the activators bound to a genelet-activator complex. If the concentration of these fragments for a particular genelet was large enough, the genelets could remain on even when repressors are present. Such RNA waste build-up could possibly explain why Core 2N was not able to completely shut Core 1N off during a third state change (Supplementary Fig. 11). Other RNases besides RNase H have been tested in genelet circuits in an attempt to prevent the accumulation of RNA waste products that impede circuit function. However, the utility of these RNases was unclear as they either did not produce the desired reduction in the concentration of waste RNA's or increased the degradation rate of the RNA repressors too much to allow for proper circuit operation[3].

A decrease in the transcription rate over the course of the experiment could also slow down or prevent Core 2N from shutting Core 1N off during a third state change. The effective transcription rate of T7 RNAP has been shown to decrease over time due to degradation of the enzyme[13,14] and accumulation of transcription products that change the reaction conditions and lower the effective transcription rate (such as increasing free Mg^{2+} over the course of the reaction)[15,16]. To test the extent to which the transcription rate slowed in our experiments, we measured the time required for each Core node to fully repress the other after different periods of active transcription of an unrelated transcript. We found that after 8 hours of transcription of the unrelated transcript (produced from 100 nM of a transcription template), the time required for either Core node to shut off the other increased at least 4-fold over the time required for either Core node to shut off the other without any prior transcription of the unrelated transcript (Supplementary Fig. 12c). The time required for each Core node to repress the other increased even more over the course of 8 hours if the transcription rate of the unrelated transcript was increased. In this case, the Core nodes could not fully repress each other when they were added after 8 hours of active background transcription (Supplementary Fig. 12d). Similarly, the time that each Core node could keep the other node completely repressed decreased both with increasing active background transcription time and with increasing transcription rate of the unrelated transcript (Supplementary Fig. 12e,f).

It's likely that both of the above mechanisms contribute to the finite operational lifetime of the bistable genelet network[3,10]. We did find that the circuits could be operated for longer by adding more T7 RNAP during circuit operation (Supplementary Fig. 33) which suggests that sustained state changes could be

possible in an open reaction system where dialysis or flow conditions allow fresh enzyme and nucleotides to be replenished and waste products to be removed.

While we were only able to successfully switch the bistable network two times (suggesting reliable dynamic operation times of 6-8 hours), oscillating genelet modules have been shown to robustly oscillate for 15-20 hours[7,10,11]. A possible explanation for the longer dynamic operation times in the oscillating genelet modules compared to the bistable module we studied could be the differences in the reaction phase space of these two different functional modules. For example, the oscillating modules typically use 2-3 times more T7 RNAP and 5-10 times more RNase H than used in the bistable circuit. Additionally, in the bistable network, the activators are in 10-fold excess of their respective genelets while in the oscillating networks the activators are typically only in 2 to 5-fold excess of their respective genelets[3,7,10,11]. Further, in an oscillating network, the genelets do not turn all the way on or off but oscillate around an intermediate activation level compared to the bistable network where the genelet activation levels have to completely invert during state changes. These differences, which in part give rise to the different functional behaviors of the two networks, might make the bistable module more sensitive to changes in reaction rates over the course of an experiment compared to the oscillating modules. Consistent with these ideas, a previous study on a bistable genelet module found that the module could only maintain a given initial state (without any state changes) for up to 11 hours[3].

Interestingly, discrepancies in the dynamic operation times between bistable modules and oscillating modules have also been observed in other synthetic networks such as the DNA-based polymerase, exonuclease, nickase (PEN) toolbox[17]. For a switchable bistable PEN toolbox module, the authors were able to switch states twice (constituting a dynamic operation time of 7-10 hours). However, oscillating modules constructed with the PEN toolbox were able to robustly oscillate for at least 30 hours[18] (and in some cases over 60 hours[17]). The authors speculate these differences could be due to an inherent lower robustness in bistable modules (which must maintain a delicate balance between two nodes to remain bistable) compared to oscillating modules.

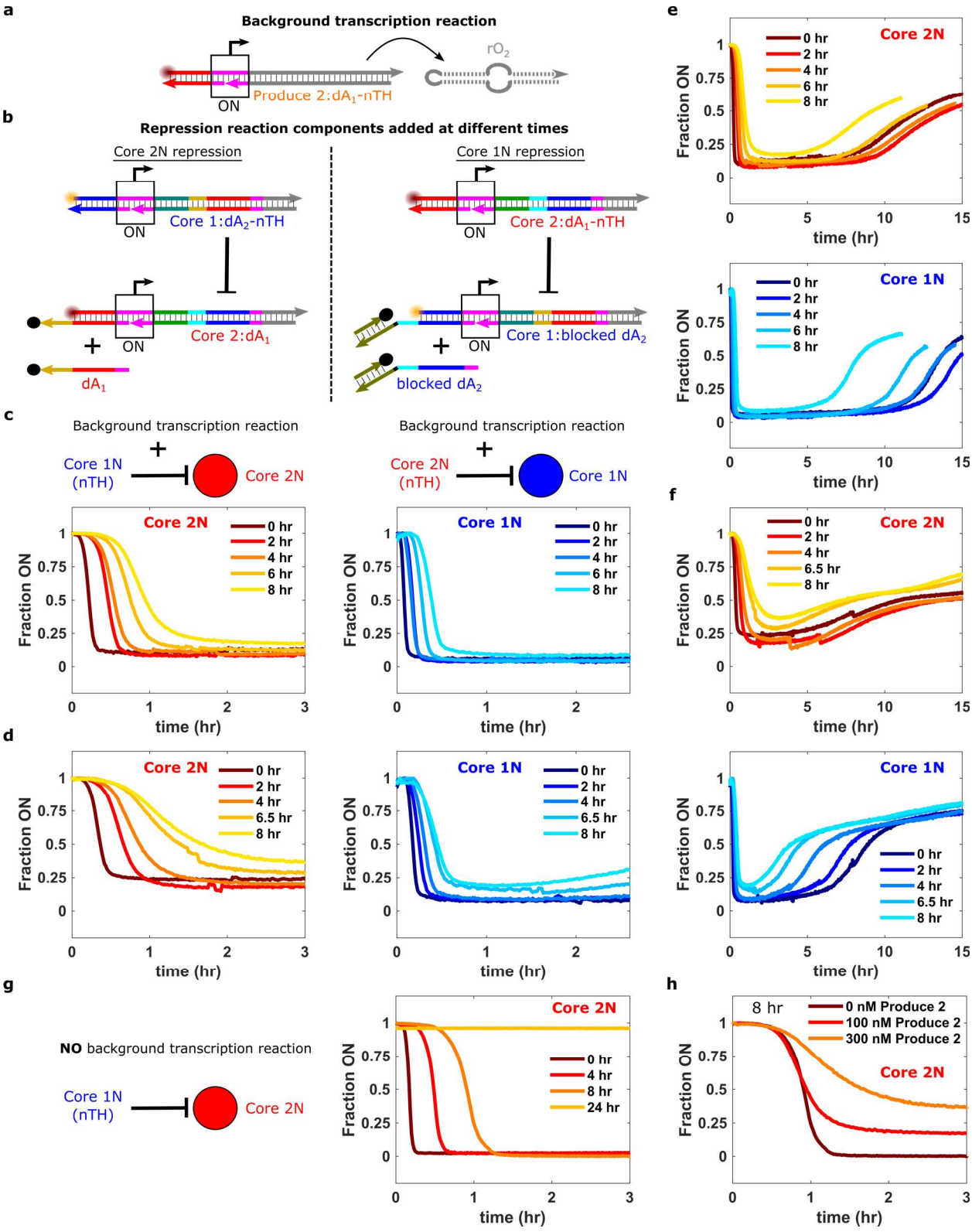
a
Background transcription reaction
rO2
Produce 2:dA1-nTH
ON
b
Repression reaction components added at different times
Core 2N repression
Core 1:dA2-nTH
ON
Core 2:dA1
dA1
Core 1N repression
Core 2:dA1-nTH
Core 1:blocked dA2
blocked dA2
c
Background transcription reaction
Core 1N (nTH)
Core 2N
Core 2N
Core 1N
Fraction ON
time (hr)
0 hr
2 hr
4 hr
6 hr
8 hr
d
6.5 hr
e
f
g
NO background transcription reaction
24 hr
h
8 hr
0 nM Produce 2
100 nM Produce 2
300 nM Produce 2

Supplementary Figure 12 | The time it takes for one of the *i*BN nodes to repress the other increases as the time of active transcription increases. To characterize the extent to which transcription rates of a genelet slow down over increasing transcription times, we used a background transcription reaction in all of the samples (**a**). The time required for each *i*BN node to repress the other was compared after different periods of time of active background transcription (**b**). **a**, The background transcription reaction present in all samples. The Produce 2 node (introduced in Fig. 4 of the main text) was used for background transcription with a variant of dA_1 that is missing the 8-base repression toehold (dA_1-nTH) so that the Produce 2 node is expressed constitutively and not affected by the addition of the *i*BN components. The background transcription output (rO_2) is designed to be a hairpin structure[19] so it should not interact with any of the *i*BN components and cannot be degraded by RNase H. *[Produce 2]* and *[dA_1-nTH]* = 100 nM in (**c**,**e**) and 300 nM in (**d**,**f**). **b**, The *i*BN components added to the samples after different periods of active background transcription. Left: to measure Core 2N repression, the Core 2 genelet, the dA_1 activator, the Core 1 genelet, and a variant of dA_2 that is missing the 8-base repression toehold (dA_2-nTH) were used. This circuit allowed Core 1N to repress Core 2N, but did not allow Core 2N to repress Core 1N. Right: to measure Core 1N repression, the Core 1 genelet, the blocked dA_2 activator (Supplementary Section 10), the Core 2 genelet, and a variant of dA_1 that is missing the 8-base repression toehold (dA_1-nTH) were used. This circuit allowed Core 2N to repress Core 1N, but did not allow Core 1N to repress Core 2N. The Core 1 and Core 2 genelets were added to a final concentration of 100 nM, all activators were added to final concentrations of 1000 nM. **c**,**d**, Normalized activation levels of network nodes during repression of Core 2N (left) or Core 1N (right) after the Core nodes were added to samples after differing periods of background transcription (legends). *[Produce 2]* and *[dA_1-nTH]* = 100 nM (**c**) or *[Produce 2]* and *[dA_1-nTH]* = 300 nM (**d**). As the time of active background transcription increases before the addition of the Core nodes, the time it takes either Core node to fully repress the other increases. In the results presented in (**d**) where a higher concentration of background transcription template was used, the Core nodes cannot completely shut each other off after 6.5 hours. **e**,**f**, Extended plots of the data in (**c**) and (**d**), respectively. As the time of active background transcription increases before the addition of the Core nodes, the time either Core node can keep the other node fully repressed decreases. Comparing (**e**) and (**f**), the higher the rate of active background transcription, the shorter the time each Core node can keep the other fully repressed. **g**, Normalized activation levels of Core 2N after the Core nodes were added to samples with differing incubation periods of the reaction enzymes in transcription conditions without any transcription template. The repression of Core 2N slows down the longer the enzymes are incubated in transcription conditions even in the absence of a transcription template. **h**, Normalized activation levels of Core 2N after the Core nodes were added after 8 hours of background transcription with different Produce 2 template concentrations. Increasing the concentration of the background template slows down the Core 2N repression reaction. Reactions were conducted as described in the Methods of the main text for the *i*BN with *[T7 RNAP]* = 3.57 U/μL, *[RNase H]* = 0.0089 U/μL.

6. Characterizing Core 1N autoinhibition

Characterization of the *i*BN showed that Core 1N slowly began turning off after the network was initialized in S1 (Fig. 2b of the main text). Core 1N could turn off in S1 if Core 2N in the OFF state was being transcribed at a significant rate. To test whether activity of Core 2N while in the OFF state was responsible for the observed change in Core 1N activation, we initialized the *i*BN without the Core 2 genelet in S1 (Supplementary Fig. 13a (*I.*)) and tracked the activation levels of Core 1N after the addition of T7 RNAP and RNase H. Despite the absence of the Core 2 genelet, Core 1N turned all the way off (Supplementary Fig. 13b). Thus off transcription of Core 2N alone could not explain why Core 1N was turning off in our *i*BN experiments. Additionally, we tested whether Core 1N would turn off on its own in the presence of T7 RNAP and RNase H (Supplementary Fig. 13a (*II.*)) or just T7 RNAP alone (Supplementary Fig. 13a (*III.*)) and found that, in both cases, Core1N still turned off. These results suggest that Core 1N slowly turning off in S1 of our *i*BN experiments is the result of an undesired reaction that is dependent on T7 RNAP and the contents of Core 1N alone. We termed this undesired reaction Core 1N autoinhibition. Given all the conditions tested in Supplementary Fig. 13 yielded similar autoinhibition results for Core 1N we selected case *III.* as our primary assay conditions for characterizing autoinhibition further. Using these assay conditions we also tested whether Core 2N in isolation exhibited autoinhibition and found that it did not (Supplementary Fig. 14), consistent with our experimental results for the *i*BN (Fig. 2c of the main text).

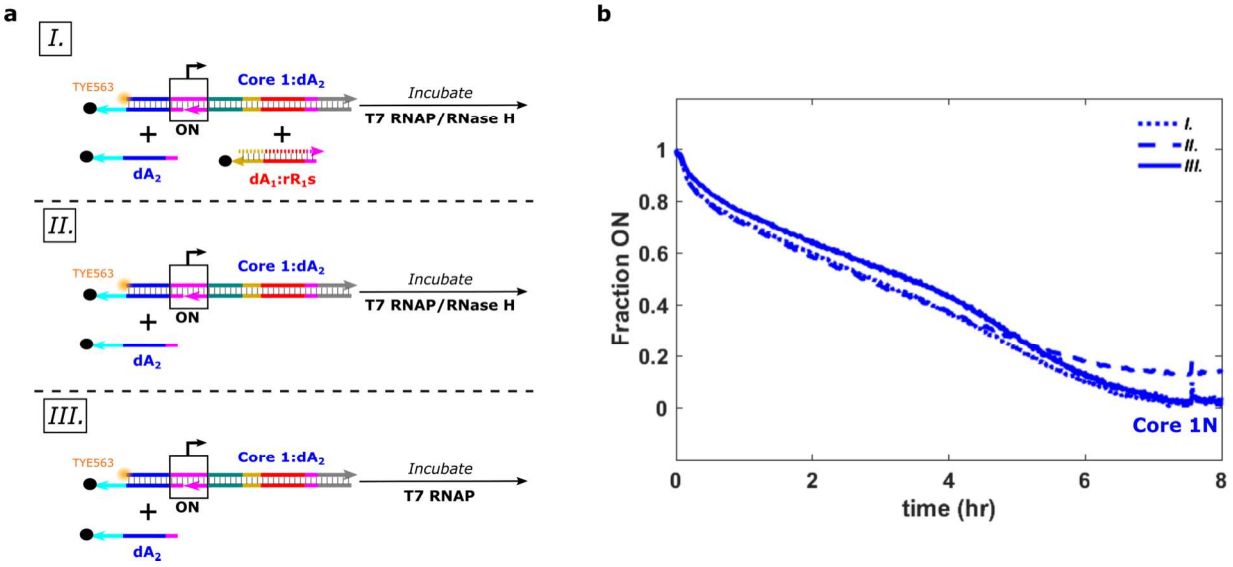

Supplementary Figure 13 | Core 1N turns off when incubated with T7 RNAP even in the absence of Core 2N. a, Diagram of the experiments presented in (**b**). The *i*BN was set in S1 in the absence of the Core 2 genelet and then incubated with T7 RNAP and RNase H (*I.*). Core 1N in the ON state was incubated with T7 RNAP and RNase H (*II.*). Core 1N in the ON state was incubated with just T7 RNAP (*III.*). **b**, Normalized activation levels of Core 1N during incubation with the enzymes and other components depicted in (**a**). Reactions were conducted in NEB RNAPol reaction buffer with BSA, $MgCl_2$, NTP, T7 RNAP, and RNase H (where noted) concentrations as described in the Methods of the main text for the *i*BN. For all experiments: *[Core 1]:* 100 nM, *[dA_2]:* 1000 nM. Additionally, for (*I.*) *[dA_1]:* 1000 nM and *[rR_1s]:* 1100 nM.

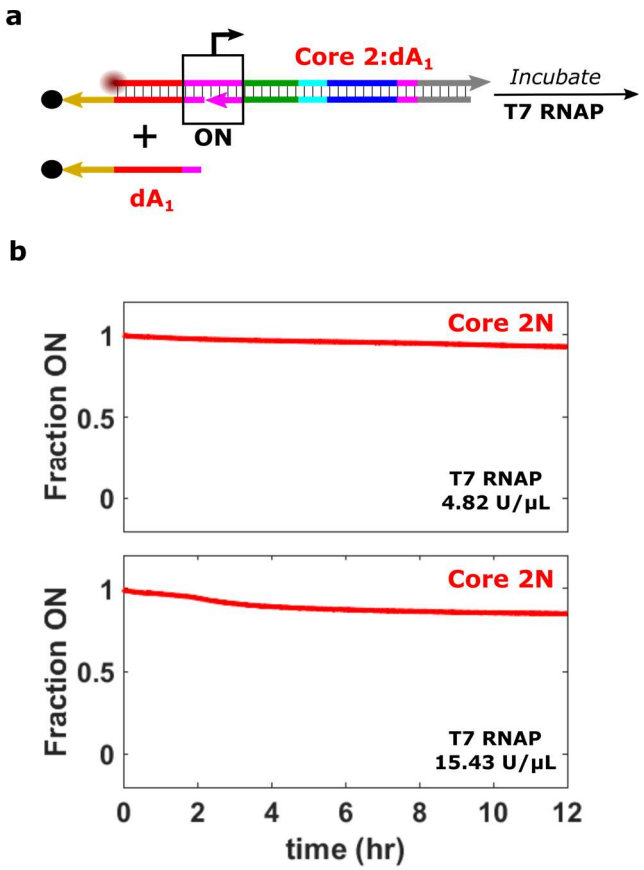

Supplementary Figure 14 | Core 2N alone does not exhibit autoinhibition. a, Diagram of the autoinhibition experiment for Core 2N. **b**, Normalized activation levels of Core 2N during incubation with T7 RNAP at the concentrations shown in the plots. Reactions were conducted in NEB RNAPol reaction buffer with BSA, $MgCl_2$, and NTP concentrations as described in the Methods of the main text for the *i*BN. For both experiments: *[Core 2]:* 100 nM, *[dA$_2$]:* 1000 nM.

We next asked whether Core 1N autoinhibition involved RNA produced during incubation with T7 RNAP. We first incubated Core 1N with T7 RNAP until Core 1N turned completely off (Supplementary Fig. 15b), and then added a high concentration of RNase H (16-fold more than the concentration of RNaseH used for the *i*BN experiments in the main text) to the reaction to rapidly digest any RNA bound to DNA in the sample. After the addition of RNase H, Core 1N quickly turned back on (Supplementary Fig. 15c), suggesting that Core 1N autoinhibition is caused by RNA that binds to a DNA strand in the system.

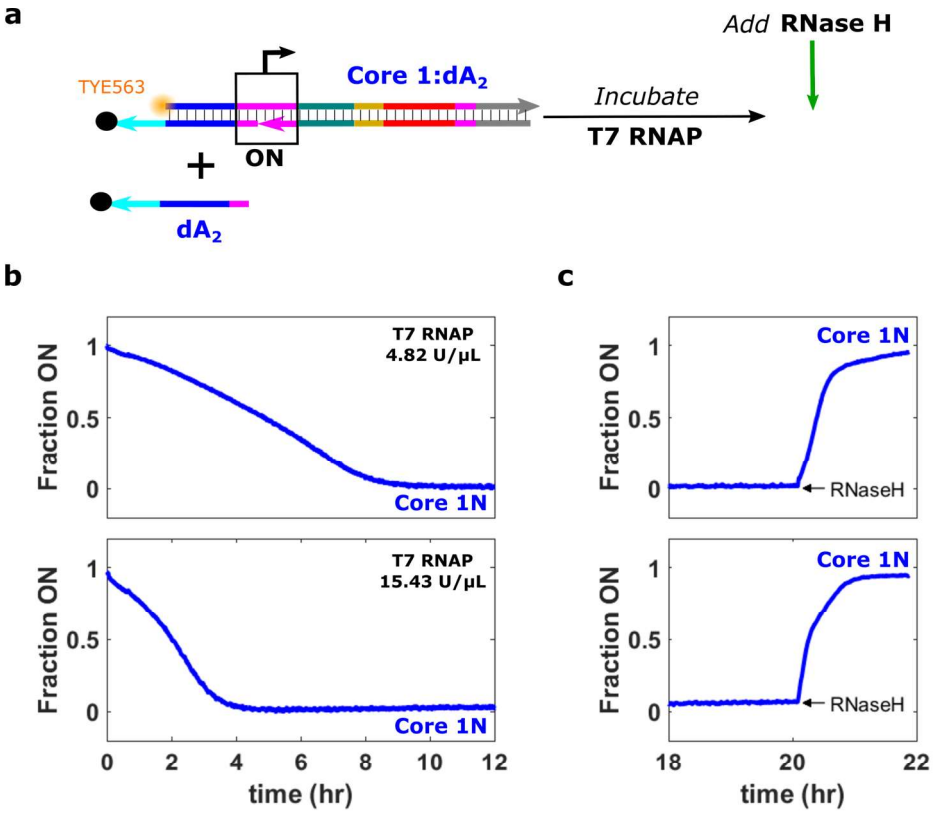

Supplementary Figure 15 | Core 1N autoinhibition is reversed by the addition of a large amount of RNase H. a, Diagram of the experiments presented in (**b**) and (**c**). Core 1N in the ON state was first incubated with T7 RNAP and then RNase H was added to the samples following incubation. **b**, Normalized activation levels of Core 1N during incubation with T7 RNAP at the concentrations shown in the plots. **c**, Normalized activation levels of Core 1N after Core 1N was incubated with T7 RNAP for 18 hours and RNase H (final concentration: 0.071 U/μL) was added after about 20 total hours of incubation. Reactions were conducted in NEB RNAPol reaction buffer with BSA, $MgCl_2$, and NTP concentrations as described in the Methods of the main text for the *i*BN. For both experiments: *[Core 1]:* 100 nM, *[dA_2]:* 1000 nM.

Given the manner in which the activation level of Core 1N is characterized (Fig. 1a of the main text), autoinhibition was likely the result of dA_2 being displaced from the Core 1:dA_2 complex. This observation, along with the fact that autoinhibition appeared to be due to RNA-DNA binding, suggested two plausible mechanisms for autoinhibition: an RNA molecule produced during the incubation of Core 1N with T7 RNAP either (1) removes dA_2 from the Core 1:dA_2 complex to form an RNA-DNA duplex with dA_2 and leaves the Core 1 genelet with an exposed activator binding domain or (2) binds to the activator binding domain of Core 1 in the Core 1:dA_2 complex, thereby displacing dA_2 to create a complex of Core 1 with RNA bound to its activator binding domain. To determine whether Core 1N autoinhibition created the products of mechanism (1) or (2), we characterized the components of a solution in which Core 1:dA_2 and dA_2 (Core 1N in the ON state) were incubated with T7 RNAP using PAGE (Supplementary Fig. 16). Incubation of Core 1:dA_2 and dA_2 with T7 RNAP resulted in a product that migrated at the same rate that the Core 1 genelet (without bound dA_2) did. Furthermore, digestion of the sample of Core 1:dA_2 and dA_2 incubated with T7 RNAP with either RNase H (which degrades RNA bound to DNA) or RNase A (which degrades all RNA[20]) resulted in a product that migrated at the same rate as the Core 1:dA_2 complex did. These results suggest that Core 1N autoinhibition involves an RNA species binding to and removing dA_2 from the Core 1:dA_2 complex (mechanism 1 described above).

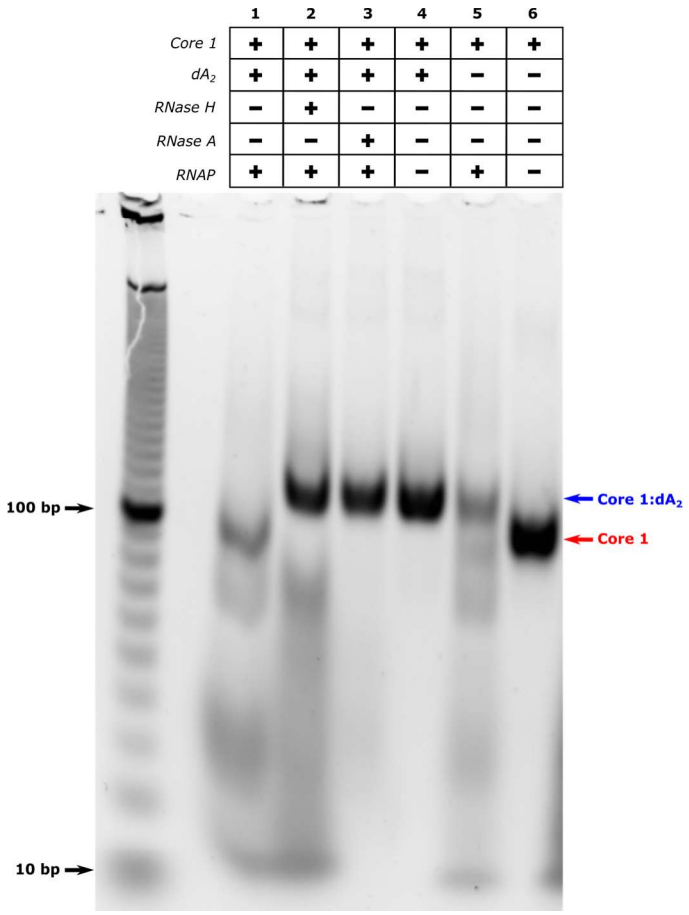

Supplementary Figure 16 | PAGE analysis of Core 1N autoinhibition products. Colored arrows (right of plot) indicate the bands corresponding to Core 1 (red) or Core 1:dA_2 (blue) in each lane. Reactions were conducted in NEB RNAPol reaction buffer with BSA, $MgCl_2$, and NTP concentrations as described in the Methods of the main text for the *i*BN. Additionally: *[Core 1]:* 100 nM, *[dA_2]:* 1000 nM, and *[T7 RNAP]:* 4.82 U/µL. The sample in lane 1 was incubated with T7 RNAP for 7.5 hours, at which point two aliquots were taken from it and RNase H (final concentration: 0.24 U/µL) was added to one aliquot and RNase A (final concentration: 2.04 µg/µL) was added to the other. These samples were then incubated at 37°C for 16 hours. All other samples were incubated at 37°C for the entire duration of the experiment (23.5 hours) without interruption. Gel electrophoresis was conducted with a 6% polyacrylamide gel run at 75V for 2.5 hours and imaged after staining with SYBR Gold (ThermoFisher Scientific) with a Syngene EF2 G:Box gel imager equipped with a blue light transilluminator (emission max ~450 nm) and a UV032 filter (bandpass 572-630 nm). The gel was run with a 10 bp dsDNA ladder (Invitrogen).

Having established that autoinhibition involved an RNA molecule that could bind to and remove dA_2 from Core 1:dA_2, we next investigated where the RNA molecule involved in this process might come from. Since the designed RNA transcript of Core 1N is rR_1 (Fig. 1a of the main text) we first asked whether rR_1 could turn Core 1N off. NUPACK[9] did not predict any interaction between rR_1 and dA_2, suggesting that rR_1 should not be able to bind dA_2 and remove it from Core 1:dA_2. To further test whether rR_1 could turn Core 1N off, we added 3 µM of a chemically synthesized RNA molecule (rR_1s, sequence in Supplementary Table 1) that has the same sequence as rR_1, except it does not have the short 5' variable region or the 3' HP domain (Supplementary Section 1.4), to Core 1N in the ON state and incubated this sample without T7 RNAP. rR_1s did not turn Core 1N off (Supplementary Fig. 17) suggesting that Core 1N autoinhibition is not caused by the designed transcriptional output of Core 1N.

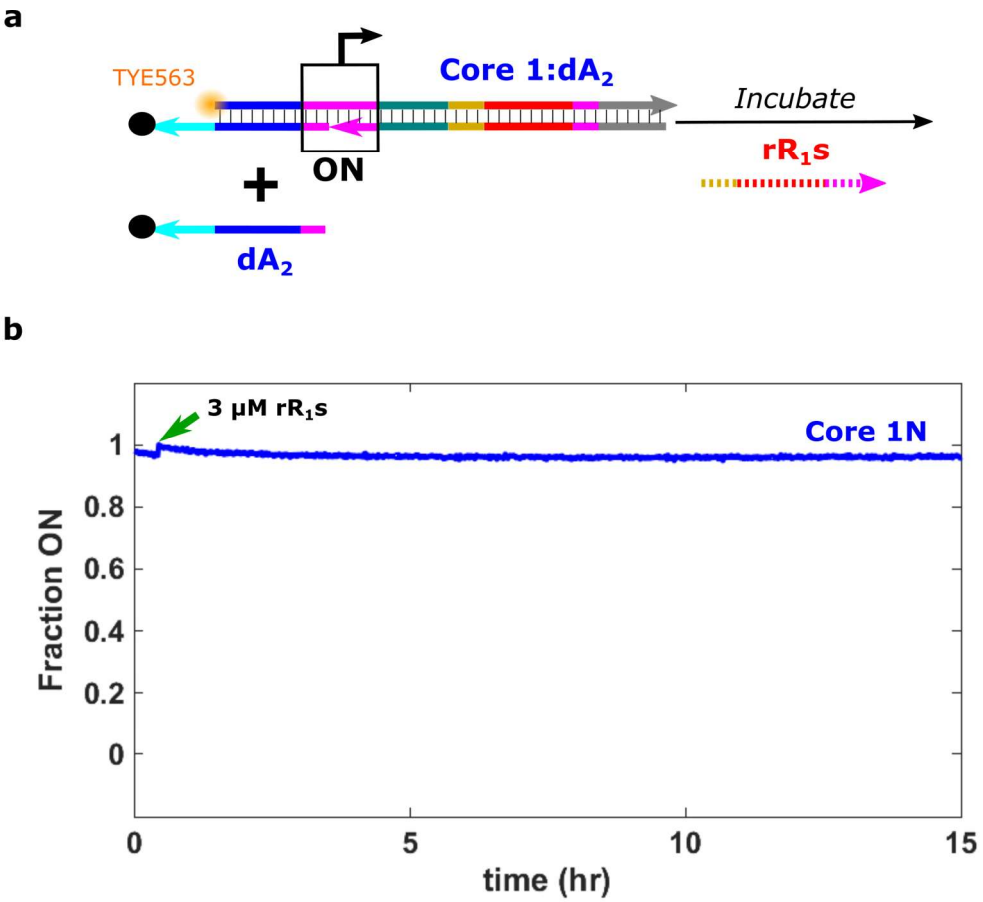

Supplementary Figure 17 | rR_1s does not turn Core 1N off. a, Diagram of the experiment presented in (**b**). **b**, Normalized activation levels of Core 1N during incubation with rR_1s as depicted in (**a**). The reaction was conducted in NEB RNAPol buffer with 1 mg/ml BSA, $MgCl_2$ at a final concentration of 20 mM, and 5 mM of each NTP. Additionally: *[Core 1]:* 100 nM, and *[dA_2]:* 1000 nM.

Since Core 1N autoinhibition did not seem to be caused by the designed transcriptional output of Core 1N, the RNA molecule(s) involved in autoinhibition were likely the product(s) of non-specific transcription. We termed this hypothetical non-specific transcript (or set of transcripts) rAI.

Since rAI could bind to and remove dA_2 from Core 1:dA_2, rAI likely contained sequence elements of rR_2, the repressor of Core 1N. If rAI were similar to rR_2, we would expect Core 1N autoinhibition to be suppressed by rI_2, the inducer RNA that inhibits rR_2 from removing dA_2 from Core 1:dA_2. To investigate whether rI_2 prevented Core 1N autoinhibition, we incubated Core 1N in the ON state with T7 RNAP and 5 μM of rI_2. Indeed, rI_2 significantly suppressed Core 1N autoinhibition (Supplementary Fig. 18), supporting that rAI contains sequence elements of rR_2.

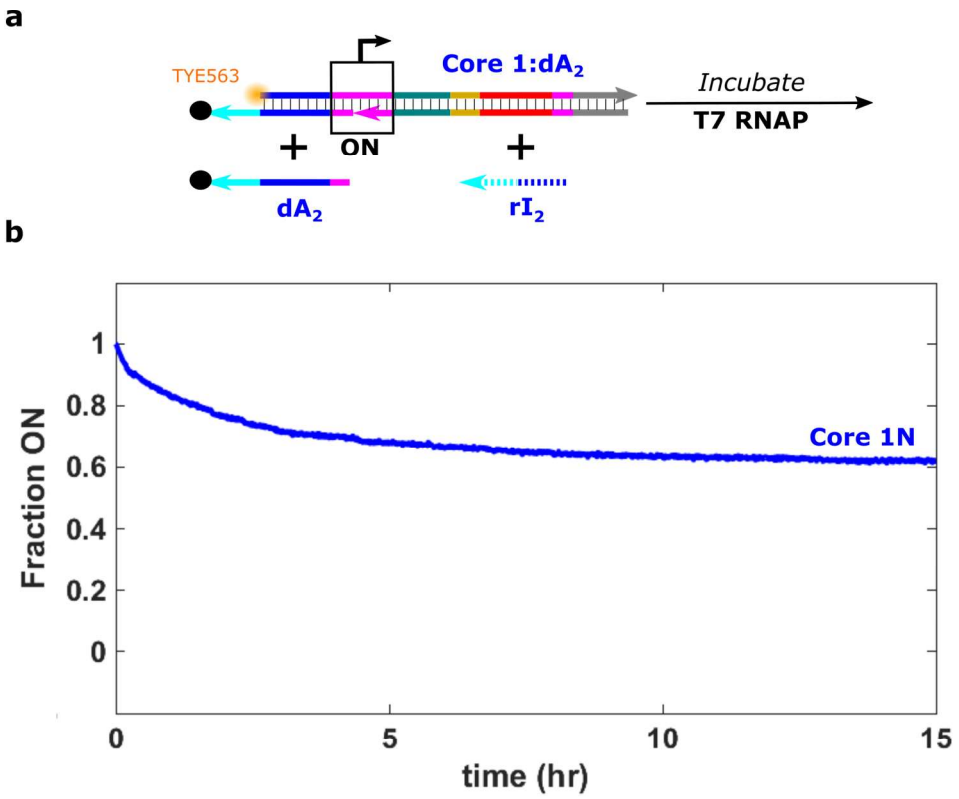

Supplementary Figure 18 | rI_2 reduces the extent of Core 1N autoinhibition. a, Diagram of the experiment presented in (**b**). **b**, Normalized activation levels of Core 1N during incubation with T7 RNAP and rI_2 as depicted in (**a**). Reactions were conducted in NEB RNAPol reaction buffer with BSA, $MgCl_2$, and NTP concentrations as described in the Methods of the main text for the *i*BN. Additionally: *[Core 1]:* 100 nM, *[dA_2]:* 1000 nM, *[rI_2]:* 5000 nM, and *[T7 RNAP]:* 4.82 U/µL.

Given rAI seemed to contain sequence elements of rR_2 and could bind to and remove dA_2 from Core 1:dA_2, we expected increasing the concentration of dA_2 to slow or delay autoinhibition in a manner similar to rI_2. However, we found that increasing the concentration of dA_2 did not change the kinetics of Core 1N autoinhibition (Supplementary Fig. 19).

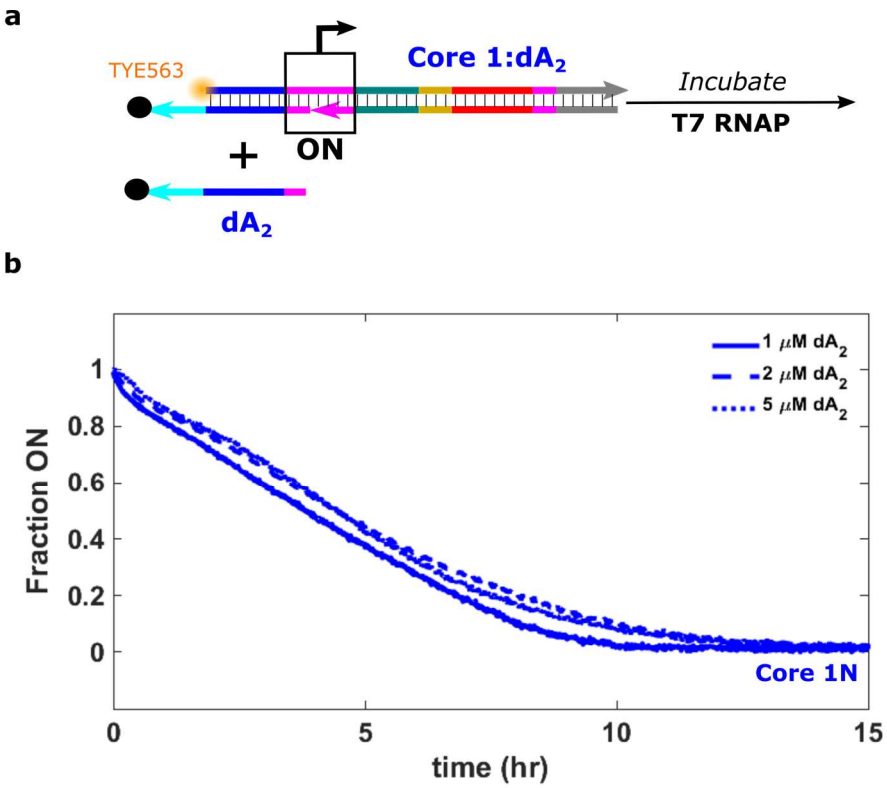

Supplementary Figure 19 | Increasing the concentration of dA_2 does not influence the rate of Core 1N autoinhibition. a, Diagram of the experiment presented in (**b**). **b**, Normalized activation levels of Core 1N during incubation with T7 RNAP and the total concentration of dA_2 indicated in the plot. Reactions were conducted in NEB RNAPol buffer with 1 mg/ml BSA, $MgCl_2$ at a final concentration of 20 mM, and 5 mM of each NTP. Additionally: *[Core 1]:* 100 nM and *[T7 RNAP]:* 4.82 U/μL, and *[dA_2]* as shown in the plot.

We theorized that increasing the concentration of dA_2 might not influence the kinetics of Core 1N autoinhibition if free dA_2 was being transcribed to produce rAI. If free dA_2 were being transcribed to produce rAI, increasing the concentration of dA_2 would proportionally increase the rate of production of rAI. Such non-specific transcription of single-stranded DNA species by viral RNA polymerases has been reported previously[21,22] and transcription of dA_2 would produce RNA species capable of removing dA_2 from Core 1:dA_2, consistent with our previous observations. To investigate whether free dA_2 was being transcribed by T7 RNAP, we incubated dA_2 with T7 RNAP, then stopped transcription after 2 hours by heat denaturing T7 RNAP. We then split each sample that underwent this process into two aliquots. One aliquot was incubated with RNase H while the other was left to incubate undisturbed. PAGE analysis of these samples showed the appearance of bands corresponding to RNA products (Supplementary Fig. 20). The intensity of the RNA bands was higher for samples that contained higher concentrations of dA_2 during the T7 RNAP incubation period. Since dA_2 was the only DNA present in the reaction, these results suggest dA_2 serves as a substrate for transcription by T7 RNAP. The RNA-containing bands in the gel likely contained a combination of RNA products bound to dA_2 and excess RNA which is consistent with previous reports that non-specific transcription of ssDNA templates can produce multiple copies of RNA per single-stranded template[21]. All of the RNA produced in these reactions appeared to be complementary to dA_2 since RNase H degradation completely removed the bands corresponding to the RNA species.

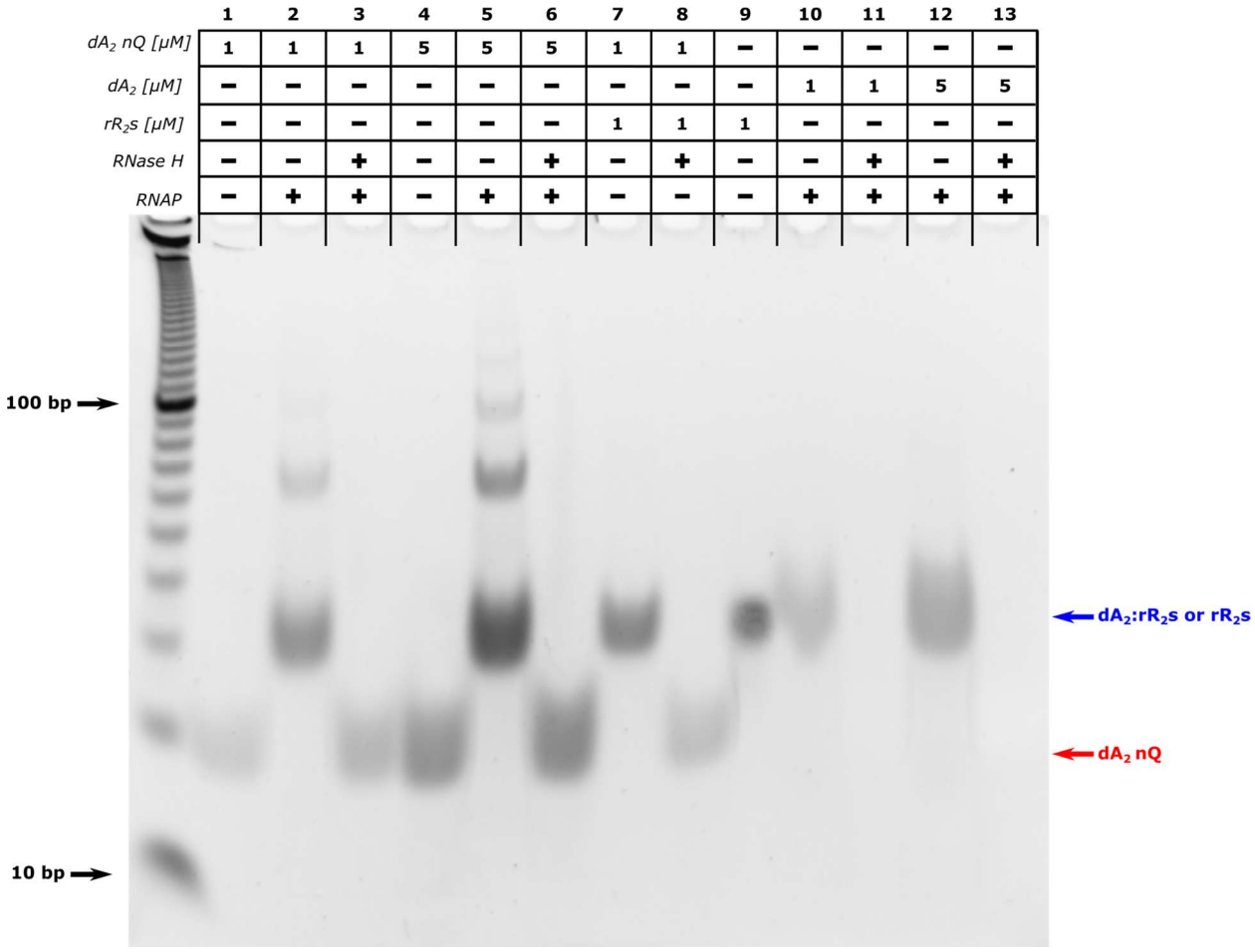

Supplementary Figure 20 | PAGE analysis of RNA products produced during incubation of T7 RNAP with different concentrations of dA_2. The reactions were conducted both with dA_2 modified with Black Hole Quencher 1 (dA_2) and dA_2 without the quencher modification (dA_2 nQ) as the quencher prevented visualization of dA_2 in the gel. The blue arrow indicates bands with mobilities similar to the mobilities of rR_2s (the exact RNA complement of dA_2) or rR_2s bound to dA_2. The red arrow indicates bands corresponding to dA_2 nQ. Reactions were conducted in NEB RNAPol reaction buffer with BSA, $MgCl_2$, and NTP concentrations as described in the Methods of the main text for the *i*BN with *[T7 RNAP]:* 4.82 U/μL where indicated. The concentrations of other species in the reactions are indicated in the grid above the gel. The samples were first incubated with or without T7 RNAP for 2 hours. Transcription was stopped by heat denaturing T7 RNAP at 75°C for 30 minutes. Samples listed as containing RNase H were then incubated with RNase H (0.086 U/μL) at 37°C for 20 hours. Samples listed as not containing RNase H were also held at 37°C for the same 20 hour period. PAGE was conducted with a 10% gel run at 100V for 2 hours and imaged after staining with SYBR Gold (ThermoFisher Scientific) with a Syngene EF2 G:Box gel imager equipped with a blue light transilluminator (emission max ~450 nm) and a UV032 filter (bandpass 572-630 nm). The gel was run with a 10 bp dsDNA ladder (Invitrogen). No bands were visible for the samples containing only dA_2 (modified with Black Hole Quencher 1), possibly because this modification quenched much of the fluorescence from the stain. Incubation of dA_2 with T7 RNAP resulted in the appearance of bands with similar mobilities to rR_2s and dA_2:rR_2s. These bands disappeared with RNase H digestion. These results suggest dA_2 is transcribed by T7 RNAP and that the major transcription product is RNA that is complementary to dA_2. Higher molecular weight products were also observed for the dA_2 nQ samples incubated with T7 RNAP. Such larger transcripts have been observed previously for viral RNAP transcription of single-stranded DNA templates[23].

Since free dA_2 is transcribed by T7 RNAP, we next asked whether removing free dA_2 would prevent Core 1N autoinhibition. We incubated just Core 1:dA_2 with T7 RNAP and found that significant autoinhibition still occurred even in the absence of free dA_2 (Supplementary Fig. 21). These results suggest that the production of rAI is not solely from free dA_2. rAI could also be produced from the Core 1:dA_2 complex since this complex contains a single-stranded 3' end. T7 RNAP has been shown to initiate transcription at single-stranded 3' ends of transcription templates even when the T7 promoter is present elsewhere in the template[24,25]. Initiation of transcription at the 3' single-stranded end of dA_2 in the Core 1:dA_2 complex would produce an RNA species complementary to dA_2 which could explain why autoinhibition still occurred in the absence of free dA_2.

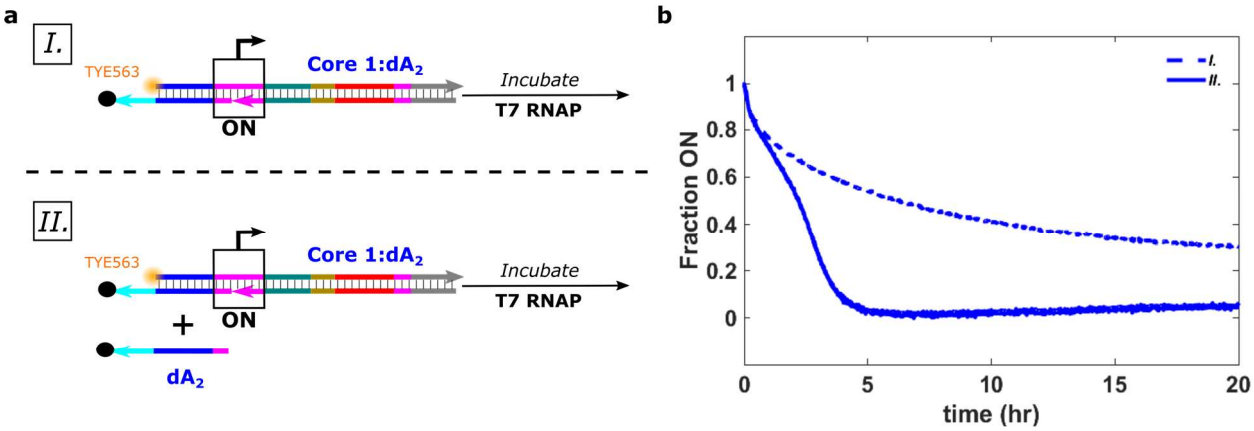

Supplementary Figure 21 | Significant autoinhibition of Core 1N still occurs in the absence of free dA_2. a, Diagram of the experiment presented in (**b**). **b**, Normalized activation levels of Core 1N during incubation with or without free dA_2 and T7 RNAP as depicted in (**a**). Reactions were conducted in NEB RNAPol reaction buffer with BSA, $MgCl_2$, and NTP concentrations as described in the Methods of the main text for the *i*BN. For both experiments: *[Core 1]:* 100 nM and *[T7 RNAP]:* 4.82 U/µL. For (*I.*) *[dA_2]:* 100 nM and (*II.*) *[dA_2]:* 1000 nM.

A plausible mechanism for Core 1N autoinhibition that is consistent with our experimental findings and the previous literature is as follows: rAI is transcribed from both Core 1:dA_2[24,25] and free dA_2[21,22] resulting in an rAI species with a sequence similar to rR_2. Since rAI is similar to rR_2, it acts as a repressor of Core 1N and can bind to free dA_2 or remove dA_2 from Core 1:dA_2. Further, rI_2 can bind to rAI and prevent it from repressing Core 1N. Additionally, rAI bound to dA_2 is degraded by RNase H. A diagram of these putative reactions is shown Supplementary Fig. 23. Given we did not observe much autoinhibition for Core 2N (Supplementary Fig. 14) it is likely the propensity for these reactions to occur is dependent on the sequences of the genelets/activators. Experiments testing for autoinhibition in other genelet nodes used in this study also showed that different sequences result in different degrees of autoinhibition (Supplementary Section 8.8).

Although beyond the scope of our current study, RNA-seq analysis might provide further insight into the autoinhibition mechanism and the identity of the rAI species. In a recent study, RNA-seq was successfully used to uncover the mechanism of another non-specific T7 RNAP transcription reaction[26]. A similar RNA-seq method could be used to further characterize autoinhibition or to rapidly uncover other non-specific transcription reactions in genelet based circuits.

Although genelet autoinhibition was only explicitly studied for T7 RNA polymerase here, the non-specific transcription reactions that appear to cause autoinhibition have also been observed for many other RNA polymerases. Other bacteriophage RNA polymerases (such as SP6 RNAP) have also been shown to non-specifically transcribe single-stranded DNA[21] and initiate transcription at single-stranded 3' overhangs on DNA templates[25]. E. coli RNA polymerase has also been shown to non-specifically initiate transcription on single-stranded DNA templates[27], single-stranded 3' overhangs[28], and within single-stranded regions of mismatched bases on DNA templates[29]. Even some eukaryotic RNA polymerases have been shown to initiate non-specific transcription at single-stranded 3' overhangs[28] and at nicks and/or single-stranded gaps in DNA templates[30]. Thus it is plausible that genelet autoinhibition may be observed with many other common RNA polymerases.

7. Kinetic model of the *i*BN

7.1. Assumptions, reactions, and fitting procedure

Model assumptions:

To build a mass action kinetic model of the *i*BN, we first enumerated designed transcription, activation, repression, inhibition, and degradation reactions for each network node (Supplementary Fig. 22). RNA transcription and degradation are driven by T7 RNAP and RNase H, respectively, and we modeled these reactions using a first order approximation for enzyme kinetics as previously described for genelet networks[6–8]. The rates of production of transcribed RNA are therefore given by: $k_{p_i}[\mathrm{Core\ i{:}dA_j}]$ where k_{p_i} is the apparent first order rate constant for production of RNA from $\mathrm{Core\ i{:}dA_j}$ and the rates of degradation for the repressors are given by: $k_{d_i}[\mathrm{dA_i{:}rR_i}]$ where k_{d_i} is the apparent first order rate constant for degradation of RNA repressor i. We also assumed that the rate of transcription of genelet templates not bound to their activators was low enough to be neglected.

In addition to the designed reactions of the network, we also included a set of reactions that could capture Core 1N autoinhibition (Supplementary Section 6) that are shown in Supplementary Fig. 23. While it is reasonable to expect that Core 1N autoinhibition may involve a larger set of reactions than those presented in Supplementary Fig. 23, these reactions should be able to capture the aspects of autoinhibition that could be directly measured and might affect the behavior of our networks. To keep the number of fitting parameters to a minimum, the rate constant for the reaction between rI_2 and rAI was assumed to be the same as the rate constant for the reaction between rI_2 and rR_2 (k_{IIC_2}) since both of these reactions likely involve RNA hybridization events with >15 bases. Likewise, the rate constant for the binding of rAI to free dA_2 was assumed to be the same as the rate constant for rR_2 binding to dA_2 (k_{AI_2}). The rate of RNase H-catalyzed degradation of rAI within a dA_2:rAI complex was also assumed to be the same as the rate of RNase H-catalyzed degradation of rR_2 within the dA_2:rR_2 complex (k_{D_2}). The autoinhibition process is then characterized by three other rate parameters: k_{PAI_1}, the apparent first order rate constant for the production of rAI from Core 1:dA_2; k_{PAI_2}, the apparent first order rate constant for the production of rAI from free dA_2; and $k_{R_{AI}}$, the rate constant for the removal of dA_2 from Core 1:dA_2 by rAI.

Model reactions:

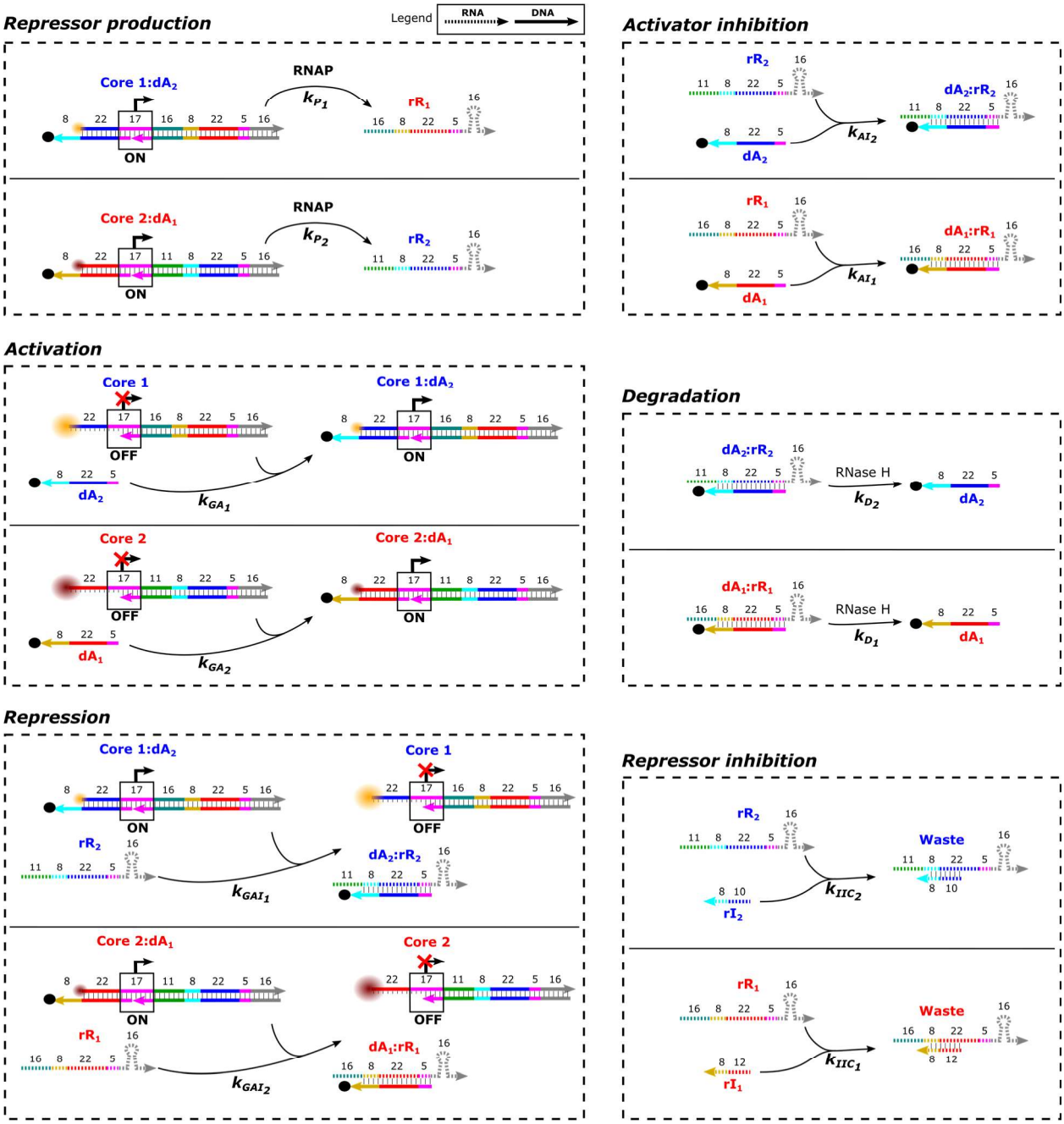

Supplementary Figure 22 | Designed reactions included in the kinetic model of the *i*BN.

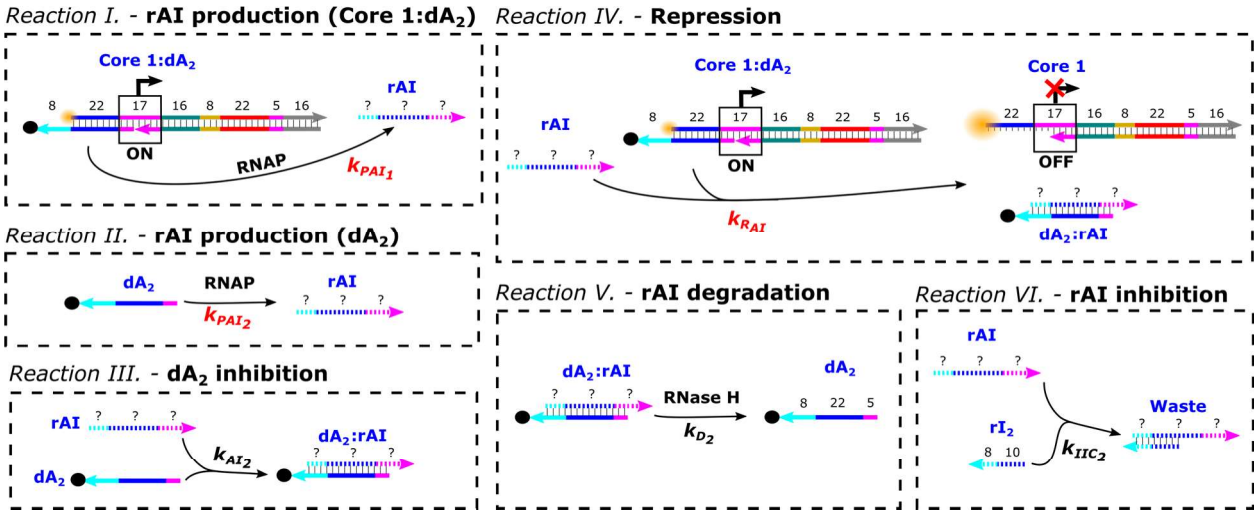

Supplementary Figure 23 | The reactions included in the kinetic model of the *i*BN to capture Core 1N autoinhibition. Autoinhibition is the result of an RNA molecule(s), termed rAI, and the reactions modeled were derived from the experiments described in Supplementary Section 6. We modeled rAI as being produced from both Core 1:dA_2 (Supplementary Fig. 21) and free dA_2 (Supplementary Fig. 20) as shown in *Reactions I.* and *II.*, respectively. rAI was modeled as being able bind to either free dA_2 (Supplementary Fig. 20) or remove dA_2 from Core 1:dA_2 (Supplementary Fig. 16) as shown in *Reactions III.* and *IV.*, respectively. rAI bound to dA_2 was modeled as being a substrate for RNase H degradation (Supplementary Fig. 15, 16, and 20) as shown in *Reaction V*. If rI_2 was present in a reaction it was modeled as being able to bind to rAI to produce inert waste (Supplementary Fig. 18) as shown in *Reaction VI.* Red rate constants represent rate parameters specific to the autoinhibition process only.

The mass action kinetic equations used to model the reactions depicted in Supplementary Fig. 22 (black text) and Supplementary Fig. 23 (red text) are:

$$(7)\ \frac{d[rR_1]}{dt} = -k_{GAI_2}[\text{Core 2:dA}_1][rR_1] - k_{AI_1}[dA_1][rR_1] - k_{IIC_1}[rI_1][rR_1] + k_{P_1}[\text{Core 1:dA}_2]$$

$$(8)\ \frac{d[rR_2]}{dt} = -k_{GAI_1}[\text{Core 1:dA}_2][rR_2] - k_{AI_2}[dA_2][rR_2] - k_{IIC_2}[rI_2][rR_2] + k_{P_2}[\text{Core 2:dA}_1]$$

$$(9)\ \frac{d[dA_1]}{dt} = k_{D_1}[dA_1{:}rR_1] - k_{GA_2}[\text{Core 2}][dA_1] - k_{AI_1}[dA_1][rR_1]$$

$$(10)\ \frac{d[dA_2]}{dt} = k_{D_2}[dA_2{:}rR_2] - k_{GA_1}[\text{Core 1}][dA_2] - k_{AI_2}[dA_2][rR_2] - k_{AI_2}[dA_2][rAI] + k_{D_2}[dA_2{:}rAI]$$

$$(11)\ \frac{d[\text{Core 1:dA}_2]}{dt} = k_{GA_1}[\text{Core 1}][dA_2] - k_{GAI_1}[\text{Core 1:dA}_2][rR_2] - k_{R_{AI}}[\text{Core 1:dA}_2][rAI]$$

$$(12)\ \frac{d[\text{Core 2:dA}_1]}{dt} = k_{GA_2}[\text{Core 2}][dA_1] - k_{GAI_2}[\text{Core 2:dA}_1][rR_1]$$

$$(13)\ \frac{d[rI_1]}{dt} = -k_{IIC_1}[rI_1][rR_1]$$

$$(14)\ \frac{d[rI_2]}{dt} = -k_{IIC_2}[rI_2][rR_2] - k_{IIC_2}[rI_2][rAI]$$

$$(15)\ \frac{d[rAI]}{dt} = -k_{R_{AI}}[\text{Core 1:dA}_2][rAI] - k_{AI_2}[dA_2][rAI] - k_{IIC_2}[rI_2][rAI] + k_{PAI_1}[\text{Core 1:dA}_2] + k_{PAI_2}[dA_2]$$

$$(16)\ \frac{d[dA_2{:}rR_2]}{dt} = k_{GAI_1}[\text{Core 1}{:}dA_2][rR_2] + k_{AI_2}[dA_2][rR_2] - k_{D_2}[dA_2{:}rR_2]$$

$$(17)\ \frac{d[dA_2{:}rAI]}{dt} = k_{R_{AI}}[\text{Core 1}{:}dA_2][rAI] + k_{AI_2}[dA_2][rAI] - k_{D_2}[dA_2{:}rAI]$$

Mass balances are used to infer the concentrations of some of species in equations (7)-(17) over time:

$$(18)[dA_1{:}rR_1] = [dA_1]_{TOTAL} - [dA_1] - [\text{Core 2}{:}dA_1]$$

$$(19)[\text{Core 1}] = [\text{Core 1}]_{TOTAL} - [\text{Core 1}{:}dA_2]$$

$$(20)[\text{Core 2}] = [\text{Core 2}]_{TOTAL} - [\text{Core 2}{:}dA_1]$$

The kinetic model of *i*BN has fifteen fitting parameters to be determined:

Supplementary Table 2 | Rate parameters to be determined for the model. Red parameters correspond to rates specific to autoinhibition reactions only.

Core 1N	Core 2N
k_{P_1} (s^{-1})	k_{P_2} (s^{-1})
k_{D_2} (s^{-1})	k_{D_1} (s^{-1})
k_{GA_1} $(M^{-1}s^{-1})$	k_{GA_2} $(M^{-1}s^{-1})$
k_{GAI_1} $(M^{-1}s^{-1})$	k_{GAI_2} $(M^{-1}s^{-1})$
k_{AI_2} $(M^{-1}s^{-1})$	k_{AI_1} $(M^{-1}s^{-1})$
k_{IIC_2} $(M^{-1}s^{-1})$	k_{IIC_1} $(M^{-1}s^{-1})$
k_{PAI_1} (s^{-1})	– –
k_{PAI_2} (s^{-1})	– –
$k_{R_{AI}}$ $(M^{-1}s^{-1})$	– –

Fitting procedure:

The kinetic model was created to accurately predict the dynamics of switching the state of the *i*BN as a function of inducer RNA concentration and the time of induction with the goal of being able to inform the design of larger genelet networks that incorporate the *i*BN. We selected data to fit the rate parameters of the model with the goal of capturing these dynamics in the fits of the rate parameters of the model.

To fit the rate parameters, we included experimental data from single state switches in both directions at 0.5, 2, and 4 hours (data shown in Supplementary Fig. 4, Fig. 2b,c of the main text (top plots), and Fig. 2b,c of the main text (bottom plots), respectively). We also included the three two state change experiments from Supplementary Fig. 10 to capture the dynamics of sequential switches in response to different concentrations of the first inducer RNA. Additionally, to better inform the fitting of the rate parameters for Core 1N autoinhibition, the experiments where Core 1N autoinhibition was monitored in response to increasing concentrations of dA_2 (Supplementary Fig. 19) were also included in the fitting.

The 15 model parameters shown Supplementary Table 2 for the model were simultaneously fit to the 12 data sets described above by numerically integrating the model's differential equations using MATLAB's *ode23s* function for different parameter sets and minimizing the sum of squared errors between the normalized activation levels of the *i*BN's nodes predicted by the model and recorded in the corresponding experiments using MATLAB's *lsqnonlin* function. For the experiments starting in S2 with rI_2 added at 2 or 4 hours the data from the beginning of the experiments until 30 minutes before rI_2 was added was not included in the sum of squared errors calculation since these periods did not contain any useful dynamics to inform the fitting. To maximize the probability of finding the global minimum of the error, the optimization process was initialized at a few predetermined initial parameter guesses and at 500 random initial guesses using MATLAB's *MultiStart* function. The parameters resulting in the lowest sum of squared errors were selected as the best fit. To ensure that the fit values for the parameters were physically reasonable, each parameter was constrained to lie within a range deemed reasonable for that parameter, which typically spanned a few orders of magnitude (Supplementary Table 3).

The best fits for the parameters are shown in Supplementary Table 4. The 95% confidence intervals for the parameter values were calculated using the MATLAB function *nlparci*. The model fit to the experimental data used for the fitting is shown in Supplementary Fig. 24. The model fits the experimental data well and is able to capture state changes in both directions induced at different times (Supplementary Fig. 24a,b). Additionally, it captures the dynamics of switching states sequentially with increasing amounts of the first inducer RNA (Supplementary Fig. 24c). Finally, the model captures the Core 1N autoinhibition kinetics, including the independence of the autoinhibition rate on increasing concentrations of dA_2 (Supplementary Fig. 24d). We also used the model to simulate the results of additional state change experiments not used to fit the model parameters and found good agreement with these experimental results as well (Supplementary Fig. 25). The rate parameters obtained from the fitting primarily fall within the range of parameters previously described for genelet based circuits[3,7,10].

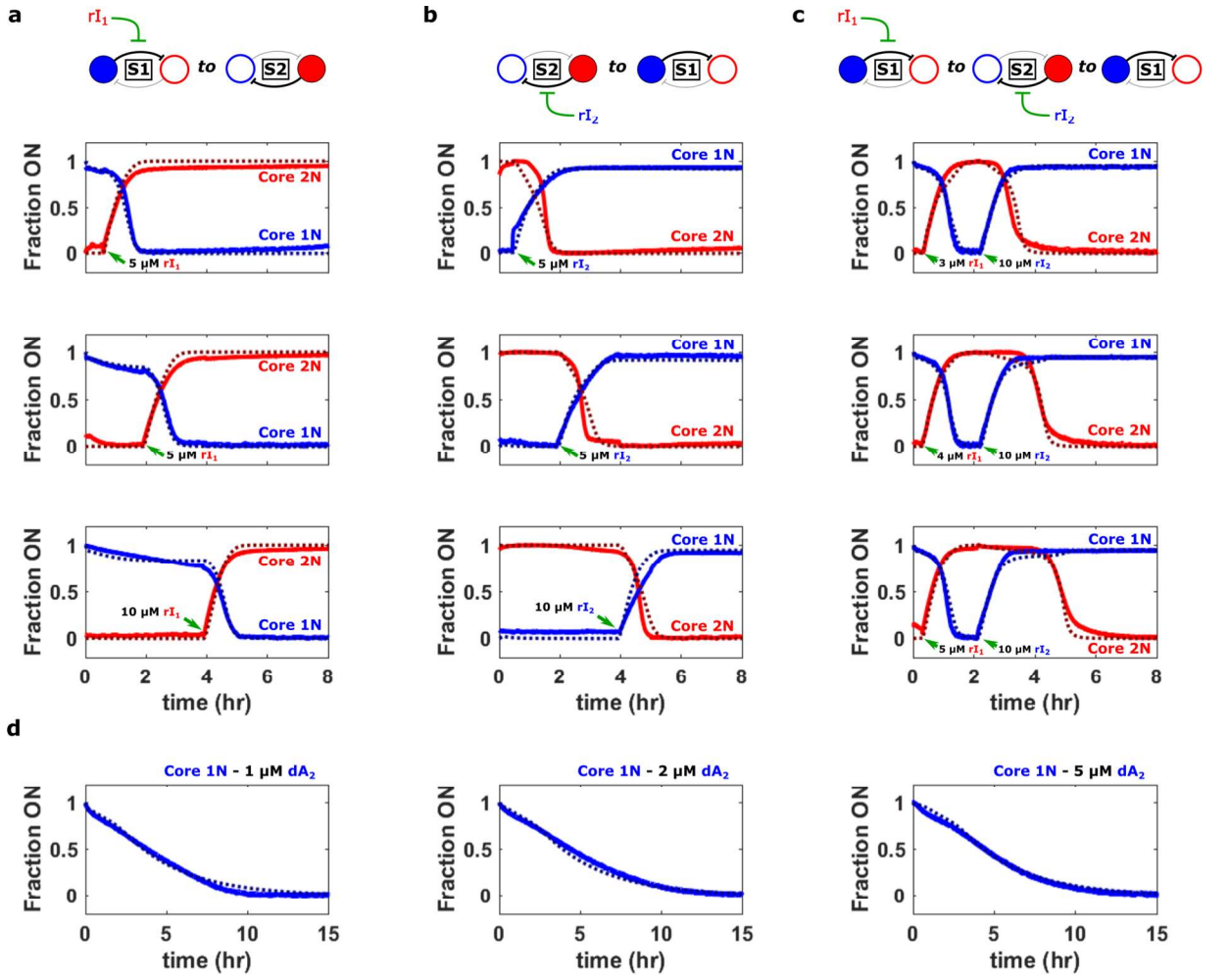

Supplementary Figure 24 | Fits of the kinetic model to the data used to fit the model parameters. a, Normalized activation levels of network nodes during switches from S1 to S2 at either 0.5 hours (top), 2 hours (middle), or 4 hours (bottom). **b**, Normalized activation levels of network nodes during switches from S2 to S1 at either 0.5 hours (top), 2 hours (middle), or 4 hours (bottom). **c**, Normalized activation levels of network nodes during sequential switches from S1 to S2 using either 3 μM rI_1 (top), 4 μM rI_1 (middle), or 5 μM rI_1 (bottom) and back to S1 using 10 μM rI_2 in each case. Reaction conditions for (**a**,**b**,**c**) were otherwise as described in the Methods of the main text for the *i*BN. **d**, Normalized activation level of Core 1N during autoinhibition experiments where Core 1N and increasing concentrations of dA_2 were incubated with T7 RNAP. Reactions for (**d**) were otherwise as described in Supplementary Fig. 19. Experimental data: solid lines, model simulations: dashed lines. The fit rate parameters for the model are in Supplementary Table 4.

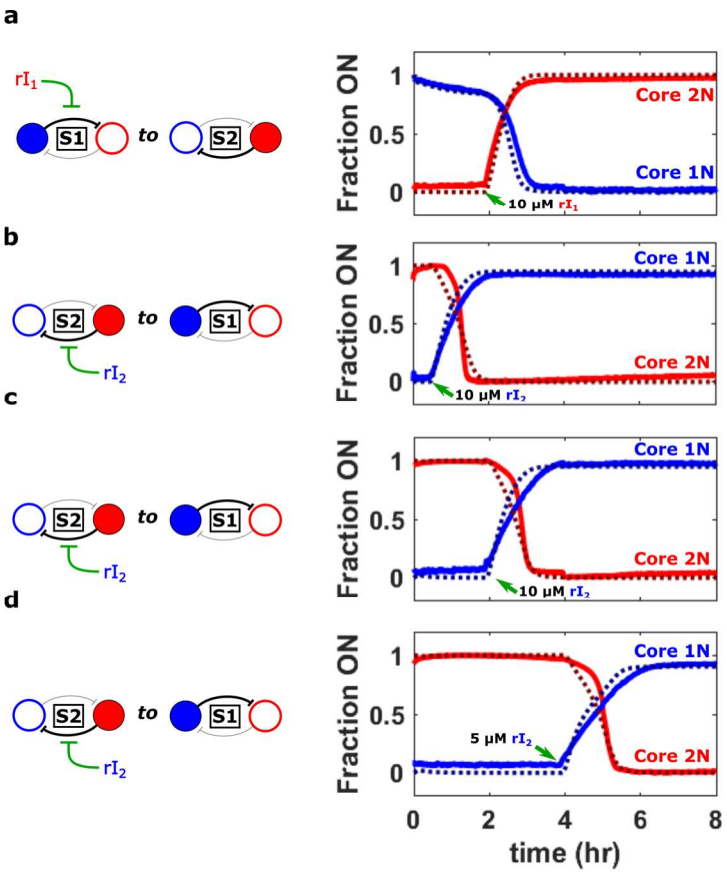

Supplementary Figure 25 | Simulations of the *i*BN kinetic model compared with the results of additional experiments that were not used to fit the model parameters. a, Normalized activation levels of network nodes during a switch from S1 to S2 at 2 hours *via* addition of 10 μM rI_1. **b-d**, Normalized activation levels of network nodes during switches from S2 to S1 at either 0.5 hours (**b**), 2 hours (**c**), or 4 hours (**d**) *via* addition of 10 μM rI_2 (**b**), 10 μM rI_2 (**c**), or 5 μM rI_2 (**d**). Reaction conditions were otherwise as described in the Methods of the main text for the *i*BN. Experimental data: solid lines, model simulations: dashed lines. The rate parameters used in the model are in Supplementary Table 4.

7.2. Rate parameters for the kinetic model of the *i*BN

Supplementary Table 3 | Parameter bounds for model fitting. Bounds were set to include the full range of values fit for similar rate parameters in related studies[3,7,10].

Parameters	Min	Max
k_P (s^{-1})	$1.0x10^{-4}$	$1.0x10^{-1}$
k_D (s^{-1})	$1.0x10^{-5}$	$1.0x10^{-2}$
k_{GA} ($M^{-1}s^{-1}$)	$1.0x10^{3}$	$1.0x10^{6}$
k_{GAI} ($M^{-1}s^{-1}$)	$1.0x10^{3}$	$1.0x10^{6}$
k_{AI} ($M^{-1}s^{-1}$)	$1.0x10^{3}$	$1.0x10^{6}$
k_{IIC} ($M^{-1}s^{-1}$)	$1.0x10^{3}$	$1.0x10^{6}$
$k_{P_{AI1}}$ (s^{-1})	$1.0x10^{-6}$	$1.0x10^{-1}$
$k_{P_{AI2}}$ (s^{-1})	$1.0x10^{-6}$	$1.0x10^{-1}$
$k_{R_{AI}}$ ($M^{-1}s^{-1}$)	$1.0x10^{1}$	$1.0x10^{6}$

Supplementary Table 4 | Fits of the rate parameters for the kinetic model of the *i*BN. Red parameters are for parameters unique to Core 1N autoinhibition. Parameter ranges indicate 95% confidence intervals.

Parameters	Core 1N	Core 2N
k_P (s^{-1})	$4.50\pm0.03 \times 10^{-3}$	$2.23\pm0.15 \times 10^{-3}$
k_D (s^{-1})	$6.14\pm0.33 \times 10^{-5}$	$6.78\pm0.40 \times 10^{-5}$
k_{GA} ($M^{-1}s^{-1}$)	$3.37\pm0.33 \times 10^{4}$	$1.32\pm0.07 \times 10^{4}$
k_{GAI} ($M^{-1}s^{-1}$)	$5.79\pm1.7 \times 10^{4}$	$1.12\pm0.16 \times 10^{5}$
k_{AI} ($M^{-1}s^{-1}$)	$3.87\pm0.85 \times 10^{4}$	$1.00\pm0.29 \times 10^{3}$
k_{IIC} ($M^{-1}s^{-1}$)	$4.29\pm0.77 \times 10^{3}$	$7.13\pm0.91 \times 10^{4}$
$k_{P_{AI1}}$ (s^{-1})	$7.43\pm0.11 \times 10^{-5}$	– –
$k_{P_{AI2}}$ (s^{-1})	$6.04\pm0.24 \times 10^{-4}$	– –
$k_{R_{AI}}$ ($M^{-1}s^{-1}$)	$1.62\pm0.36 \times 10^{5}$	– –

8. Design and characterization of the *i*BN-*u*A

8.1. Simulations of the *i*BN with transcription of the inducer RNAs

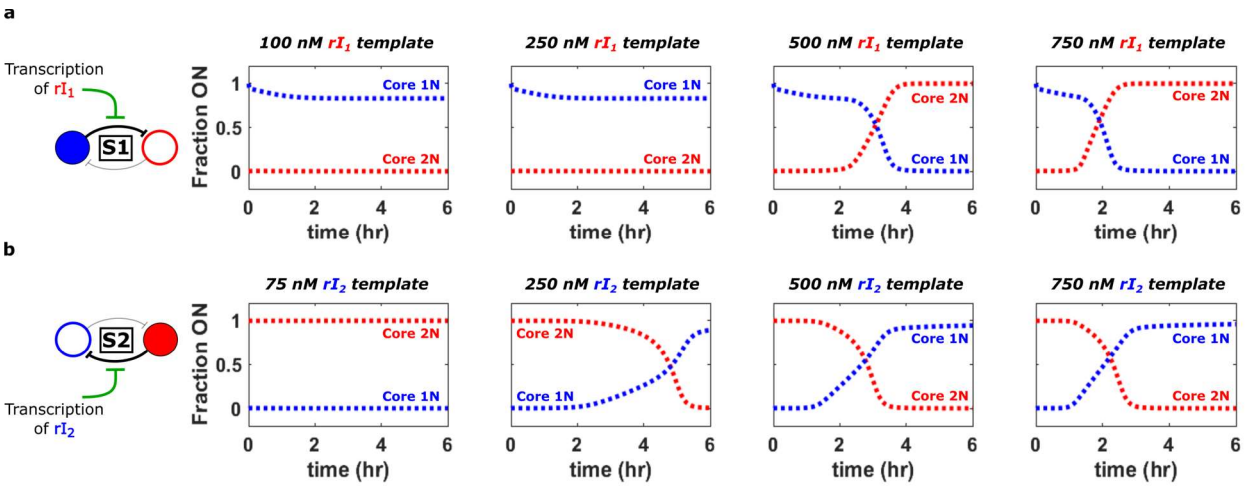

Supplementary Figure 26 | Simulations of the *i*BN where the inducer RNAs are transcribed predicts that the state of the network can be switched if the concentrations of the inducer RNA templates are higher than the concentrations of the *i*BN genelets. a, Simulations of the *i*BN initialized in S1 with a transcription template for rI_1 introduced after 30 minutes to the final concentrations indicated above the plots. **b**, Simulations of the *i*BN initialized in S2 with a transcription template for rI_2 introduced after 30 minutes to the concentrations indicated above the plots. For all simulations the model presented in Supplementary Section 7 was used with additional reaction terms added for the production of the inducer RNAs (k_P[Transcription template]). The concentrations of the *i*BN components in the simulations were as described for the *i*BN experiments in Supplementary Section 1.2. The transcription rate parameter (k_P) for the transcription templates of the inducer RNAs was set to 1×10^{-3} s^{-1}, slightly lower than the transcription rates fit for the genelets in the *i*BN. The rate parameters for the rest of the *i*BN reactions were taken from Supplementary Table 4.

8.2. NUPACK design of Induce nodes

To construct the *i*BN-*u*A, we needed to add two upstream nodes to the *i*BN. There were two major design constraints that we considered when designing these upstream nodes. First, the components of these nodes (genelet activator binding domains, activators, and repressors) should not have any spurious interactions with the existing components of the *i*BN. We defined a spurious interaction as a significant hybridization interaction between two species that are not designed to interact. We considered a spurious interaction to be significant if it resulted in >25% of the limiting species in an unintended interaction to be hybridized with another reactant at equilibrium in our simulated conditions. Second, we sought to satisfy the first criteria without redesigning any of the sequences of the existing *i*BN components.

To design the sequences for the components of the upstream nodes we used NUPACK[9] with a temperature of 37°C and default salt conditions (1 M Na^+, 0 M Mg^{2+}) since estimating the concentration of free magnesium is difficult in our experiments given the high concentration of NTPs. Since NUPACK does not model DNA-RNA interactions, we modeled all of the species in the network as RNA molecules. Since RNA-RNA/RNA-DNA interactions tend to be stronger than DNA-DNA interactions[31] these simulations served as a worst case scenario in terms of spurious interactions across components.

8.3. Adding nodes to the *i*BN with the KWW genelet design results in spurious interactions between the components of the *i*BN-*u*A

Initially we designed the sequences for the additional upstream nodes of the *i*BN-*u*A for genelets with 27-base single-stranded activator binding domains and 35-base single-stranded activators and repressors following the design of the genelets presented in Kim, White, and Winfree[3] (Fig. 1a). We termed components with this design KWW components (Supplementary Fig. 27). NUPACK was not able to produce sequences for the components of the additional KWW nodes that were not predicted to have significant spurious interactions (Supplementary Section 8.2) with components in the *i*BN. Particularly, cross-activation, where one activator could bind to a genelet other than its target genelet was predicted. After several rounds of design without much success, we decided to determine whether the spurious interactions predicted by simulations would be observed in experiments.

To determine whether the designed additional KWW genelets might exhibit the crosstalk predicted by NUPACK, we tested whether the additional KWW genelets would be spuriously activated by the Core 1 or Core 2 activators dA_1 and dA_2. We incubated each additional KWW genelet individually and added dA_1 (a species predicted to spuriously interact with the activator binding domains of the additional KWW genelets) to each sample while tracking the fluorescence of the samples. If dA_1 could bind to either additional KWW genelet's activator binding domain, we would expect to see a drop in fluorescence since dA_1 is modified with a quencher and each genelet is labeled with a fluorophore. To validate that observed drops in fluorescence were due to activator-genelet binding, the DNA complement of dA_1 (*i.e.* dR_1s) was subsequently added in excess at the end of the experiments to remove any activator that might have bound to the genelets. Thus, a fluorescence drop upon dA_1 addition followed by a fluorescence increase upon dR_1s addition signified a binding interaction between the genelets and dA_1. We observed interactions between both the additional KWW genelets we designed and dA_1 (Supplementary Fig. 27). The fact that these effects were observed in experiments suggested other spurious interactions predicted by NUPACK that are not directly observable could also influence network functionality. These spurious interactions thus indicated a considerable challenge for scaling genelet networks to a large number of nodes using the KWW genelet design, especially in the case where it is desired to add more nodes to an existing network without sequence redesign.

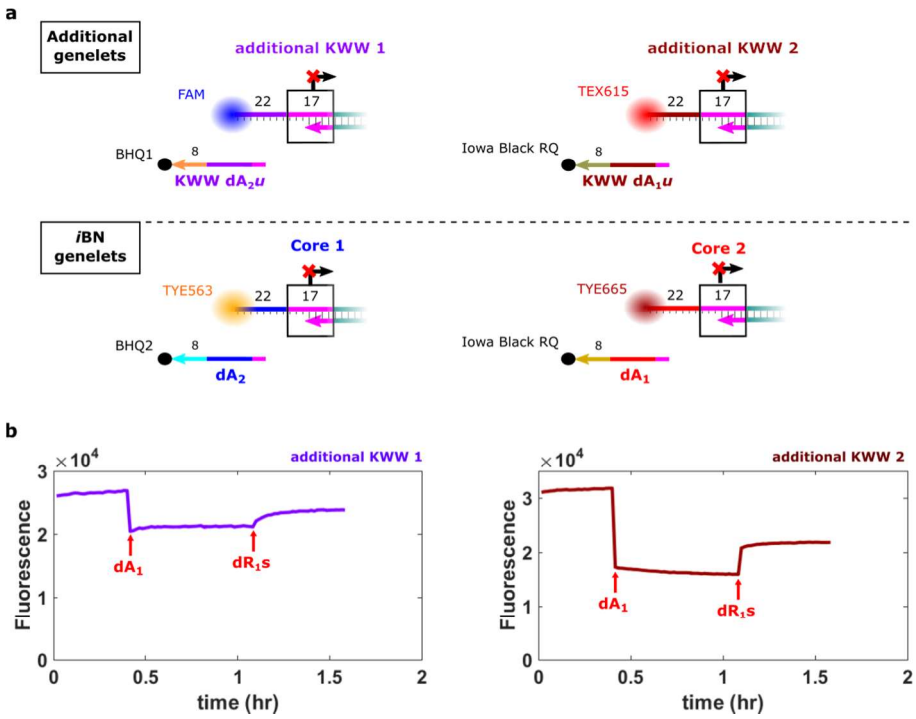

Supplementary Figure 27 | Spurious interactions between designed additional KWW genelets and dA_1. a, Schematic of the activator binding domains of the additional KWW genelets and their respective activators (Sequences, Supplementary Table 1). The schematics for the activators and activator binding domains of Core 1 and Core 2 are also shown for reference. **b**, Fluorescence kinetic data showed spurious activation of the additional KWW genelets by dA_1. dA_1 and dR_1s were added at the times indicated by the labeled arrows to a final concentration of 1000 nM and 15000 nM, respectively. Reactions were conducted in NEB RNAPol buffer with 1 mg/ml BSA, $MgCl_2$ at a final concentration of 20 mM, 5 mM of each NTP, and *[additional KWW genelets]:* 100 nM.

8.4. Limitations to scaling the number of KWW genelets in a circuit without encountering significant crosstalk

We sought to determine the extent to which the KWW genelet design (the design for genelets presented in Fig. 1a of the main text) allows for the *de novo* construction of multiple orthogonal genelets without crosstalk. Our initial goal was to use this design to extend the *i*BN. However, we were unable (as discussed in the main text and Supplementary Section 8.3) to find sequences to create additional nodes that did not have significant crosstalk with the existing *i*BN nodes. The goal of this investigation was to determine whether the limitation on the number of orthogonal genelet nodes that could be designed was due to the specific choice of preset *i*BN sequences (in which case larger networks might be constructed by redesigning the *i*BN) or whether a propensity for crosstalk is inherent to the KWW genelet design.

We attempted to design 6 orthogonal activator/repressor pair sequences *de novo* using NUPACK. The designs were carried out to minimize the crosstalk between the different activators, crosstalk between the different repressors, and crosstalk between activators and non-target repressors (see the example script below). The best sequences that NUPACK could produce in these designs were still predicted to have an average of roughly 15% of their bases incorrectly paired at equilibrium (normalized ensemble defect[9]).

In the above designs, the sequences of the activators and repressors could be composed of any of the 4 standard nucleotides. We also tried designing 6 sets of activator/repressor pairs where we restricted the RNA repressors to only have the bases A, U, or C. This strategy of using a restricted nucleotide alphabet has worked well for increasing the size of enzyme free DNA strand displacement networks[32]. However, this strategy produced slightly worse results than the unrestricted sequence design, with the best sequences that NUPACK could produce predicted to have a roughly 17% normalized ensemble defect. Such a result is not unexpected, since a given genelet activator/repressor pair must be complementary but orthogonal activators and repressors will exist as single-stranded species so all activators will have an A, U, or G sequence while all repressors will have an A, U, or C sequence resulting in a high propensity for activators to interact with non-target repressors.

These issues with *de novo* design of orthogonal sequences for only a 6 node genelet network signify a potential issue for building large networks with the KWW genelet design.

Below is an example NUPACK script used for these design exercises with the KWW genelet design. In the below script, the sequences can be composed of any of the 4 standard bases. To restrict the repressor sequences to only be composed of the bases A, U, or C, the sequence domains b1 through b6 were restricted (*e.g.* domain sequence definitions were changed from N30 to D30). The script was modified for the HPC genelet design (Supplementary Section 8.6) by changing the activator and repressors structures from U35 to U8 D7 (U5) U8 and increasing the number or activators/repressors to 10.

```
# parameters for design
material = rna
temperature[C] = 37.0
trials = 5
# target structures using DU+ notation
#####################################
# Defining the single-stranded activators
structure A1 = U35
```

```
structure A2 = U35
structure A3 = U35
structure A4 = U35
structure A5 = U35
structure A6 = U35
# Defining the single-stranded repressors
structure R1 = U35
structure R2 = U35
structure R3 = U35
structure R4 = U35
structure R5 = U35
structure R6 = U35
# sequence domains
########################################
# defining the sequence domains where N indicates
# A, T, G, or C can be used in the designed sequences
domain a = TAATA
domain b1 = N30
domain b2 = N30
domain b3 = N30
domain b4 = N30
domain b5 = N30
domain b6 = N30
# thread sequence domains onto target structures
################################################
# defining the activator sequences
A1.seq = a b1
A2.seq = a b2
A3.seq = a b3
A4.seq = a b4
A5.seq = a b5
A6.seq = a b6
# defining the repressor sequences
R1.seq = b1* a*
R2.seq = b2* a*
R3.seq = b3* a*
R4.seq = b4* a*
R5.seq = b5* a*
R6.seq = b6* a*
# Tube to prevent binding of the activators
tube tubeA = A1 A2 A3 A4 A5 A6
# Tube to prevent binding of the repressors
tube tubeR = R1 R2 R3 R4 R5 R6
# Tubes to prevent binding between the activators
# and their non-target repressors
tube tube1 = A1 R2 R3 R4 R5 R6
tube tube2 = A2 R1 R3 R4 R5 R6
tube tube3 = A3 R1 R2 R4 R5 R6
tube tube4 = A4 R1 R2 R3 R5 R6
tube tube5 = A5 R1 R2 R3 R4 R6
tube tube6 = A6 R1 R2 R3 R4 R5
# design against all off-target ordered complexes of up to this
# 2 strands (dimers)
tubeA.maxsize = 2
tubeR.maxsize = 2
tube1.maxsize = 2
tube2.maxsize = 2
tube3.maxsize = 2
```

```
tube4.maxsize = 2
tube5.maxsize = 2
tube6.maxsize = 2
# preventing repeated sequence patterns
prevent = AAAAA, CCCCC, GGGGG, UUUUU, KKKKKKKK, MMMMMMMM, RRRRRRRR, SSSSSSSS,
WWWWWWWW, YYYYYYYY
```

8.5. Adding nodes to the *i*BN with the HPC design prevents most spurious interactions between the components of the *i*BN-*u*A

A central difficulty in designing suitable sequences for the additional KWW nodes of the *i*BN-*u*A was that adding more nodes to the *i*BN resulted in a network with many different long, single-stranded nucleic acid components, most of which would be present at high concentrations and not hybridized to any extent in the reactions. To reduce the lengths of the single-stranded domains in the *i*BN-*u*A, we developed a genelet design with "hairpin clamp" (HPC) motifs in the activator binding domains (Supplementary Fig. 28). The activator binding domains of the HPC genelets were designed to fold into hairpins when not bound to their activators. The activators and repressors of HPC genelets were likewise designed to fold into hairpins when not bound to their intended targets in the network. The bases within these hairpins should then not be available to spuriously interact with other components in the network. Using NUPACK, we were able to design sequences for the components of the two additional nodes of the *i*BN-*u*A with the HPC design that were predicted to have little to no crosstalk between network components. After the design process, we tested whether there was any spurious activation (*i.e.* cross-activation) of any of the four genelets of the *i*BN-*u*A by any activators other than their designed activators using the assay described in Supplementary Fig. 27. No cross-activation was observed in this network (Supplementary Fig. 28).

Hairpins have also been incorporated into transcriptional templates not to reduce the total length of single-stranded DNA or RNA in a circuit for less crosstalk, but instead to use hairpin folding for regulation rather than the association and dissociation of activating strands, thus enabling the creation of a single-stranded transcriptional switches[33].

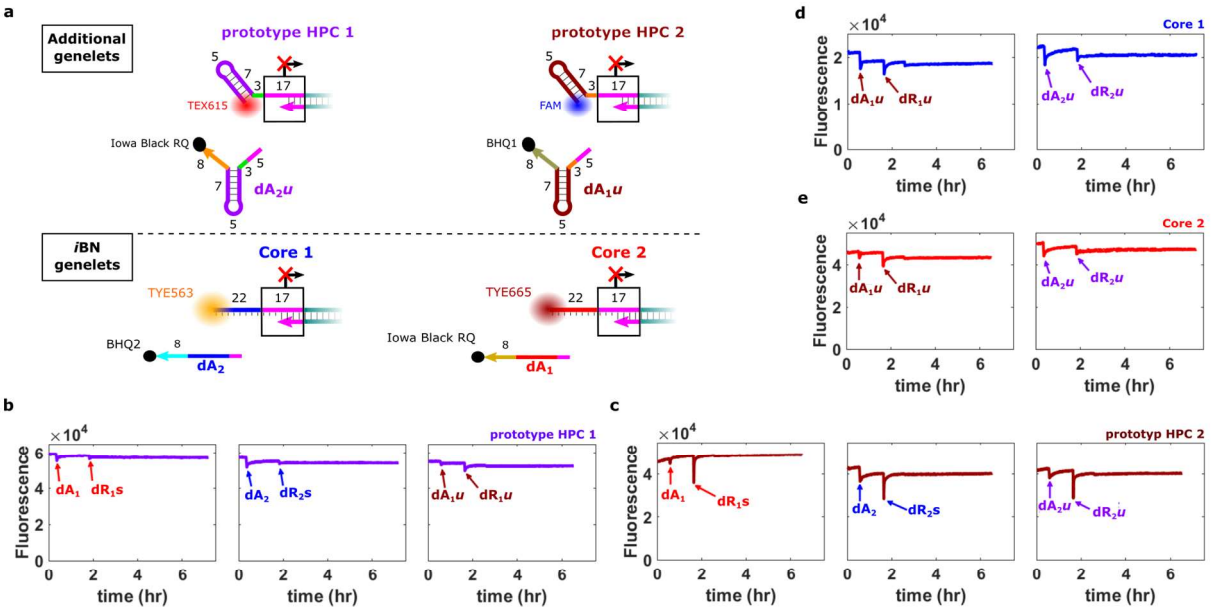

Supplementary Figure 28 | There is no cross-activation between the genelets of the *i*BN and the prototype HPC genelets. a, Schematics of the four genelets tested for spurious activation and their activators (sequences, Supplementary Table 1). **b**, The effects of dA_1, dA_2, and dA_1u on prototype HPC 1 fluorescence. **c**, The effects of dA_1, dA_2, and dA_2u on prototype HPC 2 fluorescence. **d**, The effects of dA_1u and dA_2u on Core 1 fluorescence. **e**, The effects of dA_1u and dA_2u on Core 2 fluorescence. Activators and repressors were added at the times indicated by the arrows. dA_1 and dA_2 were added to a final concentration of 1 µM. dR_1s and dR_2s were added to a final concentration of 1.5 µM. dA_1u and dA_2u were added to a final concentration of 0.5 µM. dR_1u and dR_2u were added to a final concentration of 1 µM. Reactions were conducted in NEB RNAPol buffer with 1 mg/ml BSA, $MgCl_2$ at a final concentration of 20 mM, 5 mM of each NTP. Genelets were present at 100 nM in each experiment. Prototype HPC 1 and prototype HPC 2 were designed to test the HPC genelet design and have the same activator and repressor sequences as Induce 1 and Induce 2 used in the main text, respectively, but possess different sequences than Induce 1 and 2 downstream of the T7 RNAP promoter domain.

8.6. Scalability of the HPC genelet design compared to the KWW genelet design

The HPC genelets are designed to decrease the number of exposed bases on genelet activator binding domains and activators/repressors compared to the KWW genelets. We sought to estimate the extent to which HPC genelets might allow for the design of larger genelet networks without significant crosstalk between network nodes.

The key requirement for multiple genelet nodes to operate together or to be connected in larger networks is that the activator and repressor for each activation domain interact well with one another but not with other activators or repressors, *i.e.* off-target interactions are minimized. We estimate the number of such domains that could achieve specific action without crosstalk as follows:

In the current design, all of the activators and repressors must contain at least 5 complementary bases because each activator is required to have the 5 bases of the T7 RNAP promoter at its 5' end. To estimate the number of orthogonal activator/repressor pairs, we thus need to determine how many unique activator sequences there are that are sufficiently different from each other so that they won't interact with another activator's repressor.

In the HPC design, each activator and repressor contain two 8-base single-stranded domains that could facilitate a spurious interaction between an activator and another activator's repressor. For simplicity in

our estimation, we consider these domains as a single 16 base single-stranded region. Since each activator has to have the same TATTA sequence at the 5' end, there are only 11 free bases that can be changed in this single-stranded region. Naively, there are then 4^{11} unique activator sequences. Of course, two activators that are different by only a few bases will have enough complementarity with each other's repressors, so the true number of orthogonal HPC genelet sequences is much smaller.

To estimate how much crosstalk could be allowed, we used the NUPACK nucleic acid modeling software and tested the strength of potential interactions between a repressor and activator (see Supplementary Section 8.2 for NUPACK details). A series of trials of measuring these interactions suggests that two activators that contain the same 5 base sequence anywhere along this 11 base single stranded region will have significant crosstalk with each other's repressors, where significant crosstalk is defined, roughly, as >25% of an activator is predicted to be bound to an off target repressor at equilibrium when both species are present at 1 μM. Thus, a conservative estimate for the number of unique sequences would be the number of 11 base activator sequences that do not share any consecutive 5 base sequences.

To get an estimate for how many such sequences exist, we wrote a simple MATLAB algorithm to generate random pools of 11 base sequences that did not share any 5 base consecutive subsequences. Running this stochastic algorithm numerous times revealed libraries of 116-125 different activator sequences that fit this criterion.

Thus, in principle, on order 100 orthogonal genelets might be assembled into a network without significant crosstalk using the HPC design presented in this work. While this metric is conservative in terms of off-target interactions, there are other practical issues that were not considered that could mean some of the sequences could not be used in a circuit or would introduce undesired interactions by other means. For example, this analysis does not take secondary structure into account and some sequences might exhibit significant autoinhibition or slow reaction kinetics which could prohibit their use. However, even if 50-75% of the possible sequences are not viable, the HPC genelets should allow for 30-60 orthogonal genelet activation domains with low crosstalk to be designed.

It is worth contrasting this estimate with the sequence space available using the KWW genelet design without hairpins. For the KWW genelet design, all 35 bases of a DNA activator are single-stranded so we looked for pools of 30-base activator sequences that did not share any consecutive 5 base sequences to estimate the viable sequence space for the KWW design. Using the stochastic algorithm described above we found libraries of 16-19 activator sequences for the KWW design. Again, assuming only 25-50% of these sequences are experimentally viable, the KWW design could potentially allow for 5-10 orthogonal genelet activation domains. Based on this analysis the HPC genelet design could potentially increase the number of orthogonal genelet activation domains roughly 5 to 6-fold compared to the KWW genelet design.

The estimate of 5-10 possible orthogonal nodes for the KWW genelet design determined in the analysis above is consistent with the results of our NUPACK designs in Supplementary Section 8.4 where we were unable to obtain 6 activator/repressor pairs that did not have significant crosstalk or undesired secondary structure. To further compare the HPC genelet design to the KWW design, we used NUPACK to design 10 orthogonal HPC activator/repressor pairs as described in Supplementary Section 8.4. NUPACK found sequences for these 10 HPC activator/repressor pairs that were predicted to have a <1% normalized ensemble defect, indicating that the HPC design should in principle be much more scalable than the KWW genelet design.

8.7. Activation and repression of the prototype HPC genelets

For the prototype HPC genelets designed for the *i*BN-*u*A, activation and repression occur *via* a 4-way branch migration process compared to the 3-way branch migration activation and repression of the genelets in the *i*BN. Many 4-way branch migration reactions utilize two initiation toeholds, one on each side of the duplex to be invaded[34–36]. The activation and repression of the HPC genelets can be viewed similarly but with toeholds of length 8 and 0 bases[37]. For example, the activation of a HPC genelet is initiated *via* the 8-base toehold at the 5' end of the activator (termed the activation toehold) to invade the hairpin on the genelet (Supplementary Fig. 29a). The repression of a HPC genelet-activator complex is initiated *via* the 8-base toehold at the 3' end of the activator (termed the repression toehold). Repression begins as a 4-way branch migration process which converts to a 3-way branch migration process to ultimately remove the activator from the genelet (Supplementary Fig. 29a). We termed this process 4-way initiated 3-way branch migration[38]. The interaction between a free HPC activator and its corresponding repressor is initiated using both of the 8-base toeholds on the activator (Supplementary Fig. 29a). We found that the 4-way branch migration activation and repression of the HPC genelets worked as designed (Supplementary Fig. 29b,c).

We observed that the rate of HPC genelet repression can vary depending on the HPC activator sequence. For example, the repression kinetics of prototype HPC 2N were considerably slower than the repression kinetics of prototype HPC 1N (Supplementary Fig. 29). Given the free energy change of toehold binding is generally a better predictor of strand displacement reaction rates than toehold length alone[37,39], we theorized the difference in the rates of repression between the two HPC sequences was due to the lower GC content (and therefore the less negative free energy change of binding) of the 8-base repression toehold of dA_1u compared to that of dA_2u. To test whether the less negative free energy change of toehold binding for dA_1u was causing the slower repression rate of prototype HPC 2N compared to prototype HPC 1N, we replaced the 8-base repression toehold of dA_1u with the 8-base repression toehold of dA_2u and tested the activation and repression kinetics of prototype HPC 2N with this new activator/repressor pair. We found a significant increase in the repression rate of prototype HPC 2N when using the dA_1u variant with the dA_2u repression toehold (Supplementary Fig. 30c). We also designed another variant of dA_1u with a new 8-base repression toehold sequence that had a more negative free energy change of toehold binding than the original dA_1u repression toehold and tested its activation and repression kinetics with prototype HPC 2N. Again we found this dA_1u variant exhibited fast repression kinetics (Supplementary Fig. 30d). These results suggest that relatively fast activation and repression kinetics may be obtained for HPC genelets by selecting activator toeholds with moderate GC content.

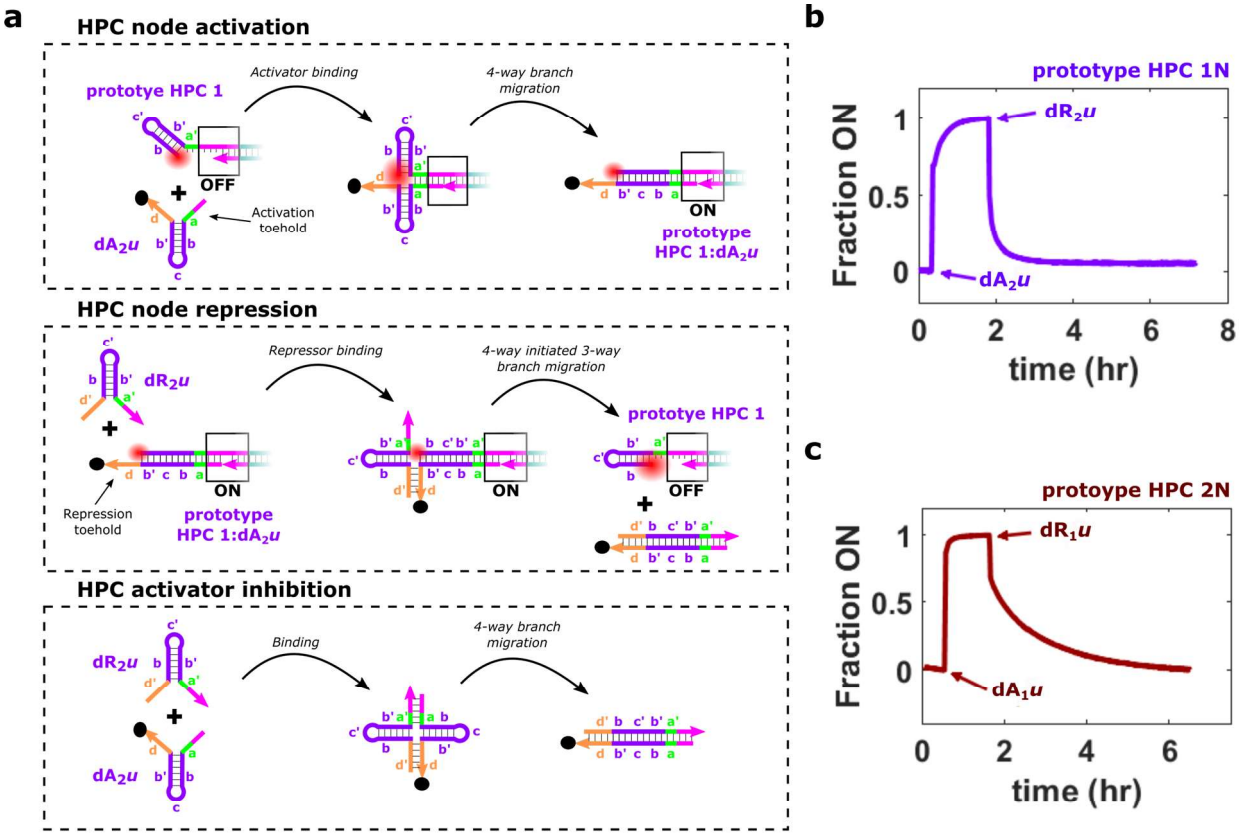

Supplementary Figure 29 | HPC genelets can be activated and repressed by their corresponding HPC activators and repressors. a, Reaction schemes for prototype HPC 1N activation and repression. Activation and repression proceed analogously for prototype HPC 2N. Letters on colored domains indicate sequence identity. A domain's complement is denoted with an apostrophe. **b**,**c**, Normalized activation levels during activation and repression of prototype HPC 1N (**b**) and prototype HPC 2N (**c**). Each node was activated *via* addition of its respective activator and subsequently repressed *via* addition of its respective DNA repressor. Activators and repressors were added at the times indicated by the labeled arrows to a final concentration of 500 nM and 1000 nM, respectively. Reactions were conducted in NEB RNAPol buffer with 1 mg/ml BSA, $MgCl_2$ at a final concentration of 20 mM, 5 mM of each NTP, and *[prototype HPC genelets]:* 100 nM. See Supplementary Section 12.2 for data normalization procedure for these experiments. Prototype HPC 1 and prototype HPC 2 were designed to test the HPC genelet design and have the same activator and repressor sequences as Induce 1 and Induce 2 used in the main text, respectively, but possess different sequences than Induce 1 and 2 downstream of the T7 RNAP promoter domain (sequences, Supplementary Table 1).

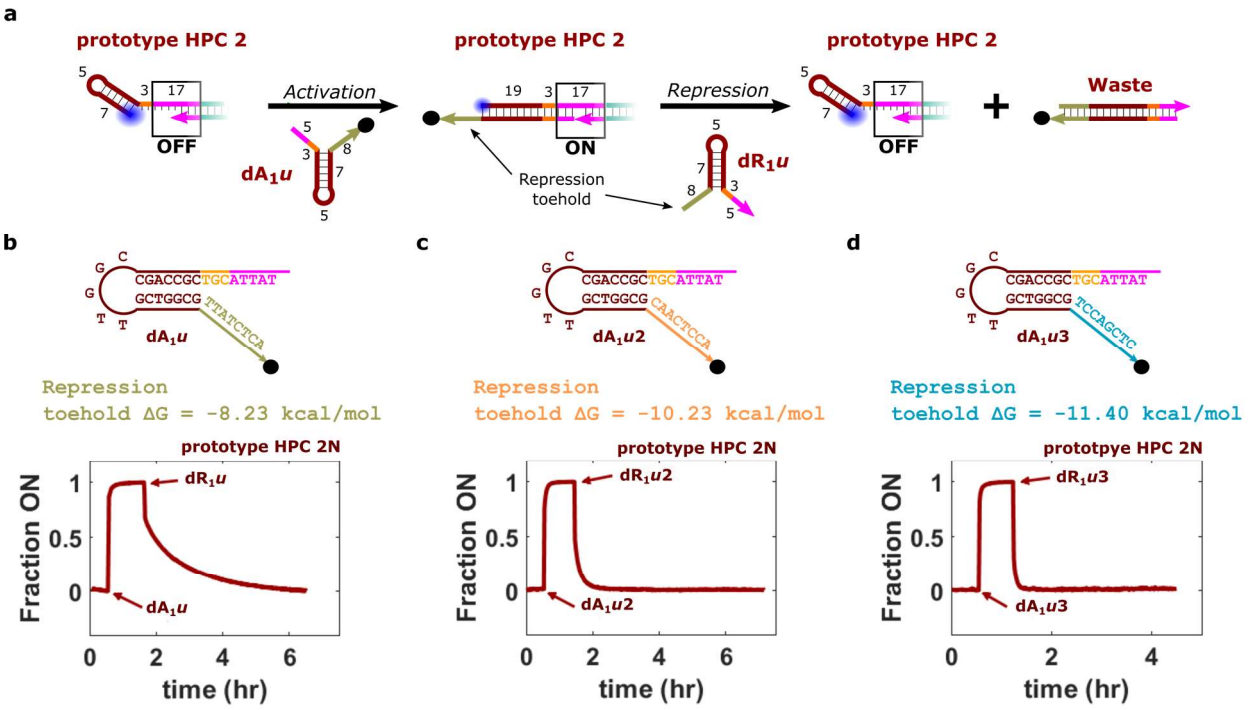

Supplementary Figure 30 | The rate of repression of HPC genelets increases with increasing binding strength of the repression toehold of the activators. a, Schematic of the genelet activation and repression experiment conducted in (**b**). The prototype HPC 2 genelet was activated by the addition of dA_1u and subsequently repressed by the addition of dR_1u. Similar experiments were conducted in (**c**) and (**d**) but using the activator variants shown above the plots and the corresponding DNA repressors complementary to those activators. **b**-**d**, Normalized genelet activation levels for activation and repression of prototype HPC 2N with dA_1u and dR_1u (**a**), dA_1u2 and dR_1u2 which contain the repression toeholds of dA_1u and dR_1u (**b**), and dA_1u3 and dR_1u3 which contain a repression toehold designed to have a large negative free energy change of toehold binding (*i.e.* strong binding) (**c**). The sequence of the activator and the free energy of the repression toehold (8 bases at the 3' end) are shown above the plots. Repression toeholds with more negative free energy changes of toehold binding result in lower rates of dissociation between an invading repressor and an activator bound to the genelet which increases the rate of 4-way branch migration[37]. Reactions were conducted in NEB RNAPol buffer with 1 mg/ml BSA, $MgCl_2$ at a final concentration of 20 mM, 5 mM of each NTP, *[prototype HPC 2]:* 100 nM, *[activators]:* 500 nM, and *[repressors]:* 1000 nM. See Supplementary Section 12.2 for data normalization procedure for these experiments. Prototype HPC 2 was designed to test the HPC genelet design and has the same activator and repressor sequences as Induce 2 used in the main text but possess a different sequence than Induce 2 downstream of the T7 RNAP promoter domain (sequences, Supplementary Table 1).

8.8. Autoinhibition of Induce 1N and Induce 2N

To determine the extent to which the autoinhibition behavior observed for Core 1N is general to genelets, we measured the degree of autoinhibition for the Induce 1N and Induce 2N nodes. To assess autoinhibition Induce 1N and Induce 2N were each incubated alone with T7 RNAP in transcription conditions. Induce 1N exhibited relatively little autoinhibition (<10% inactivation over 20 hours) and Induce 2N displayed a moderate amount of autoinhibition, about 50% inactivation over 20 hours (Supplementary Fig. 31). The autoinhibition of Induce 2N did not appear to affect the results of our experiments with the *i*BN-*u*A (Fig. 3 of the main text), likely because Induce 2N is only activated for a short time in these experiments and autoinhibition only becomes significant over longer timeframes. Additionally, the *i*BN-*u*A reactions also contain RNase H which can degrade autoinhibition products and additional transcriptional templates that likely reduce spurious T7 RNAP activity, limiting the autoinhibition that occurs during network operation. Thus in many cases moderate autoinhibition, as observed for Induce 2N, may not hinder network operation.

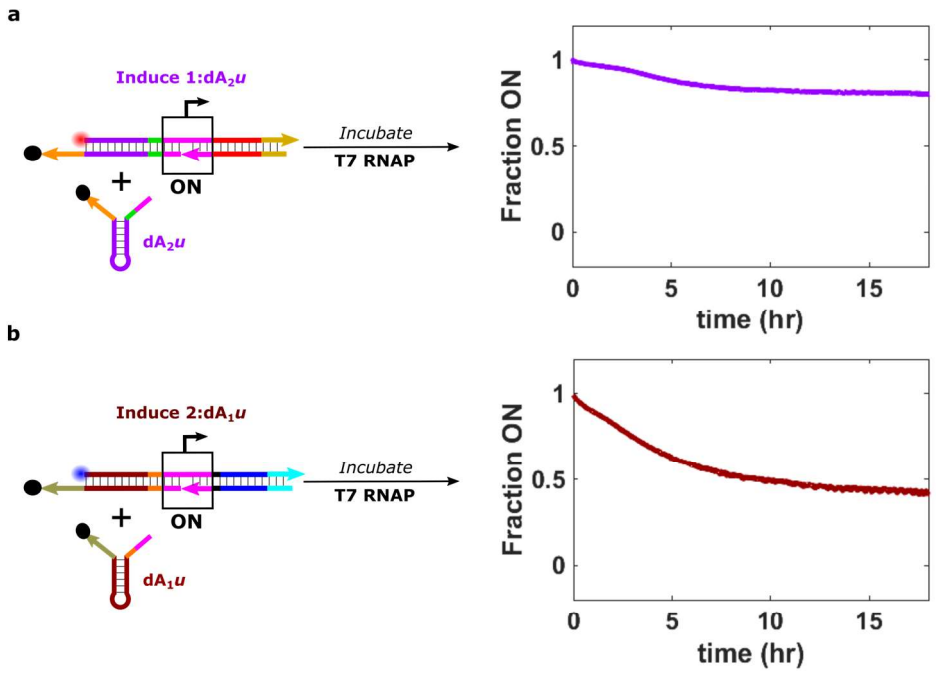

Supplementary Figure 31 | Autoinhibition of the Induce nodes. a, Normalized activation levels of Induce 1N during incubation with T7 RNAP as depicted in the schematic to the left of the plot. **b**, Normalized activation levels of Induce 2N during incubation with T7 RNAP as depicted in the schematic to the left of the plot. Reactions were conducted in NEB RNAPol reaction buffer with BSA, $MgCl_2$, and NTP concentrations as described in the Methods of the main text for the *i*BN. For both experiments: *[Induce 1] or [Induce 2]:* 100 nM, *[dA₂u] or [dA₁u]:* 1000 nM, and *[T7 RNAP]:* 4.82 U/µL.

8.9. Additional *i*BN-*u*A experiments

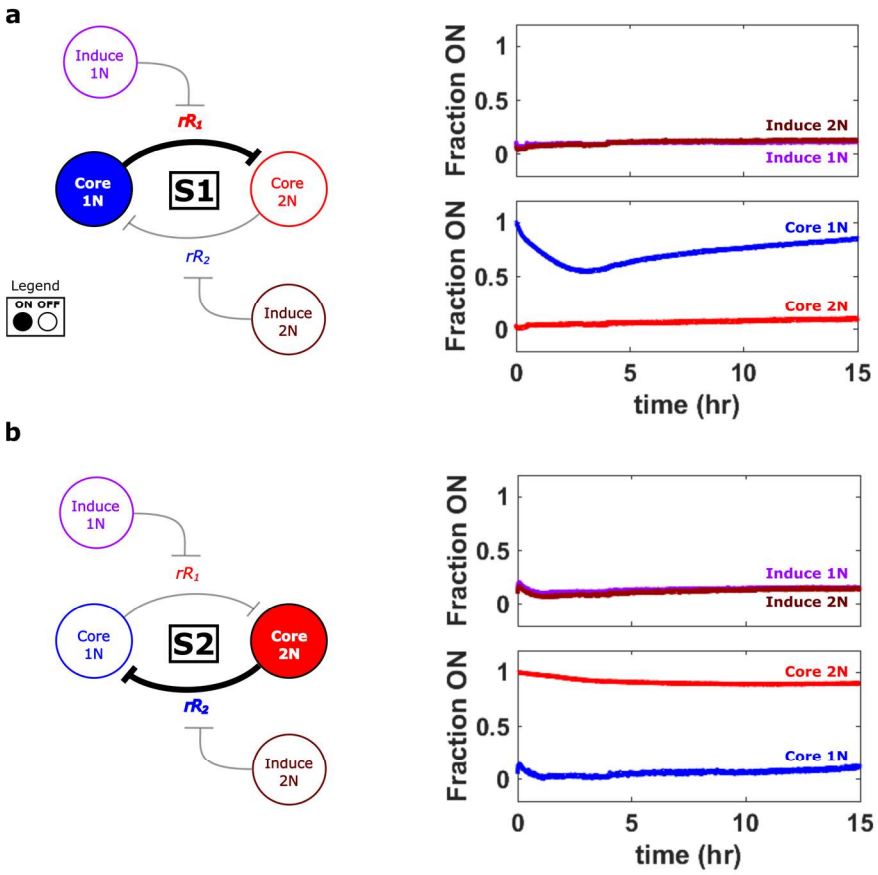

Supplementary Figure 32 | The *i*BN-*u*A is bistable. a,**b**, Normalized activation levels of network nodes of the *i*BN-*u*A after initialization in S1 (**a**) or S2 (**b**). Schematics of the state of the network at the start of each experiment are shown to the left of the plots. Reactions were conducted as described in the Methods of the main text for the *i*BN-*u*A. As seen with the *i*BN experiments, significant Core 1N autoinhibition was observed when the network was initialized in S1.

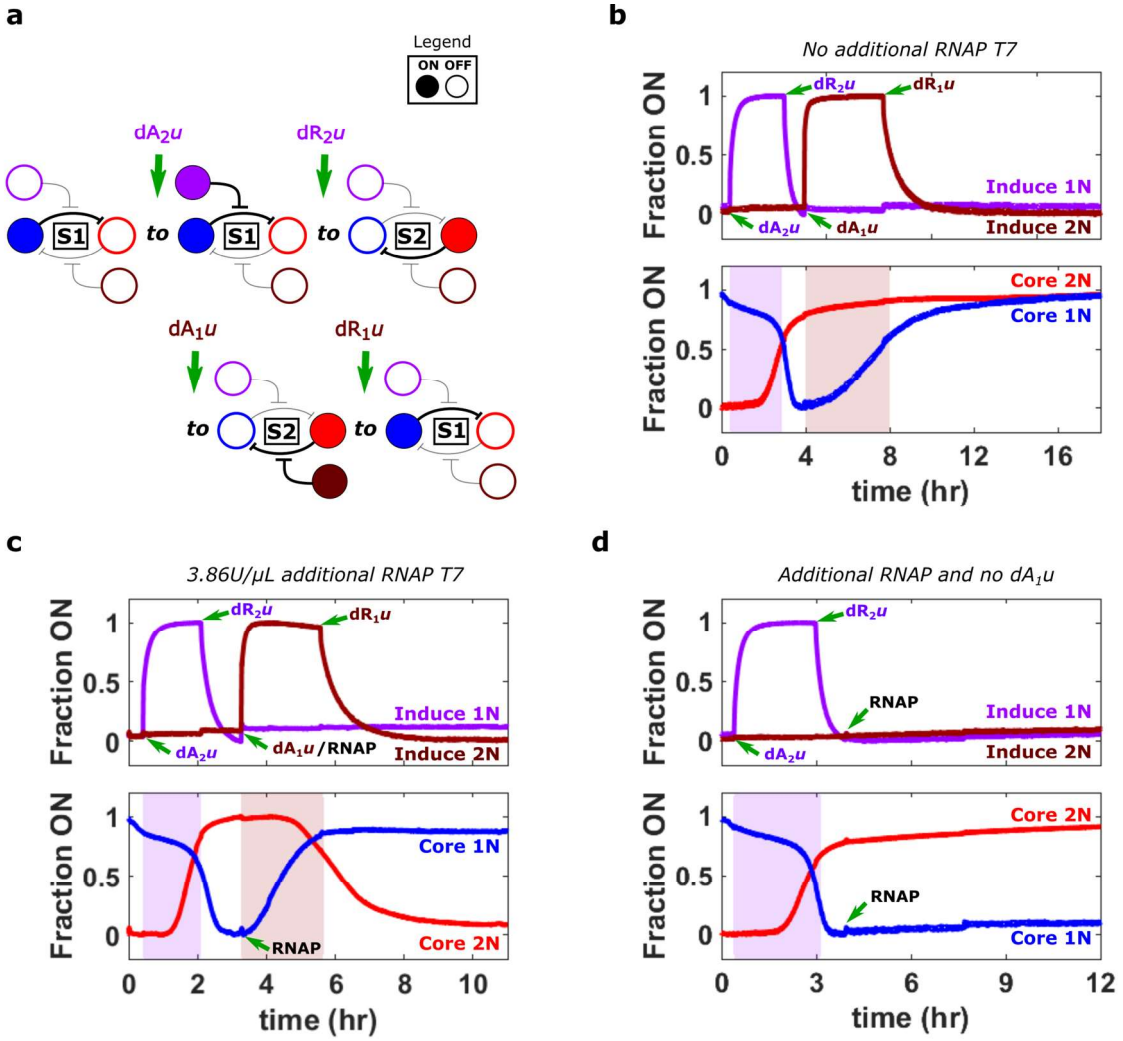

Supplementary Figure 33 | Additional T7 RNAP extends the transcriptional lifetime of the *i*BN-*u*A during two state changes without influencing network state. a, The set of steps used to switch the state of the *i*BN-*u*A from S1 to S2 then back to S1. **b**, Normalized activation levels of network nodes during an attempted switch from S1 to S2 then back to S1 without the addition of more RNAP. The first state change occurred as desired. During the second induced state change, Core 1N turned on after the addition of dA_1u but Core 2N did not turn off. To combat the negative effects of long reaction times on circuit function (Supplementary Section 5.2), we added additional T7 RNAP at the start of the second switch. **c**, Normalized activation levels of network nodes during a switch from S1 to S2 then back to S1 with an additional 3.86U/μL of T7 RNAP added when dA_1u was added. The additional polymerase enabled the second state switch. **d**, Normalized activation levels of network nodes during a control experiment to assess the effect of adding T7 RNAP on network state. The network was initialized in S1 and Induce 1N was turned on and then turned off as in (**a**) and (**b**), and then T7 RNAP (a total of 4.82 U/μL) was added 30 minutes after the network had completed switching to S2 (roughly the same time as when dA_1u was added in (**a**) and (**b**)). T7 RNAP alone did not change the activation levels of the network nodes. Shaded regions in the bottom plots indicate when the Induce nodes were on during the experiments. Reactions were otherwise conducted as described in the Methods section of the main text for the *i*BN-*u*A.

9. Kinetic model of the *i*BN-*u*A

9.1. Assumptions, reactions, and fitting procedure

Model assumptions:

The assumptions presented in Supplementary Section 7.1 were also made here when formulating the additional reactions for the Induce nodes.

Model reactions:

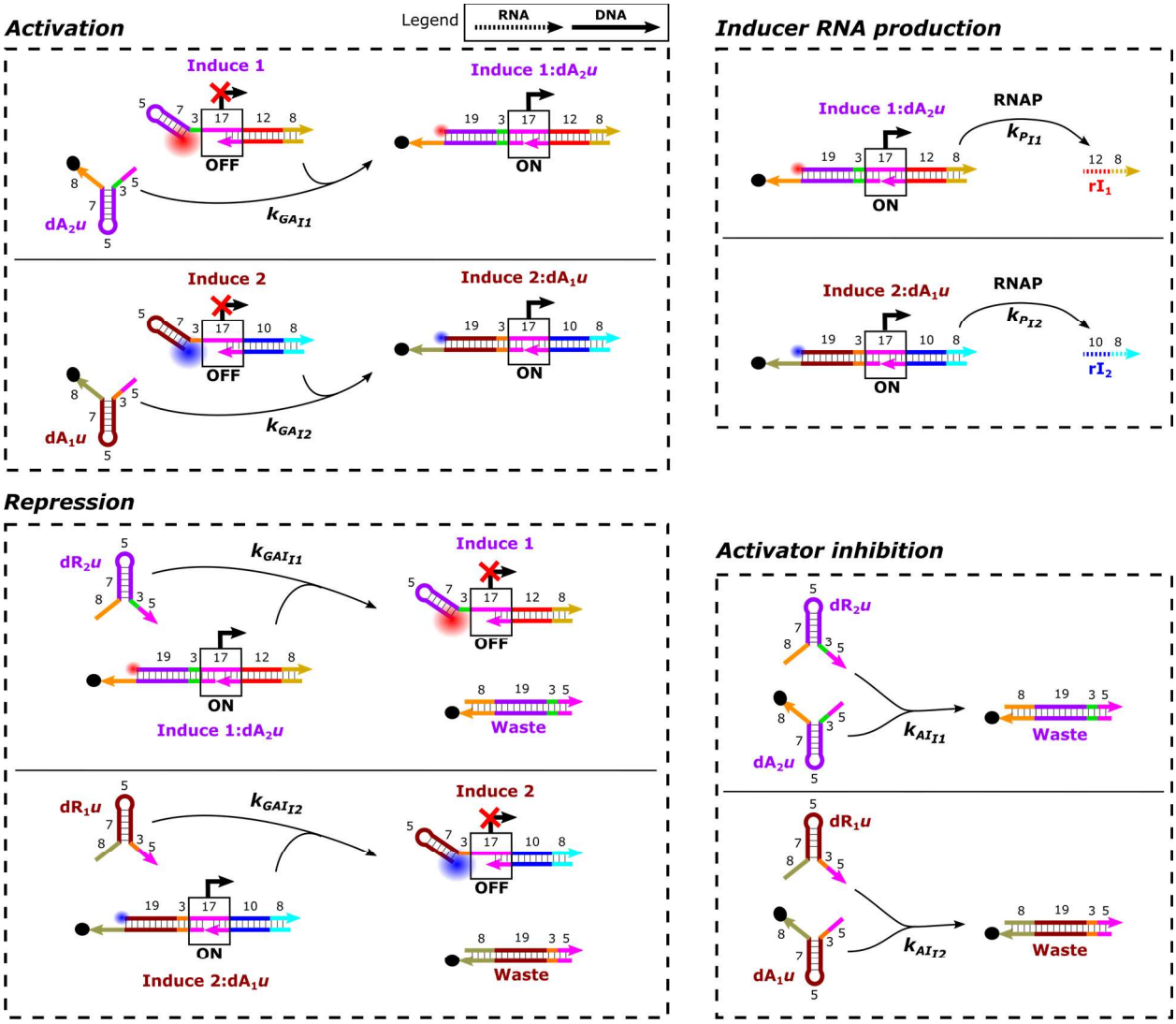

Supplementary Figure 34 | Reactions added to the kinetic model for the *i*BN (Supplementary Section 7) to create the kinetic model for the *i*BN-*u*A.

The mass action kinetic equations that were modified from or added to the kinetic model of the *i*BN to model the *i*BN-*u*A are shown below. **Bold** terms show equations or reaction terms added to the model of the *i*BN from Supplementary Section 7. Red terms show equations and reaction terms pertaining to Core 1N autoinhibition. The model of the *i*BN-*u*A also includes equations (7)-(20) presented in Supplementary Section 7 for the *i*BN except equations (13) and (14) are replaced with equations (21) and (22) below.

$$(21)\ \frac{d[rI_1]}{dt} = \mathbf{k_{P_{I1}}[Induce\ 1{:}dA_2u]} - k_{IIC_1}[rI_1][rR_1]$$

$$(22)\ \frac{d[rI_2]}{dt} = \mathbf{k_{P_{I2}}[Induce\ 2{:}dA_1u]} - k_{IIC_2}[rI_2][rR_2] - k_{IIC_2}[rI_2][rAI]$$

$$(23)\ \mathbf{\frac{d[Induce\ 1{:}dA_2u]}{dt} = k_{GA_{I1}}[Induce\ 1][dA_2u] - k_{GAI_{I1}}[Induce\ 1{:}dA_2u][dR_2u]}$$

$$(24)\ \mathbf{\frac{d[Induce\ 2{:}dA_1u]}{dt} = k_{GA_{I2}}[Induce\ 2][dA_1u] - k_{GAI_{I2}}[Induce\ 2{:}dA_1u][dR_1u]}$$

$$(25)\ \mathbf{\frac{d[dA_1u]}{dt} = -k_{GA_{I2}}[Induce\ 2][dA_1u] - k_{AI_{I2}}[dA_1u][dR_1u]}$$

$$(26)\ \mathbf{\frac{d[dA_2u]}{dt} = -k_{GA_{I1}}[Induce\ 1][dA_2u] - k_{AI_{I1}}[dA_2u][dR_2u]}$$

$$(27)\ \mathbf{\frac{d[dR_1u]}{dt} = -k_{GAI_{I2}}[Induce\ 2{:}dA_1u][dR_1u] - k_{AI_{I2}}[dA_1u][dR_1u]}$$

$$(28)\ \mathbf{\frac{d[dR_2u]}{dt} = -k_{GAI_{I1}}[Induce\ 1{:}dA_2u][dR_2u] - k_{AI_{I1}}[dA_2u][dR_2u]}$$

Mass balances are used to infer the concentrations of some of species in equations (21)-(28) over time:

$$(29)\ \mathbf{[Induce\ 1] = [Induce\ 1]_{TOTAL} - [Induce\ 1{:}dA_2u]}$$

$$(30)\ \mathbf{[Induce\ 2] = [Induce\ 2]_{TOTAL} - [Induce\ 2{:}dA_1u]}$$

Supplementary Table 5 | Additional modeling parameters to fit for the kinetic model of the *i*BN-*u*A

Induce 1N	Induce 2N
$k_{P_{I1}}$ (s^{-1})	$k_{P_{I2}}$ (s^{-1})
$k_{AI_{I1}}$ $(M^{-1}s^{-1})$	$k_{AI_{I2}}$ $(M^{-1}s^{-1})$
$k_{GA_{I1}}$ $(M^{-1}s^{-1})$	$k_{GA_{I2}}$ $(M^{-1}s^{-1})$
$k_{GAI_{I1}}$ $(M^{-1}s^{-1})$	$k_{GAI_{I2}}$ $(M^{-1}s^{-1})$

Model fitting procedure:

The goal for developing a model for the *i*BN-*u*A was to validate our design approach where the model for the *i*BN was expanded to predict the behavior of the *i*BN-*u*A to aid in this network's design. From a network design perspective it is desirable to be able to individually characterize the behavior of smaller motifs in a larger network prior to constructing the overall network, but this approach is only valid if the behavior of the smaller motifs in isolation translates to their behavior in larger networks. Thus, to investigate if our model of the *i*BN in isolation was consistent with the behavior of the *i*BN in the *i*BN-*u*A we extended our kinetic model to include the reactions for the Induce nodes of the *i*BN-*u*A. We then asked if the rate parameters obtained for the *i*BN in isolation could be used to recapitulate our experimental results for the *i*BN-*u*A.

The model of the *i*BN-*u*A contained 8 more parameters (Supplementary Table 5) than the model of the *i*BN did. These 8 additional parameters were fit using the two experimental datasets shown in Fig. 3c,d of the main text while the 15 parameters from the kinetic model for the *i*BN in isolation (Supplementary Table 4) were maintained during the fitting process. The parameter fitting procedure was conducted as described for the kinetic model of the *i*BN (Supplementary Section 7.1) with the 8 parameters constrained to be within reasonable ranges (Supplementary Table 6) during the fitting. The objective function for these fits minimized the sum of squared errors between the simulated and the experimental activation levels of Core 1N and Core 2N and the Induce node that was turned on to switch states in a given experiment (the Induce node that was off over the course of the experiment was not considered in the objective function since this data contained no dynamics to inform the fitting). The final parameters of this fit are given in Supplementary Table 7 in bold and the model fit to the experimental data is shown in Fig. 3c,d of the main text. The model of the *i*BN-*u*A shows good agreement with the experimental dynamics of the network. Additionally, the significant autoinhibition that was experimentally observed for Core 1N when the network was initialized in S1 is captured. These results indicate our model and rate parameters for the *i*BN are consistent with the behavior of the expanded *i*BN-*u*A network.

The fitted parameters for the activation and repression of the HPC genelets fall within an expected range based on studies of similar 4-way branch migration reactions[37]. The rate parameters for the reactions between the free activators and the free repressors ($\mathrm{k_{AI}}$'s) have large error bounds, which is reasonable given the datasets used for the fitting. We only directly measured the rate of removal of the activator from the genelet-activator complex in the *i*BN-*u*A experiments; these experiments did not contain any explicit information about the rates at which the free repressors and free activators react. So we would expect to have low confidence in the values of $\mathrm{k_{AI}}$ for the HPC nodes. Likely a range of values for $\mathrm{k_{AI}}$ would fit the repression kinetics equally well and additional experiments characterizing the direct kinetics between the free activators and their repressors would be needed if more confidence in the parameter values were desired.

9.2. Rate parameters for the kinetic model of the *i*BN-*u*A

Supplementary Table 6 | Parameter bounds for fitting the model parameters of the *i*BN-*u*A.

Parameters	Min	Max
k_P (s^{-1})	$1.0x10^{-6}$	$1.0x10^{-1}$
k_{GA} ($M^{-1}s^{-1}$)	$1.0x10^{1}$	$1.0x10^{6}$
k_{GAI} ($M^{-1}s^{-1}$)	$1.0x10^{0}$	$1.0x10^{6}$
k_{AI} ($M^{-1}s^{-1}$)	$1.0x10^{0}$	$1.0x10^{6}$

Supplementary Table 7 | Fit model parameters for the kinetic model of the *i*BN-*u*A. The bold parameters were fit using the *i*BN-*u*A data in Fig. 3c,d from the main text. The remaining parameters were taken from the fitting of the *i*BN (Supplementary Section 7). Parameter ranges indicate 95% confidence intervals.

Parameters	Core 1N	Core 2N	Induce 1N	Induce 2N
k_P (s^{-1})	$4.50\pm0.03 \times 10^{-3}$	$2.23\pm0.15 \times 10^{-3}$	$\mathbf{8.54\pm0.12 \times 10^{-4}}$	$\mathbf{4.55\pm0.04 \times 10^{-4}}$
k_D (s^{-1})	$6.14\pm0.33 \times 10^{-5}$	$6.78\pm0.40 \times 10^{-5}$	– –	– –
k_{GA} ($M^{-1}s^{-1}$)	$3.37\pm0.33 \times 10^{4}$	$1.32\pm0.07 \times 10^{4}$	$\mathbf{4.88\pm0.54 \times 10^{3}}$	$\mathbf{1.24\pm0.22x\ 10^{4}}$
k_{GAI} ($M^{-1}s^{-1}$)	$5.79\pm1.7 \times 10^{4}$	$1.12\pm0.16 \times 10^{5}$	$\mathbf{2.10\pm0.36 \times 10^{3}}$	$\mathbf{5.64\pm0.27 \times 10^{2}}$
k_{AI} ($M^{-1}s^{-1}$)	$3.87\pm0.85 \times 10^{4}$	$1.00\pm0.29 \times 10^{3}$	$\mathbf{0.472\pm1.6 \times 10^{3}}$	$\mathbf{0.025\pm2.3 \times 10^{6}}$
k_{IIC} ($M^{-1}s^{-1}$)	$4.29\pm0.77 \times 10^{3}$	$7.13\pm0.91 \times 10^{4}$	– –	– –
$k_{P_{AI1}}$ (s^{-1})	$7.43\pm0.11 \times 10^{-5}$	– –	– –	– –
$k_{P_{AI2}}$ (s^{-1})	$6.04\pm0.24 \times 10^{-4}$	– –	– –	– –
$k_{R_{AI}}$ ($M^{-1}s^{-1}$)	$1.62\pm0.36 \times 10^{5}$	– –	– –	– –

10. Mitigating Core 1N autoinhibition by blocking the 3' end of dA_2

Our results in Supplementary Section 6 suggested that autoinhibition of Core 1N is the result of the non-specific production of an RNA species (rAI), whose sequence is similar to the repressor of Core 1N (rR_2) that removes dA_2 from Core 1:dA_2. These results suggest there are likely two pathways for the production of rAI, with one pathway being the transcription of free dA_2 (Supplementary Fig. 20) and another pathway in which the transcription of rAI is independent of free dA_2 (Supplementary Fig. 21). We theorized that the pathway that is independent of free dA_2 might involve initiation of transcription at the single-stranded 3' end of dA_2 in the Core 1:dA_2 complex based on precedent in the literature[24,25]. If transcription initiated at the 3' end of dA_2 in the Core 1:dA_2 complex, we reasoned that sequestering the single-stranded 3' end of dA_2 in a double-stranded DNA domain might decrease the rate of autoinhibition by blocking the initiation of non-specific transcription at this site. To test this hypothesis, we extended the 3' end of dA_2 by 21 bases (termed "extended dA_2" in Supplementary Table 1) and added another strand (termed "quenched blocker" in Supplementary Table 1) complementary to 20 bases of this extended region to sequester the 3' end of the activator in dsDNA. We termed this modified activator blocked dA_2. The use of blocked dA_2 in place of dA_2 markedly decreased Core 1N autoinhibition (Supplementary Fig. 35). Blocked dA_2 was thus used in place of dA_2 in the *i*BN-*u*A-*d*SP (Fig. 4 of the main text) and the *i*BN-*u*AFO-*d*SPC (Fig. 5 of the main text) experiments.

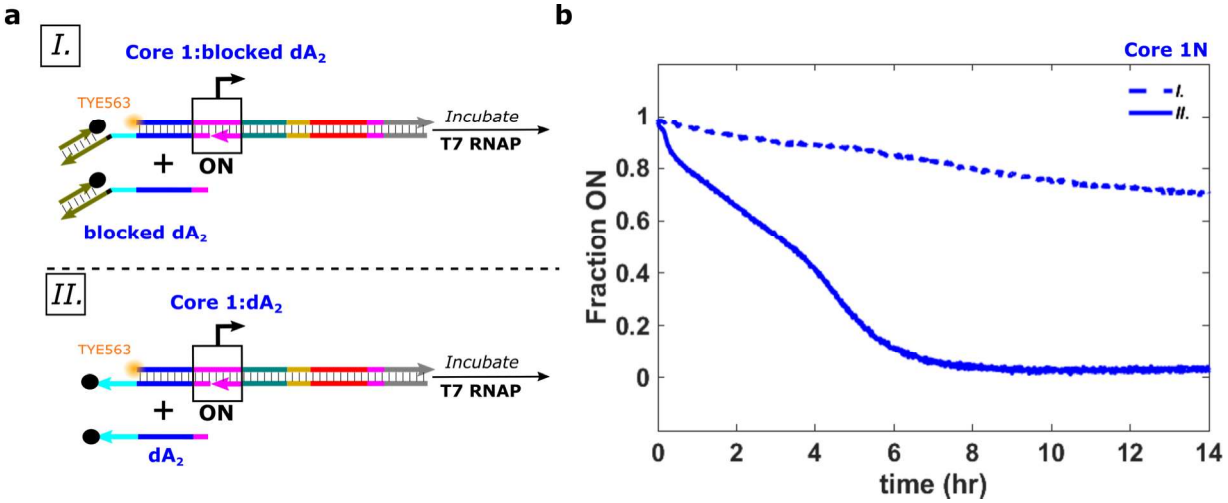

Supplementary Figure 35 | Blocked dA_2, which contains a double-stranded domain at its 3' end, mitigates Core 1N autoinhibition. a, Diagram of the experiments presented in (**b**). **b**, Normalized activation levels of the Core 1N variants shown in (**a**) during individual incubation with T7 RNAP. Reactions were conducted in NEB RNAPol reaction buffer with BSA, $MgCl_2$, and NTP concentrations as described in the Methods of the main text for the *i*BN. For both experiments the genelets were at 100 nM and the activators were at 1000 nM. Blocked dA_2 was prepared prior to the experiment by cooling an equimolar amount of the quenched blocker strand with the extended dA_2 strand from 90°C to 20°C at a rate of -1°C/min in NEB RNAPol reaction buffer.

11. Additional *i*BN-*u*A-*d*SP and *i*BN-*u*AFO-*d*SPC experiments

11.1. Steady state behavior of *i*BN-*u*A-*d*SP in both stable states

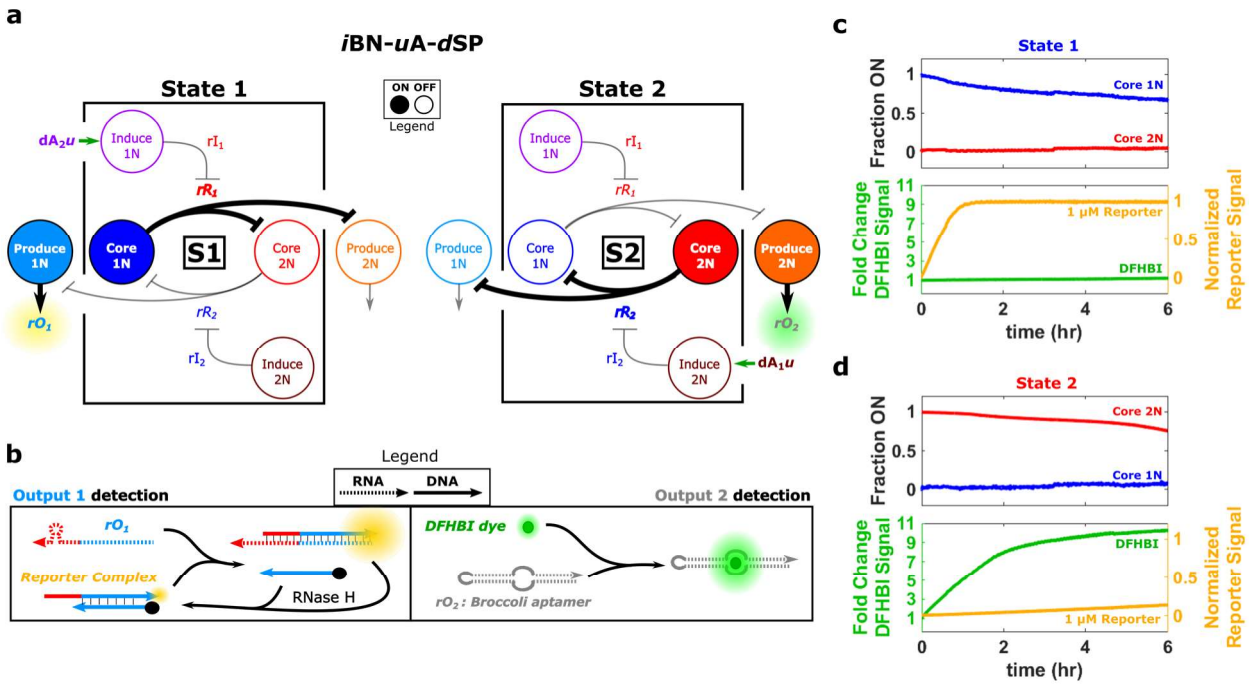

Supplementary Figure 36 | The steady state behavior of *i*BN-*u*A-*d*SP in S1 and S2. a, Architecture of the *i*BN-*u*A-*d*SP in each stable state. The *i*BN-*u*A (boxed) is connected to downstream Produce nodes that encode distinct RNA outputs. State changes are induced by activating the respective Induce node (indicated by the green arrows). **b**, Reactions used to detect the Produce nodes' RNA production. rO_1 was detected *via* displacement of a quenching strand in a dsDNA fluorophore-quencher reporter complex and rO_2 (the Broccoli aptamer) was detected *via* binding of the DFHBI fluorescent dye[19]. Sequences, Supplementary Table 1. **c**,**d**, Normalized activation levels of network nodes (top plots) and accumulation of reporting signals (bottom plots) in S1 (**c**) or S2 (**d**).

11.2. Two state changes of the *i*BN-*u*AFO-*d*SPC

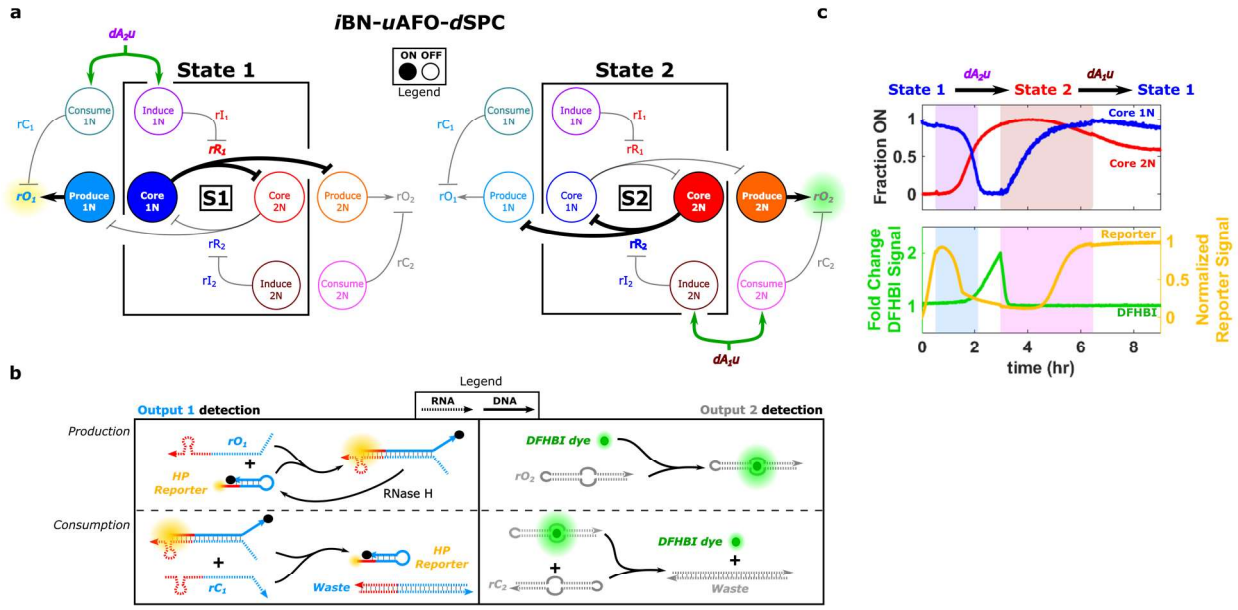

Supplementary Figure 37 | An attempt at two state changes with the *i*BN-*u*AFO-*d*SPC. a, Architecture of the *i*BN-*u*AFO-*d*SPC in each stable state. Paired Consume and Induce nodes are activated by the same input signal that initiates a state change (green arrows). **b**, Reactions used to detect production and consumption of the two downstream RNA signals. rO_1 was detected with a hairpin DNA reporter complex and rO_2 (the Broccoli aptamer) was detected *via* binding of the DFHBI fluorescent dye. Fluorescence increases or decreases as signal concentration increases or decreases respectively. Sequences, Supplementary Table 1. **c**, Normalized activation levels of network nodes (top plots) and RNA reporting signals (bottom plots) during an attempted switch from S1 to S2 to S1. Shaded regions in the plots indicate when the Induce nodes (top plots) and Consume nodes (bottom plots) were ON during the experiments. Activators and repressors used to initiate the state changes were added to a final concentration of 1 µM and 1.5 µM, respectively. In this experiment, as in Supplementary Fig. 33, we added additional T7 RNAP at the start of the second switch (a total of 7.71 U/µL T7 RNAP was added 30 minutes after the addition of dA_1u). Even with the additional polymerase, Core 2N was not completely turned off and the second state change could not fully complete. The downstream signals did complete the second state change, possibly because the total concentration of the rO_1 reporter complex was only 4.3 times that of the Produce 1 genelet (compared to the activator (dA_1) of Core 2N which was in 10-fold excess of the Core 1 genelet) (Supplementary Section 1.2 for concentrations of all species). The shorter operation time of the *i*BN-*u*A-*d*SPC compared to the *i*BN-*u*A (Supplementary Fig. 33) could be due to the *i*BN-*u*A-*d*SPC's higher total concentration of transcription templates which might lead to faster build-up of transcription waste products that negatively affect circuit reactions[15,16] (Supplementary Fig. 12).

12. Data normalization

All of the network reactions were conducted as described in the Methods of the main text where initial fluorescence readings were taken prior to setting the initial state of the network and adding the enzymes to start the reactions. These initial measurements served as a reference for the minimum fluorescence values of Core 1N and Core 2N. Additionally, DNA complements of dA_1 and dA_2 (dR_1s and dR_2s, respectively) were added in excess at the end of the experiments. Fluorescence measurements taken after the addition of dR_1s and dR_2s served as a reference for the maximum fluorescence values of Core 1N and Core 2N over the course of the experiments. The procedures used to normalize the experimental data are described below.

12.1. Experiments with the *i*BN

Default normalization procedure

The majority of the fluorescence data presented for the *i*BN was normalized as described below. Exceptions to this procedure are described in subsequent sections.

First, the fluorescence data for the two nodes (Core 1N or Core 2N) in the *i*BN were normalized as:

$$(31)\ \text{Normalized Fluorescence} = \frac{\text{data} - \min(\text{data})}{\max(\text{data}) - \min(\text{data})}$$

Where *data* is the fluorescence data obtained over an entire experiment (including the data obtained prior to setting the initial network state and after the addition of dR_1s and dR_2s) for Core 1N or Core 2N.

Second, since higher fluorescence values correspond to a higher fraction of a node in an OFF state, the normalized fluorescence was converted to node activation levels (Fraction ON):

$$(32)\ \text{Fraction ON} = 1 - \text{Normalized Fluorescence}$$

Switching network states twice

For the experiments where the state of the *i*BN was switched twice (Supplementary Fig. 10 and Fig. 2c of the main text) the fluorescence data was normalized in two parts. This was done to account for changes in the minimum and maximum fluorescence values of the network nodes over the course of these experiments. For example, the maximum fluorescence value for Core 2N at the end of these experiments (after adding an excess of dR_1s to turn Core 2N completely off) was about 10% lower than the maximum fluorescence value obtained at the beginning of the experiments when rR_1s was added to initialize the network in S1 (Supplementary Fig. 38a). This drop in the maximum fluorescence was likely due to a combination of dilution and DNA binding to the pipette tips from the addition and mixing of the enzymes, the inducer RNAs, and the DNA repressors over the course of the experiment and is consistent with previous observations for genelet circuits[3,7]. Accounting for these small changes in fluorescence intensities in our data was important since these data sets were included in the fitting of the rate parameters for the kinetic model of the *i*BN. Since the goal of our model was to be able to quantitatively capture network behavior to inform further network design we did not want the rate parameters to reflect artifacts in our measurements.

To account for any changes in the absolute range of fluorescence intensity in these two state change experiments we normalized the data in two parts, considering only the data of a single state change in each normalization (using equation (31)). Thus the data shown in Region 1 (corresponding to switching from S1 to S2) in Supplementary Fig. 38b was normalized using only the data in that region and the data in Region 2 (which corresponds to switching from S2 to S1 and the rest of the experiment – including the addition of dR_1S and dR_2S at the end of the experiment) in Supplementary Fig. 38b was normalized using only the data in that region. This two-part normalization accounts for the change in maximum fluorescence obtained for Core 2N at the end of the experiment and only marginally changes the data collected for Core 1N (less than 6% change in final Fraction ON for the two-part normalization compared to a single normalization of all the data) (Supplementary Fig. 38b).

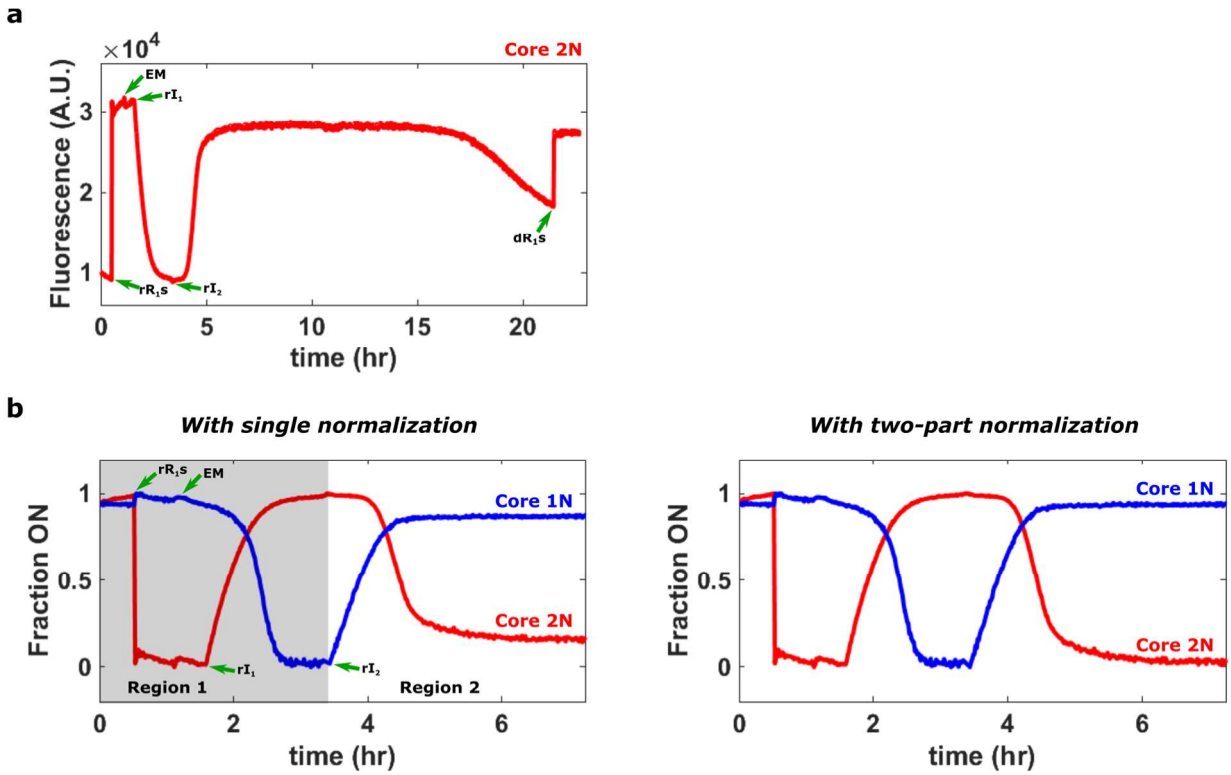

Supplementary Figure 38 | Representative example of normalization for the *i*BN experiments where the network state was switched from S1 to S2 then back to S1. a, The raw fluorescence data collected for Core 2N over the course of the experiment. Green arrows indicate the addition of different components. rR_1S was added first to set the network in S1, a mixture containing the enzymes for the reaction (EM) was then added, rI_1 and rI_2 were then sequentially added to switch the states of the network. dR_1S was added to obtain a reference for the maximum fluorescence of Core 2N at the end of the experiment. **b**, Comparison of the data normalized with the two-part normalization procedure (right plot) to all the data with a single normalization (left plot). The two regions of the data used in the two-part normalization are shown. Region 2 also extends to the end of the experiment (about 24 hours as shown in (**a**)).

12.2. Experiments with the *i*BN-*u*A

Induce nodes

The fluorescence data for the Induce nodes in the *i*BN-*u*A experiments was normalized in two parts to account for a change in the maximum fluorescence intensity after the addition of the quencher-modified HPC activators used to switch states. The addition of quencher-modified species to a fluorescent sample can alter the fluorescence intensity of the sample even without specific localization of the fluorescent and quencher species through a mechanism known as the inner filter effect[40]. At the beginning of the *i*BN-*u*A experiments, no HPC activators were in the samples and the Induce nodes had a high fluorescence. Upon subsequent activation and repression of an Induce node to switch states, the maximum fluorescence of the Induce node was less than the fluorescence obtained at the beginning of the experiment in the absence of any of its quencher-modified activator. Since an excess of the HPC repressors were used in these experiments, this difference in maximum fluorescence intensity was presumably due to the inner filter effect brought about by the addition of the quencher-modified activator. To correct for this effect in our normalization procedure we normalized Induce node activation and repression separately. Induce node activation (shown as Region 1 in Supplementary Fig. 39) was normalized (with equation (31)) using just the data contained within that region and Induce node repression (shown as Region 2 in Supplementary Fig. 39) was normalized using just the data in that region (with equation (31)). This process accounts for the different maximum intensity values of the Induce nodes prior to activation and after repression, accounting for the inner filter effect.

Core nodes of the *i*BN

The addition of quencher-modified species could also influence the fluorescence intensity values obtained for the nodes of the *i*BN depending on which quencher species is added. For example, dA_2u is modified with the dark quencher Iowa Black RQ which will absorb light over a range of wavelengths that include the excitation and emission wavelengths of the fluorophore on Core 2 (TYE665). Indeed, when dA_2u was added to switch the network from S1 to S2, a drop in the fluorescence of Core 2N was observed. Similarly, dA_1u is modified with the dark quencher Black Hole Quencher 1 which absorbs light over wavelengths that include the excitation and emission of the fluorophore on Core 1 (TYE563) and a drop in the fluorescence of Core 1N was observed when dA_1u was added to switch the network from S2 to S1 (Supplementary Fig. 39). These drops in fluorescence were not due to spurious interactions between the HPC activators and the genelets in the *i*BN (Supplementary Fig. 28) and were presumably due to the inner filter effect[40].

To correct for the effect of adding dA_2u on the fluorescence intensity of Core 2N when switching from S1 to S2, the fluorescence data for Core 2N was normalized in two parts, using either the data from before the addition of dA_2u or the data after the addition of dA_2u (Region 1 and Region 2, respectively in Supplementary Fig. 39b). Similarly, when switching from S2 to S1 the fluorescence data for Core 1N was normalized in two parts using either the data prior to or after the addition of dA_1u (Regions 1 and 2, respectively in Supplementary Fig. 39d). Equation (31) was used for each normalization.

For the experiments with the *i*BN-*u*A where two state changes were induced, the above procedures were performed in a similar manner sequentially with the exception that Core 2N was normalized as described in Supplementary Section 12.1 after the addition of dA_2u to account for the aforementioned

drop in Core 2N maximum fluorescence value after the numerous addition and mixing steps for two state changes.

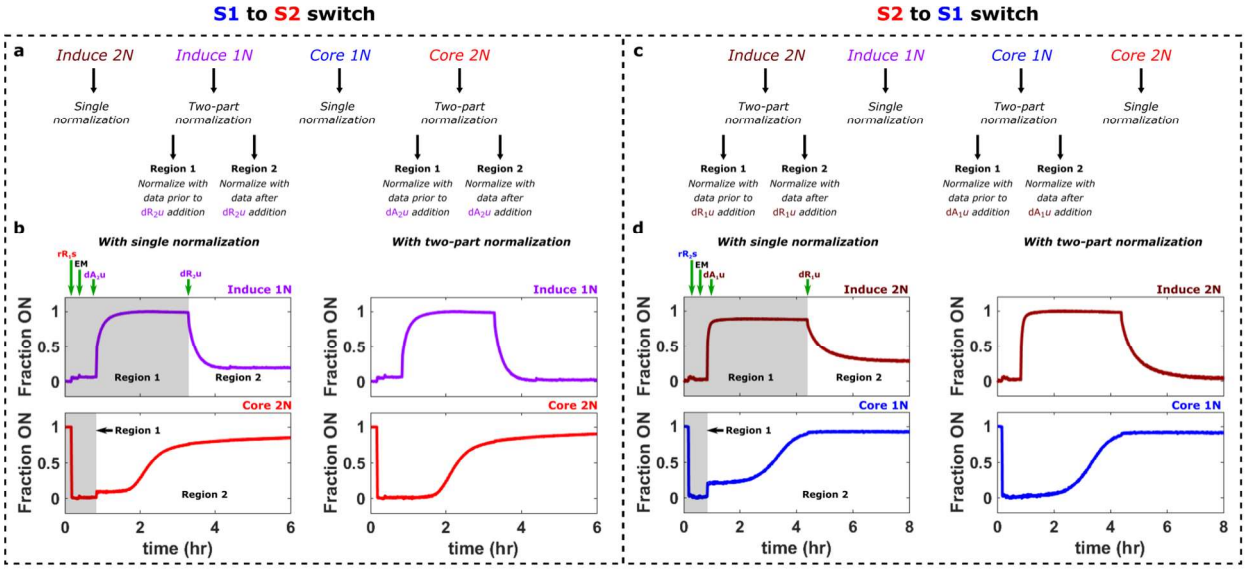

Supplementary Figure 39 | Normalization procedure for the fluorescence data obtained in the *i*BN-*u*A experiments. a, When switching the network from S1 to S2 (where dA_2u was added to switch states) the data for Induce 1N and Core 2N were normalized in two parts using the data in Region 1 in the first normalization and Region 2 in the second (regions shown in **b**). **b**, Comparison of the normalization of Induce 1N and Core 2N with the two-part normalization procedure and a single normalization of all the data. The two regions of the data used in the two-part normalization are shown. Region 2 also extends to the end of the experiment. **c**, When switching the network from S2 to S1 (where dA_1u is added to switch states) the data for Induce 2N and Core 1N were normalized in two parts using the data either in Region 1 or Region 2 (regions shown in **d**). **d**, Comparison of the normalization of Induce 2N and Core 1N with the two-part normalization procedure and a single normalization of all the data. The two regions of the data used in the two-part normalization are shown. Region 2 also extends to the end of the experiment.

12.3. Experiments with the *i*BN-*u*A-*d*SP and *i*BN-*u*AFO-*d*SPC

Normalization of activation levels of the nodes of the *i*BN

In the experiments with the *i*BN-*u*A-*d*SP and *i*BN-*u*AFO-*d*SPC, dA_1u and dA_2u were still modified with quenchers so the normalization procedures described in Supplementary Section 12.2 and Supplementary Fig. 39 were applied to the fluorescence data obtained for Core 1N and Core 2N in these experiments.

Normalization of the reporting signals for rO_1 and rO_2

For the rO_1 reporters, 5x excess of a DNA version of rO_1 (dO_1) was spiked into the samples at the end of the experiments to obtain a reference for the maximum signal of the reporter complex and the entire reporter fluorescence data set (including the addition of dO_1) was normalized as:

$$(33)\ \text{Normalized Reporter Signal} = \frac{\text{Reporter data} - \min(\text{Reporter data})}{\max(\text{Reporter data}) - \min(\text{Reporter data})}$$

For the DFHBI dye signal, the data was normalized against the minimum fluorescence values obtained over the course of the experiment (including the data collected prior to the addition of enzymes to start the reactions):

$$(34)\ \text{Fold Change DFHBI Signal} = \frac{\text{DFHBI data}}{\min(\text{DFHBI data})}$$

References

1. Milligan, J. F., Groebe, D. R., Witherell, G. W. & Uhlenbeck, O. C. Oligoribonucleotide synthesis using T7 RNA polymerase and synthetic DNA templates. *Nucleic Acids Res.* **15**, 8783–8798 (1987).
2. Kuzmine, I., Gottlieb, P. A. & Martin, C. T. Binding of the priming nucleotide in the initiation of transcription by T7 RNA polymerase. *J. Biol. Chem.* **278**, 2819–2823 (2003).
3. Kim, J., White, K. S. & Winfree, E. Construction of an in vitro bistable circuit from synthetic transcriptional switches. *Mol. Syst. Biol.* **2**, 68 (2006).
4. Alon, U. Network motifs: theory and experimental approaches. *Nat. Rev. Genet.* **8**, 450–461 (2007).
5. Gardner, T. S., Cantor, C. R. & Collins, J. J. Construction of a genetic toggle switch in Escherichia coli. *Nature* **403**, 339–342 (2000).
6. Kim, J., Hopfield, J. & Winfree, E. Neural network computation by in vitro transcriptional circuits. in *Advances in Neural Information Processing Systems 17* (eds. Saul, L. K., Weiss, Y. & Bottou, L.) 681–688 (MIT Press, Boston, MA, 2005).
7. Franco, E. *et al.* Timing molecular motion and production with a synthetic transcriptional clock. *Proc. Natl. Acad. Sci. USA* **108**, E784–E793 (2011).
8. Cuba Samaniego, C., Giordano, G., Kim, J., Blanchini, F. & Franco, E. Molecular titration promotes oscillations and bistability in minimal network models with monomeric regulators. *ACS Synth. Biol.* **5**, 321–333 (2016).
9. Zadeh, J. N. *et al.* NUPACK: Analysis and design of nucleic acid systems. *J. Comput. Chem.* **32**, 170–173 (2011).
10. Kim, J. & Winfree, E. Synthetic in vitro transcriptional oscillators. *Mol. Syst. Biol.* **7**, 465 (2011).
11. Weitz, M. *et al.* Diversity in the dynamical behaviour of a compartmentalized programmable biochemical oscillator. *Nat. Chem.* **6**, 295–302 (2014).
12. Lima, W. F. & Crooke, S. T. Cleavage of Single Strand RNA Adjacent to RNA-DNA Duplex Regions by Escherichia coli RNase H1. *J. Biol. Chem.* **272**, 27513–27516 (1997).
13. Arnold, S. *et al.* Kinetic modeling and simulation of in vitro transcription by phage T7 RNA polymerase. *Biotechnol. Bioeng.* **72**, 548–561 (2001).
14. Niederholtmeyer, H., Stepanova, V. & Maerkl, S. J. Implementation of cell-free biological networks at steady state. *Proc. Natl. Acad. Sci. USA* **110**, 15985 (2013).
15. Kern, J. A. & Davis, R. H. Application of solution equilibrium analysis to in vitro RNA transcription. *Biotechnol. Prog.* **13**, 747–756 (1997).
16. Young, J. S., Ramirez, W. F. & Davis, R. H. Modeling and optimization of a batch process for in vitro RNA production. *Biotechnol. Bioeng.* **56**, 210–220 (1997).
17. Padirac, A., Fujii, T. & Rondelez, Y. Bottom-up construction of in vitro switchable memories. *Proc. Natl. Acad. Sci. U. S. A.* **109**, E3212–E3220 (2012).
18. Montagne, K., Plasson, R., Sakai, Y., Fujii, T. & Rondelez, Y. Programming an in vitro DNA oscillator using a molecular networking strategy. *Mol. Syst. Biol.* **7**, 466 (2011).
19. Filonov, G. S., Moon, J. D., Svensen, N. & Jaffrey, S. R. Broccoli: rapid selection of an RNA mimic of green fluorescent protein by fluorescence-based selection and directed evolution. *J. Am. Chem. Soc.* **136**, 16299–16308 (2014).
20. Ausubel, F. M. et. al. *Current Protocols in Molecular Biology.* **1**, (John Willey & Sons, Inc, 1994).
21. Sharmeen, L. & Taylor, J. Enzymatic synthesis of RNA oligonucleotides. *Nucleic Acids Res.* **15**, 6705–6711 (1987).

22. Krupp, G. RNA synthesis: strategies for the use of bacteriophage RNA polymerases. *Gene* **72**, 75–89 (1988).
23. Krupp, G. Unusual promoter-independent transcription reactions with bacteriophage RNA polymerases. *Nucleic Acids Res.* **17**, 3023–3036 (1989).
24. Rong, M., Durbin, R. K. & McAllister, W. T. Template strand switching by T7 RNA polymerase. *J. Biol. Chem.* **273**, 10253–10260 (1998).
25. Schenborn, E. T. & Mierendorf, R. C. A novel transcription property of SP6 and T7 RNA polymerases: dependence on template structure. *Nucleic Acids Res.* **13**, 6223–6236 (1985).
26. Gholamalipour, Y., Karunanayake Mudiyanselage, A. & Martin, C. T. 3′ end additions by T7 RNA polymerase are RNA self-templated, distributive and diverse in character—RNA-Seq analyses. *Nucleic Acids Res.* **46**, 9253–9263 (2018).
27. Frieden, M., Pedroso, E. & Kool, E. T. Tightening the belt on polymerases: Evaluating the physical constraints on enzyme substrate size. *Angew. Chem. Int. Ed.* **38**, 3654–3657 (1999).
28. Kadesch, T. R. & Chamberlin, M. J. Studies of in vitro transcription by calf thymus RNA polymerase II using a novel duplex DNA template. *J. Biol. Chem.* **257**, 5286–5295 (1982).
29. Aiyar, S. E., Helmann, J. D. & deHaseth, P. L. A mismatch bubble in double-stranded DNA suffices to direct precise transcription initiation by Escherichia coli RNA polymerase. *J. Biol. Chem.* **269**, 13179–13184 (1994).
30. Chambon, P. Eukaryotic nuclear RNA polymerases. *Annu. Rev. Biochem.* **44**, 613–638 (1975).
31. Bloomfield, V. A., Crothers, D. M. & Tinoco, I. *Nucleic Acids : Structures, Properties, and Functions*. (University Science Books, Sausalito, CA, 2000).
32. Cherry, K. M. & Qian, L. Scaling up molecular pattern recognition with DNA-based winner-take-all neural networks. *Nature* **559**, 370–376 (2018).
33. Kar, S. & Ellington, A. D. In vitro transcription networks based on hairpin promoter switches. *ACS Synth. Biol.* **7**, 1937–1945 (2018).
34. Venkataraman, S., Dirks, R. M., Rothemund, P. W. K., Winfree, E. & Pierce, N. A. An autonomous polymerization motor powered by DNA hybridization. *Nat. Nanotechnol.* **2**, 490–494 (2007).
35. Green, A. A. *et al.* Complex cellular logic computation using ribocomputing devices. *Nature* **548**, 117–121 (2017).
36. Kotani, S. & Hughes, W. L. Multi-arm junctions for dynamic DNA nanotechnology. *J. Am. Chem. Soc.* **139**, 6363–6368 (2017).
37. Dabby, N. Thesis: Synthetic molecular machines for active self-assembly: prototype algorithms, designs, and experimental study. (California Institute of Technology, 2013).
38. Qian, L. & Winfree, E. Parallel and scalable computation and spatial dynamics with DNA-based chemical reaction networks on a surface. in *DNA Computing and Molecular Programming* (eds. Murata, S. & Kobayashi, S.) 114–131 (Springer International Publishing, 2014).
39. Zhang, D. Y. & Winfree, E. Control of DNA strand displacement kinetics using toehold exchange. *J. Am. Chem. Soc.* **131**, 17303–17314 (2009).
40. Parker, C. A. & Rees, W. T. Fluorescence spectrometry. A review. *Analyst* **87**, 83–111 (1962).